The University Of Sheffield.

FAULT DETECTION OF BRUSHLESS PERMANENT MAGNET MACHINE DRIVES

Bing Liu

M.Phil Thesis

Department of Electronic and Electrical Engineering

February 2014

A thesis submitted in partial fulfilment of the requirement for the degree of Master of Philosophy in Electronic and Electrical Engineering at The University of Sheffield

Abstract

In the last two decades, permanent magnet synchronous machines (PMSMs) have attracted much interest and have been largely investigated for modern industries and special applications. Although the use of the permanent magnet for the magnetic field creation brings a number of merits, the low fault tolerance capability is an inherent weak point for the PMSMs. A few short-circuit turns lead to significant increase in the faulting winding current and excessive heat generation. This may further propagate and eventually cause a catastrophic failure. Based on the above reason, fault detection in PMSMs has become crucially important and necessary, especially for applications demanding high security and reliability. This forms the basic motivation of this research work.

In this thesis, the modelling of PMSM with inter-turn short-circuit faults is presented first. The developed PMSM model can represent the motor operation under normal and short-circuit fault conditions. A winding fault detection technique is addressed by applying the sequence component theory. To eliminate the influence of disturbances on fault detection, a fuzzy logic based approach is considered in this work. The simulation results have shown that the proposed fault detection approach is capable of diagnosing the faulting phase accurately and quickly under both load and speed fluctuations.

Acknowledgement

I would like to express my deepest gratitude to my supervisor Prof. Jiabin Wang, for his expert guidance and continuous support throughout my study at the University of Sheffield. I would like to thank my external examiner Dr. Zhigang Sun and internal examiner Dr. Luke Seed for their advices to the corrections to this thesis.

Thanks also to Electrical Machines and Drives Group for providing a fantastic research environment to work in. In particular, I would like to thank Dr. Xibo Yuan and Mr. Bhaskar Sen for their brilliant advice and invaluable help. My thanks also go to Mr. Liang Chen, Mr. Shoan Mbabazi, Mr Xiao Chen, Mr. Panagiotis Lazari and Mrs. Hawa Agita for interesting discussion.

A very special thanks to Dr Philip Allsworth-Jones for his invaluable friendship.

Most of all,, I would like to thank my family, my beloved parents and my brother, who have always been enriching and inspiring my life. Lastly, I would like to thank my husband Dr Chao Ji for always being my side, loving , supporting and believing in me.

List of Contents

List of Figures

List of Tables

List of Abbreviations

PMSM	permanent magnet synchronous machine
EMI	electromagnetic interference
IPM	interior permanent magnet
SPM	surface-mounted permanent magnet
FDD	fault detection and diagnosis
MCSA	motor current signature analysis
FFT	fast fourier transform
PSD	power spectra density
DWT	discrete wavelet transformation
AI	artificial intelligence
NN	neural network
GA	genetic algorithm
FEM	finite element method
IGBT	insulated gate bipolar transistor
PWM	pulse width modulation
VSA	vibration signature analysis
AX	axial flux
SOGI	second order generalised integrator
CUSUM	cumulative sum algorithm

CCVSI	current-controlled voltage source inverter
PLL	phase locked loop

CHAPTER 1

INTRODUCTION

1.1 Electrical Machines

Built on the foundation of electromagnetic phenomena, electrical machines were first invented early in the 19th century. By the classic definition, electrical machine is the universal name of both electrical motors and generators, which are both electromechanical energy converters (i.e. converting energy between electrical and mechanical forms). Nowadays, most of the electricity consumed by humans is generated by electrical generators, and more than 60% of the electricity is consumed by different types of electrical motors. Hence, the electrical machine is ubiquitous and important in modern social and industrial applications.

There are many different ways to classify electrical machines (motors or generators), such as electrical power input (DC or AC), operating condition (AC induction or AC synchronous), and rotor structure (switching reluctance machines) etc. Permanent magnet synchronous machines (PMSMs) were not widespread until the middle of last century. Especially in the 1980s, industrial

manufacturers made progress in the improvement of the magnet characteristics, which enabled the fast development of the PMSMs [1, 2]. Compared to the traditional induction motors, the PMSMs utilise a permanent magnet to create magnetic field instead of using winding coils. This important feature brings the PMSMs with many advantages, such as higher power density, lower electromagnetic interference (EMI), higher achievable motor speed etc. Therefore, the PMSMs have been extensively used in modern industrial applications, such as hybrid automobile, aerospace drives.

1.2 Permanent Magnet Synchronous Machines

For PMSMs, the stator generally has the same form as traditional induction motors, i.e. classical three-phase stator windings. Instead of excitation windings, the rotor of the PMSM's rotor has the permanent magnet installed which is responsible for the creation of the magnetic field. According to the position of the magnet, the PMSM can be roughly divided into two categories, which are the interior permanent magnet (IPM) motor type and the surface mounted permanent magnet (SPM) motor type [3].

For the SPM motors, the permanent magnet is installed directly on the surface of the cylindrical rotor, which implies that the magnetic flux path seen by the stator windings is independent of rotor position. In contrast, the permanent magnet of the IPM motors is buried inside the rotor, which leads to magnetic reluctance variation with rotor position. Consequently, the synchronous inductance, L_d, in the direction of the rotor magnetic axis is the same as L_q, the inductance in the quadrature direction in SPM machine, but is different in IPMs.

Each type PMSM has its own advantages and drawbacks. In general, the SPM motor is relatively easy to construct and has low torque ripple and good linearity; due to the buried magnet structure, the IPM motor is difficult to build and thus the cost is slightly higher. However, the constant power capability of the IPM is better than the SPM motors [3].

Although the use of the permanent magnet brings many merits, the PMSM is very sensitive to machine or control system faults, since the magnetic field generated by the PM cannot be turned off at will. For instance, a few short-circuit turns of the stator winding will lead to an increment in the faulted winding current, and thus to excessive heat generation. This may further propagate and eventually cause a catastrophic failure.

If the control and protection system can detect abnormal events at early stage, the catastrophic failures can be avoided and the machine can be protected. Particularly for applications demanding high security and reliability (e.g. aerospace and automotive sectors), fault detection of the PMSMs has become crucially important and attracted much interest.

1.3 Fault Detection and Diagnosis

1.3.1 Introduction

Fault detection and diagnosis (FDD) plays a very important role for the PMSM operation in many industrial applications. In the real word, the engineering system is inherently complex, and faults are difficult to avoid. A simple fault may result in the whole engineering system shut-down, and potential equipment damage, etc. Due to the above reasons, FDD is of great practical significance.

Figure 1.1 illustrates the block diagram of a general FDD system. The electrical machine system is regulated by a controller and using feedback signals from the measurement sensors. A FDD system is applied to monitor both the control output and sensor measurements, in order to analyse the data and thus judge the machine operating condition. As long as any abnormal signal is observed, the FDD sends high priority control commands to protect the machine from possible faults. It should be pointed out that, the machine system and measurement device are subject to faults, disturbance and environmental noise; the disturbances and sensor noise can result in a misjudgement of the machine operating condition. It is, therefore, essential that

the FDD system must be robust in order to enhance the availability and reliability of the whole machine system.

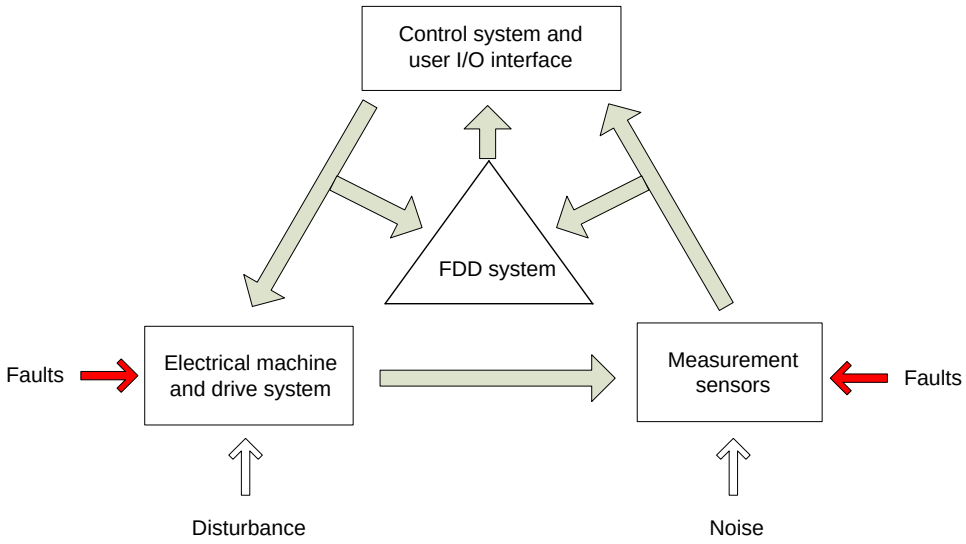

Figure 1.1 Block diagram of common FDD system.

Various techniques can be used in the FDD system. In general, they can be grouped into two categories: model-based types and knowledge-based types.

Model-based fault detection techniques are often based on linear systems models. By using linearization approaches, practical systems can be simplified and represented by a linear model around its steady state working point [4]. However, the simplified linear model of a real non-linear system is feasible only around the linearization point. This implies that model is not representative and will even result in inaccurate detection results if the system operates away for the linearization point. To overcome that, complex nonlinear models can be considered to represent the dynamic and steady state response of the practical system in a more broad operating range. However, the development of a non-linear model based fault detection technique is quite challenging and requires further research [5].

Knowledge-based methods usually employ an expert system [6, 7], as shown in Figure 1.2. The knowledge base facts and rules, also called a ‘rule-based system’, contain descriptions and rules of the characteristics of the target plant. The knowledge acquisition block is used for acquiring new facts or rules and keeping the ‘rule-based system’ updated. Based on some algorithms and

protocols, an inference engine processes the knowledge based facts and rules, and communicates with the user/plant through I/O interface.

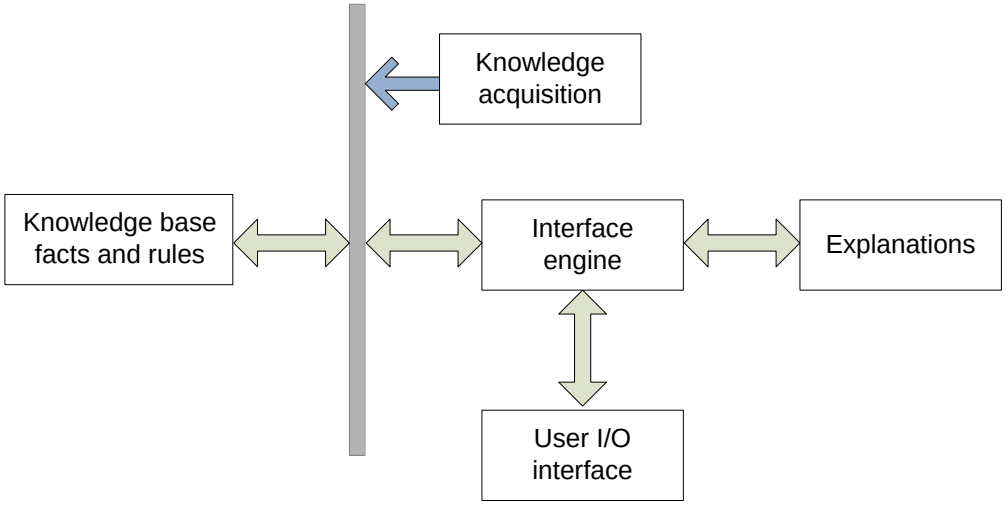

Figure 1.2 General structure of expert system for FDD [8].

1.3.2 Faults in Electric Motors

The electrical machine based FDD system was first proposed and implemented for induction machine drives [9]. In practical applications, electric motors are always exposed to non-ideal environments, e.g. overload, frequent motor starting/stopping and inadequate cooling [10, 11], and thus suffer from high risk of various faults.

Generally, faults in electric motors can be devided into three categories, which are electrical, magnetic and mechanical faults, respectively. According to IEEE Standard 493-2007 [12], the two most common faults of the electric motors are bearing faults (44%) and winding faults (26%). Mechanical faults include bearing faults, eccentricity faults and faults caused by mechanical imbalances or non-uniform air gaps. As the most frequently occurring electrical fault, winding faults (mainly in stator windings) of the electrical motors are always related to insulation breakdowns, which accounts for 36.7% [5] [13, 14]. Several possible causes of stator winding fault can be summarised as follows: unbalanced operation, transient overvoltage during start-up and loose bracing for end winding, etc.

Starting with an insignificant insulation failure between winding turns, this kind of fault may not have much noticeable effect at initial. However, it can quickly develop into phase loss and propagates quickly to other serious faults, and even lead to a catastrophic failure of the entire machine system [15, 16].

1.3.3 FDD Techniques in Electrical Motors

In the literature, various FDD techniques have been presented and demonstrated for electrical machine systems, and each fault detection technique has its own merits and limitations. Several classical approaches are studied and reviewed as follows.

Motor current signature analysis (MCSA) is a common solution that had been used for both induction motors and PMSMs [17]. In [18], the fast Fourier Transform (FFT) of the rotor current was monitored to diagnose faults of induction machines. However, this method does not perform well when the machine is subject to fluctuations (e.g. speed or load changes). This is because these fluctuations imply variations on the motor slips and thus the FFT signals. Therefore, this approach is not always reliable and the fault detection result should be treated cautiously to avoid false alarms.

With the aim of overcoming this limitation, a method based on the sequence components of the machine current variables was developed in [19] for fault diagnosis of induction machines. The inherent asymmetries of the system were removed by using pre-recorded information of sequence components under system normal conditions to isolate the fault signal and improve the reliability of the detection result.

The wavelet transform is also a suitable approach to assess motor faults under limited speed and load variation. For example in [20], the wavelet analysis of the winding current is combined with power spectral density (PSD) estimation, in order to detect inter-turn short-circuit faults of inductor motors. The wavelet analysis based PMSM fault detection approach was discussed in [21]. The stator current harmonics have noticeable relevance with inter-turn short-circuit of the PMSM, compared with normal conditions.

The discrete wavelet transformation (DWT) has been used in [22-25], as an alternative tool for fault feature extraction to detect different electrical faults under non-stationary conditions, inter-turn fault, bearing damage, etc. Barendse *et al* [22] have applied the DWT to analyse the current variables on the rotating frame. Bearing damage of the PMSMs was detected by using DWT over a wide speed range [23].

Recently, sequence component theory has been considered by many researchers as an promising solution for an electrical machine FDD system. Cheng *et al*. have demonstrated that using the sequence component approach can detect stator winding faults in induction motors [26]. The value of negative-positive-sequence impedance is dependent on the asymmetric behaviour of the machine, which is sensitive to stator short-circuit fault (even if there is a one-turn stator fault). However, the main limitation of this method is that. It demands independent current measurement [26]. In [27], the zero sequence component of the stator voltage variables was proposed for assessing winding faults when the motor speed changes. However, in the above mentioned papers, the developed methodologies have only considered the diagnosis procedure under load fluctuations, i.e. the influence of speed change, or frequency change, is not addressed.

In the last decade, artificial Intelligence (AI) techniques have attracted much interest and have been employed successfully in the fault detection area. The solicitation of expert systems, fuzzy logic theory, genetic algorithm (GA) and artificial intelligent neural networks (NN) has been considered for fault diagnosis of electric motor drive systems [28, 29]. A fuzzy logic based MCSA approach was discussed in [28], to detect inter-turn short-circuit faults in induction motors. In [30], the authors focused on the open-loop systems and applied a feed-forward NN to detect inter-turn faults. However, for all the AI techniques, a new set of training data is required when applying the technique to a new machine.

1.4 Project Objectives

Based on the above discussion an effective and reliable FDD scheme is vital for PMSM applications that demand high reliability and high security. The objective of this research work is to develop a novel fault detection and diagnosis system, which is capable of assessing, quickly and reliably, inter-turn short-circuit faults in PMSMs. The developed fault detection scheme integrates the negative sequence component analysis with fuzzy logic classifier, to improve sensitivity and robustness detection.

The main topics covered in the thesis are:

- Development of a parametric model to simulate the operation of a PMSM drive under both normal and fault conditions.
- Development of a detection technique to diagnose inter-turn short-circuit faults in PMSMs, based on negative sequence component analysis of stator current and voltage signals.
- Application of fuzzy logic classifier to improve the robustness of the sequence component analysis techniques and thereby enhance the reliability of the FDD system.

1.5 .Thesis Outline

The thesis is sectioned into five chapters as follows:

Chapter 2 develops a simulation model of a three-phase PMSM drive system with inter-turn short-circuit faults and performs simulation study of fault behaviour.

Chapter 3 presents a detailed literature review of fault detection techniques for both induction motors and PMSMs. The concept of symmetrical components is introduced and reviewed. Following this, two methods for the real-time evaluation of sequence components of the PMSM are compared and discussed. The utility of the sequence component analysis for detecting inter-turn faults is

studied, and the influences of load and speed fluctuations on the negative sequence components are highlighted and analysed.

Chapter 4 applies the fuzzy logic approach for the FDD of an inter-turn short-circuit fault in PMSM drives under load or speed change. The fundamental theory of classical set and fuzzy set is introduced as the basis of the fuzzy logic theory. Then, the membership function and the rule based inference of the fuzzy logic are discussed to provide a clear understanding of the concepts. Finally, the simulation shows that the proposed approach is capable of diagnosing faults accurately and quickly under both load and speed fluctuations.

Chapter 5 summarises the contribution of this research and discusses possible future work.

CHAPTER 2

PMSM MODELLING UNDER NORMAL AND STATOR FAULT CONDITIONS

2.1 Introduction

In the last two decades, permanent magnet synchronous machines (PMSM) have been widely investigated and applied in modern industrial areas, such as hybrid vehicles, electric trains, airplanes and military power drive applications [13, 21], due to their higher torque, higher efficiency and better dynamic performance in comparison to traditional machines with electromagnetic excitation. However, the presence of the spinning rotor magnets is a significant weak point for the PMSMs, and any fault may create special challenges. With the aim of ensuring high system reliability and extending motor life, fault detection of the PMSMs plays an important role and attracts more and more interest.

Generally, there are three kinds of faults in the PMSMs: electrical faults, magnetic faults and mechanical faults. Since magnetic faults and mechanical

faults are not related to this research work, only electrical faults will be considered. An electrical fault is typically caused by the failure of winding insulation, and can be further divided into three categories which are turn to turn, phase to phase and phase to ground faults. As the most common fault in the electrical machines, the turn-to-turn fault is particularly difficult to detect. This is because, when an inter-turn short-circuit fault takes place, the current under feedback control may not have much noticeable change. However, the current in the short-circuit turns can be many times greater than the permissible level [31]. In contrast, if a terminal short-circuit occurs, the current is limited by the phase inductance. This feature implies the machine would withstand a phase terminal short-circuit indefinitely if the phase inductance is per unit and continued operation on the healthy phases. Since the fault current has a phase shift of 90 degrees with the back-emf, neglecting fault resistance, the resultant average torque output is small [32]. Nevertheless, the induced heat may lead to phase to phase and phase to ground faults.

Therefore, the effective modelling of the PMSM inter-turn short-circuit faults is becoming crucially important in the development of fault diagnosis. It would appear that a model with high precision would be the better for this purpose. However, in reality, a compromise needs to be made between the accuracy and the complexity of the model. A promising model of the PMSM inter-turn fault should be able to describe the behaviour of one turn fault functionally and to account for the effects of the fault correctly [33].

A finite element method (FEM) approach was presented in [34, 35] to analyse the stator winding faults and inter-turns short-circuit faults. Obviously, the FEM modelling does give quite accurate results since it includes most of the physical phenomena. However, it demands a detailed machine specification and a long computational time. For this reason, the FEM models are often applied only in the fault study cases rather than in detection schemes [36]. To overcome the limitations of the FEM model, a classical dynamic model based on the three-phase circuit coordinates has been used in this work.

2.2 PMSM Healthy Condition

In this section, the transformation of the PMSM equation from the three-phase axis (ABC) to the rotating frame (DQ) is presented.

2.2.1 Brushless AC Motors in Stator ABC system

Considering a star-connected three-phase brushless AC motor with high resistivity magnet and retaining sleeves, the current components induced by the rotor can be ignored [37]. Therefore, the circuit equations of the three perfectly-balanced windings, i.e. no physical discrepancy between the windings, can be described in (2.1),

$$\begin{bmatrix} v_a \\ v_b \\ v_c \end{bmatrix} = \begin{bmatrix} R_a & 0 & 0 \\ 0 & R_b & 0 \\ 0 & 0 & R_c \end{bmatrix} \begin{bmatrix} i_a \\ i_b \\ i_c \end{bmatrix} + \frac{d}{dt} \begin{bmatrix} L_a & M_{ab} & M_{ac} \\ M_{ab} & L_b & M_{bc} \\ M_{ac} & M_{bc} & L_c \end{bmatrix} \begin{bmatrix} i_a \\ i_b \\ i_c \end{bmatrix} + \begin{bmatrix} e_a \\ e_b \\ e_c \end{bmatrix} \tag{2.1}$$

where v_a, v_b and v_c represent the three-phase voltages; i_a, i_b and i_c are the phase currents of the three windings; R_a, R_b and R_c are the resistance of the windings; L_a, L_b and L_c represent the self-inductance of each phase, while M_{ab}, M_{ac} and M_{bc} are the mutual inductance between them; e_a, e_b and e_c represent the back-emf of each phase.

Equation (2.2) presents two sources of the back-emf $\begin{bmatrix} e_a & e_b & e_c \end{bmatrix}^T$, i.e. one from the flux linkage ψ_m and another from the electrical angular speed ω.

$$\begin{bmatrix} e_a \\ e_b \\ e_c \end{bmatrix} = \begin{bmatrix} -\omega\psi_m \sin\omega t \\ -\omega\psi_m(\sin\omega t - \frac{2\pi}{3}) \\ -\omega\psi_m(\sin\omega t + \frac{2\pi}{3}) \end{bmatrix} = \begin{bmatrix} \omega\psi_m(\cos\omega t + \frac{2\pi}{3}) \\ \omega\psi_m(\cos\omega t - \frac{2\pi}{3} + \frac{\pi}{2}) \\ \omega\psi_m(\cos\omega t + \frac{2\pi}{3} + \frac{\pi}{2}) \end{bmatrix} \tag{2.2}$$

The electrical angular speed ω is determined by the pole pairs P times and the mechanical angular speed ω_m, as given in (2.3).

$$\omega = P\omega_m \tag{2.3}$$

Assuming that the rotor reluctance stays constant, the self-inductance and mutual inductance of the three windings can be considered identical to each other [38], which yields,

$$R_a = R_b = R_c = R$$

$$L_a = L_b = L_c = L \tag{2.4}$$

$$M_{ab} = M_{ac} = M_{bc} = M$$

The sum of the three-phase currents for a star-connected balanced machine equals out zero.

$$i_a + i_b + i_c = 0 \tag{2.5}$$

Based on the above definitions, (2.1) can be re-written as in (2.6).

$$\begin{bmatrix} v_a \\ v_b \\ v_c \end{bmatrix} = \begin{bmatrix} R & 0 & 0 \\ 0 & R & 0 \\ 0 & 0 & R \end{bmatrix} \begin{bmatrix} i_a \\ i_b \\ i_c \end{bmatrix} + \frac{d}{dt} \begin{bmatrix} L & M & M \\ M & L & M \\ M & M & L \end{bmatrix} \begin{bmatrix} i_a \\ i_b \\ i_c \end{bmatrix} + \begin{bmatrix} e_a \\ e_b \\ e_c \end{bmatrix} \tag{2.6}$$

The electromagnetic torque T_e can be derived as in (2.7), where T_L, J and B represent the load torque, moment of inertia and viscous friction coefficient of the motor, respectively.

$$\begin{aligned} T_e &= \frac{e_a i_a + e_b i_b + e_c i_c}{\omega_m} \\ &= T_L + B\omega_m + J\frac{d\omega_m}{dt} \end{aligned} \tag{2.7}$$

Therefore, the mechanical angular speed can be obtained as in (2.8).

$$\omega_m = \int \left(\frac{T_e - T_L + B\omega_m}{J} \right) dt \tag{2.8}$$

2.2.2 Park's Transformation

The Park's Transformation (also known as DQ transformation) has been first proposed by Robert H. Park [39] in 1929. As a mathematical transformation, it rotates the reference frame of three-phase systems in an effort to simplify the analysis of three-phase circuits. Figure 2.1 presents the physical interpretation of this transformation, where θ defines the angle between the d-axis and a stationary reference frame – usually the a-axis for simplicity.

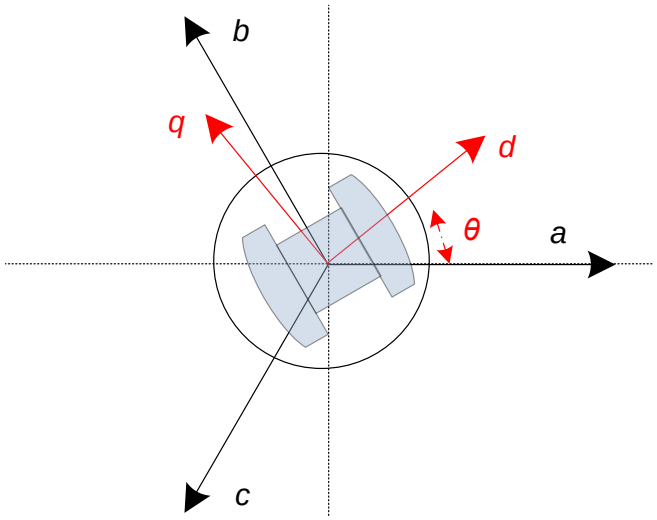

Figure 2.1 DQ rotating reference frame.

The Park's transformation can be represented by (2.9), where the variable *x* can be current, voltage or back-emf.

$$\begin{bmatrix} x_d \\ x_q \end{bmatrix} = C_{dq \leftarrow abc} \begin{bmatrix} x_a \\ x_b \\ x_c \end{bmatrix};$$
$$C_{dq \leftarrow abc} = \frac{2}{3} \begin{bmatrix} \cos\theta & \cos(\theta - \frac{2\pi}{3}) & \cos(\theta + \frac{2\pi}{3}) \\ -\sin\theta & -\sin(\theta - \frac{2\pi}{3}) & -\sin(\theta + \frac{2\pi}{3}) \end{bmatrix} \tag{2.9}$$

Combining it with (2.6), the three-phase PMSM model can be rewritten as in (2.10), where $K_e = P\psi_m$ is the back-emf constant, and $L_d = L_q = L\text{-}M$.

$$\begin{bmatrix} v_d \\ v_q \end{bmatrix} = \begin{bmatrix} R & -\omega L_q \\ \omega L_d & R \end{bmatrix} \begin{bmatrix} i_d \\ i_q \end{bmatrix} + \begin{bmatrix} L_d & 0 \\ 0 & L_q \end{bmatrix} \frac{d}{dt} \begin{bmatrix} i_d \\ i_q \end{bmatrix} + \begin{bmatrix} 0 \\ K_e \omega_m \end{bmatrix} \tag{2.10}$$

The torque equation in the DQ frame can be derived as in (2.11), where $K_t = \frac{3}{2} P \psi_m$ is the torque constant.

$$\begin{aligned} T_e &= \frac{3}{2\omega_m}(v_d i_d + v_q i_q) \\ &= \frac{3P}{2}\left[\psi_m i_q + (L_d - L_q) i_d i_q\right] \\ &= \frac{3P}{2}\psi_m i_q \\ &= K_t i_q \end{aligned} \tag{2.11}$$

2.3 PMSM under Fault Condition

Figure 2.2 shows the equivalent circuit of the three-phase winding with an inter-turn short-circuit fault. When the short-circuit fault takes place in phase A, it can be divided into two parts, a normal (healthy) part a_1 and a faulty part a_2 .The faulty part generates a corresponding magnetic field, which affects the original magnetic field. Due to the fault, two new parameters, i_f and R_f , can be defined: i_f is the short-circuit current; R_f is a resistive impedance that represents the insulation failure, the value of which is uncertain and depends on the fault severity (i.e. R_f = infinity indicates the system is in normal condition; $R_f \approx$zero indicates the winding is completely short-circuited) [40-42].

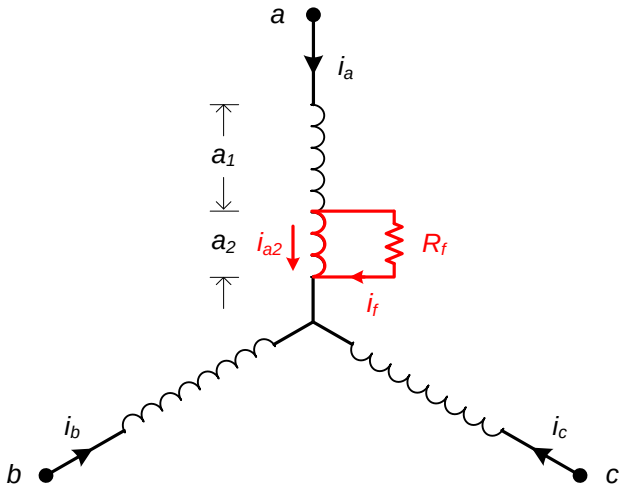

Figure 2.2 Equivalent circuit if three-phase windings with an inter-turn short-circuit fault.

The corresponding circuit equation can be derived as in (2.12) and (2.13), where R_{a2} and L_{a2} represent the resistance and self-inductance of winding a_2, respectively; M_{a1a2} is the mutual inductance between winding a_1 and a_2; M_{a1b} and M_{a1c} are the mutual inductances between winding a_1, b and c.

$$\begin{bmatrix} v_{a1} \\ v_b \\ v_c \\ v_{a2} \end{bmatrix} = \begin{bmatrix} R_{a1} & 0 & 0 & 0 \\ 0 & R_b & 0 & 0 \\ 0 & 0 & R_c & 0 \\ 0 & 0 & 0 & R_{a2}+R_f \end{bmatrix} \begin{bmatrix} i_a \\ i_b \\ i_c \\ i_{a2} \end{bmatrix} + \frac{d}{dt} \begin{bmatrix} L_{a1} & M_{a1b} & M_{a1c} & M_{a1a2} \\ M_{a1b} & L_b & M_{bc} & M_{a2b} \\ M_{a1c} & M_{bc} & L_c & M_{a2c} \\ M_{a1a2} & M_{a2b} & M_{a2c} & L_{a2} \end{bmatrix} \begin{bmatrix} i_a \\ i_b \\ i_c \\ i_{a2} \end{bmatrix} + \begin{bmatrix} e_{a1} \\ e_b \\ e_c \\ e_{a2} \end{bmatrix} \tag{2.12}$$

$$v_{a1} + v_{a2} = v_a$$
$$i_a - i_{a2} = i_f \tag{2.13}$$

Substituting (2.13) into (2.12), a 4×4 matrix of machine equations can be obtained as in (2.14).

$$\begin{bmatrix} v_a \\ v_b \\ v_c \\ v_{a2} \end{bmatrix} = \begin{bmatrix} R_a & 0 & 0 & -R_{a2} \\ 0 & R_b & 0 & 0 \\ 0 & 0 & R_c & 0 \\ -R_{a2} & 0 & 0 & R_{a2}+R_f \end{bmatrix} \begin{bmatrix} i_a \\ i_b \\ i_c \\ i_f \end{bmatrix} + \begin{bmatrix} e_a \\ e_b \\ e_c \\ -e_{a2} \end{bmatrix} + \begin{bmatrix} L_a & M_{ab} & M_{ac} & -(M_{a1a2}+L_{a2}) \\ M_{ab} & L_b & M_{bc} & -M_{a2b} \\ M_{ac} & M_{bc} & L_c & -M_{a2c} \\ -(M_{a1a2}+L_{a2}) & -M_{a2b} & -M_{a2c} & L_{a2} \end{bmatrix} \frac{d}{dt} \begin{bmatrix} i_a \\ i_b \\ i_c \\ i_f \end{bmatrix} \tag{2.14}$$

Then, the electrical model of the PMSM with inter-turn short-circuit faults on the ABC frame can be written as in (2.15).

$$\left[v_{abcf}\right] = \left[R_{abcf}\right] \cdot \left[i_{abcf}\right] + \left[L_{abcf}\right] \cdot \frac{d}{dt}\left[i_{abcf}\right] + \left[e_{abcf}\right] \tag{2.15}$$

Define μ_f as the ratio between the number of the short-circuit turns N_f and the number of total phase turns N.

$$\mu_f = \frac{N_f}{N} \tag{2.16}$$

Then, a linear relationship between μ_f and the resistance and the back-emf can be defined, and a quadratic relationship between the ratio μ_f and the inductance can be assumed. The electrical parameters for phase A with short-circuit faults can be obtained.

$$\begin{aligned} R_{a1} &= (1-\mu_f)R, \quad R_{a2} = \mu_f R \\ L_{a1} &= (1-\mu_f)^2 L, \quad L_{a2} = \mu_f{}^2 L \\ e_{a1} &= (1-\mu_f)e_a, \quad e_{a2} = \mu_f e_a \end{aligned} \tag{2.17}$$

Assuming that there is no leakage flux present between the normal winding part a_1 and faulty part a_2, the mutual inductance M_{a1a2} is equal to $\sqrt{L_{a1}L_{a2}}$.

Due to the short-circuit fault, the voltage across the faulty part is zero. Therefore, the fourth row of the matrix (2.14) can be expanded as,

$$
\begin{aligned}
&v_{a2} = 0 \\
&L_{a2}\frac{di_f}{dt} + R_{a2} i_f \\
&= R_{a2} i_a + (L_{a2} + M_{a1a2})\frac{di_a}{dt} + M_{a2b}\frac{di_b}{dt} + M_{a2c}\frac{di_c}{dt} + e_{a2}
\end{aligned}
\tag{2.18}
$$

Assuming the resistive impedance R_f that models the insulation failure is zero, based on the definitions in (2.17), the short-circuit current i_f in steady state can be derived as in (2.19).

$$
\begin{aligned}
&\left|i_f\right| = \left|\frac{\left[v_{a.rated}\right]}{R_a + j\omega L_{a2}/\mu_f}\right| \\
&\left[v_{a.rated}\right] = R_a i_a + L_a\frac{di_a}{dt} + M_{ab}\frac{di_b}{dt} + M_{ac}\frac{di_c}{dt} + e_a
\end{aligned}
\tag{2.19}
$$

The electromagnetic torque (2.7) can be re-written as follows, where

$$
\begin{aligned}
T_e &= \frac{e_{a1} i_{a1} + e_b i_b + e_c i_c + e_{a2} i_{a2}}{\omega_m} \\
&= \frac{e_a i_a + e_b i_b + e_c i_c + e_{a2} i_f}{\omega_m}
\end{aligned}
\tag{2.20}
$$

2.4 Modelling PMSM under Inter-Turn Fault

The previous section has presented the mathematical equation of the PMSM with inter-turn short-circuit faults. In this section, a simulation model is established by using the Matlab/Simulink platform, according to the PMSM machine specification.

Figure 2.3 shows the developed simulation model, while Table 2.1 summarises the nominal parameters of the PMSM. The model consists of the control block, the PMSM motor block (electrical model, mechanical model and back-emf model), the inverter stage and the d-q reference frame transformation block, which will be discussed in detail as follows.

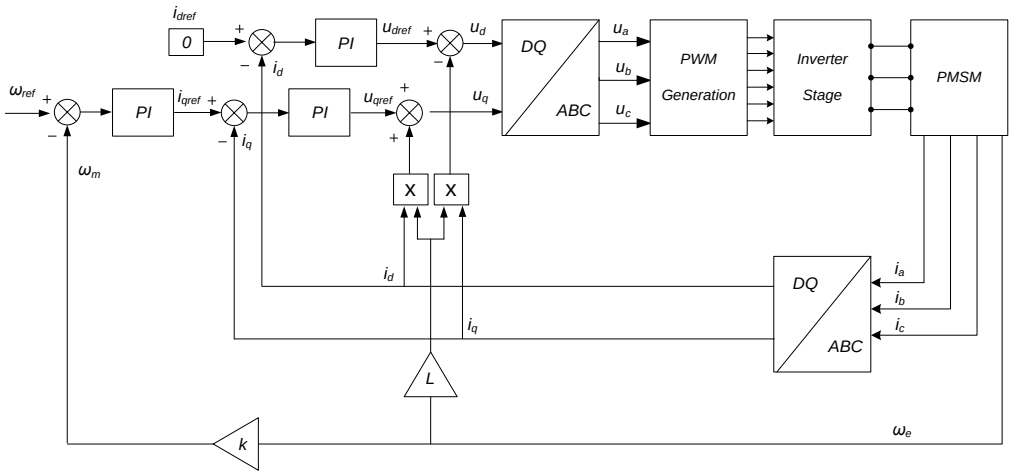

Figure 2.3 Developed simulation model for PMSM.

Table 2.1 Three-phase PMSM parameters

Rated speed	3000 rpm	No. of phases	3
Rated torque	1 Nm	No. of turns per phase	62
Rated current(peak)	6.0 A	Back-emf (peak at 3000rpm L-L)	38.1V
DC supply voltage	140 V	Phase resistance	0.5 Ω
No. of pole-pairs	6	Phase inductance	3.5 mH
Torque constant	1.77×10^{-1} Nm/A	Inertia coefficient	5×10^{-4}Kg.m

2.4.1 Motor Model

Figure 2.4 shows the implemented PMSM motor model. A switch (i.e. the block named “fault”) is utilised to change the system from a healthy to fault condition. The back-emf is simulated by a controllable voltage source block, and the control signal is from (2.2).

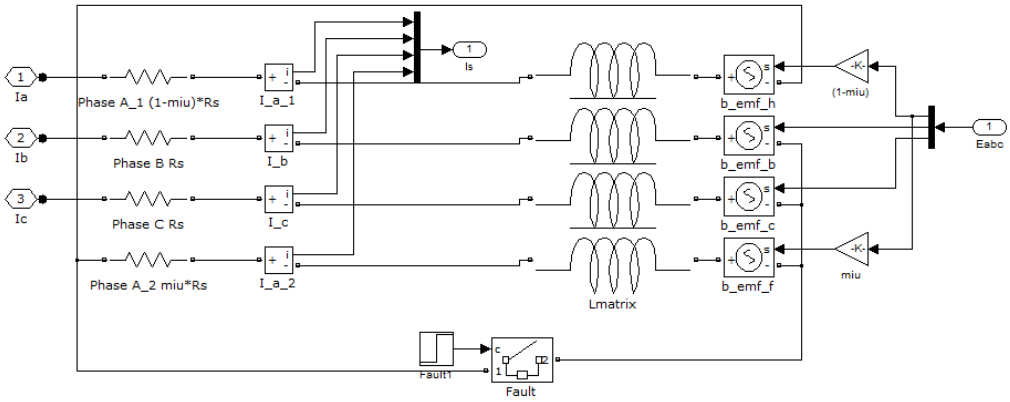

Figure 2.4 Implemented PMSM motor model.

2.4.2 PWM Generation

Figure 2.5 shows the implementation of the Pulse-width Modulation (PWM) generation. Three triangular carrier waves with a frequency of 10kHz and mutual phase shift of 120 degrees are used to compare with the reference voltage signal *Vabc* nominated reference voltage (i.e. generated by controller), in order to produce the gate signal for the voltage source inverter.

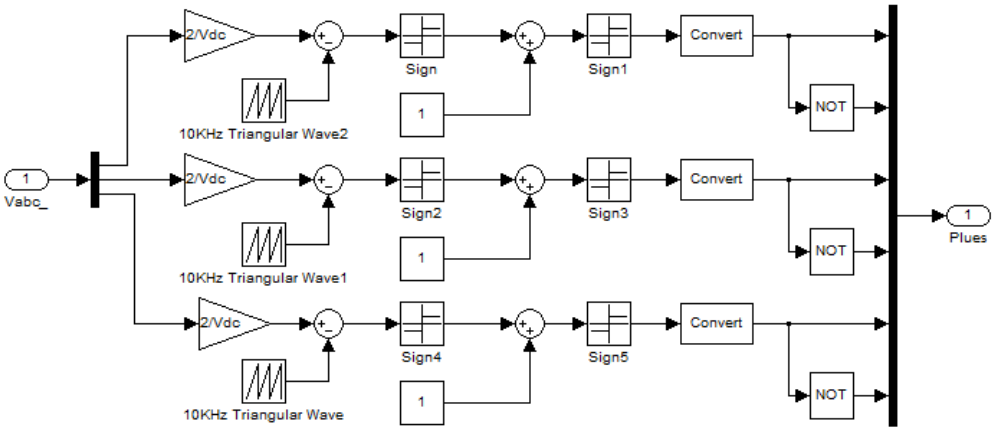

Figure 2.5 PWM generation.

2.4.3 Voltage Source Inverter Model

Supplied by a DC voltage source, the voltage source inverter is employed to produce three-phase AC voltage with variable frequency and magnitude. Figure 2.6 shows the inverter that is simulated by six switch modules, each consisting of one power switch (i.e. Insulated-gate bipolar transistor - IGBT) and one anti-parallel diode.

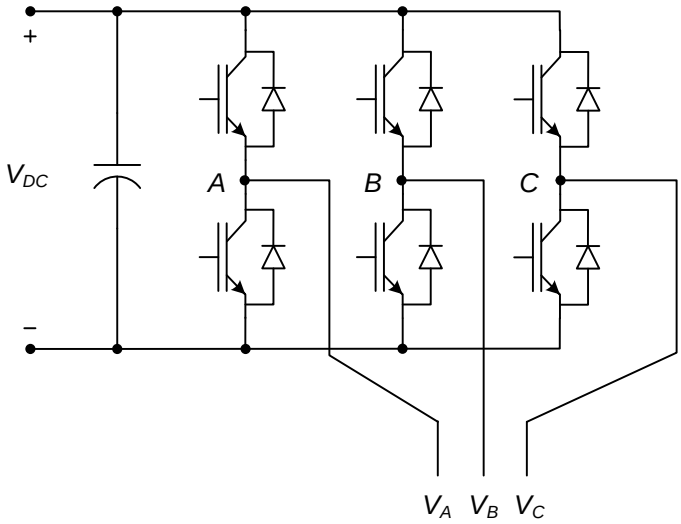

Figure 2.6 Voltage source inverter.

2.4.4 Speed and Current Controllers

For this project, vector control is selected to regulate the PMSM. The proposed control strategy, as shown in Figure 2.7, contains an outer speed control loop and an inner current control loop.

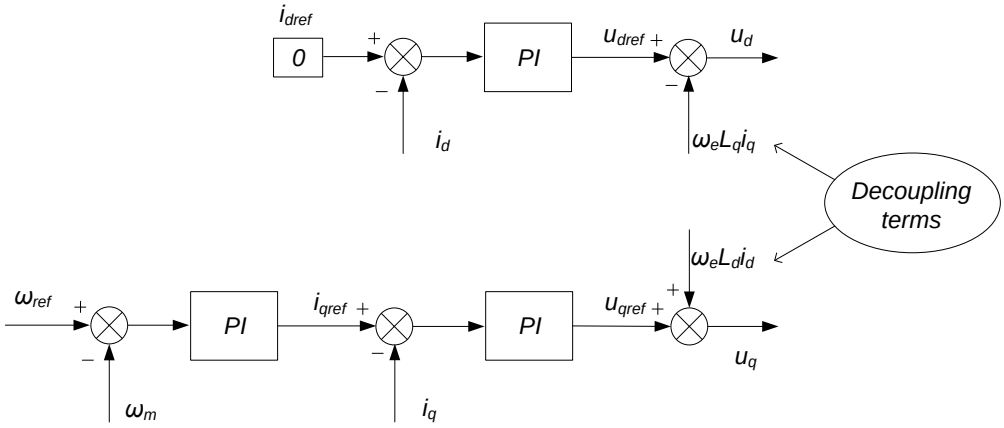

Figure 2.7 PMSM control strategy.

For the current control, the PI controller needs to be designed according to the system requirements and specifications of the PMSM. The speed control loop should be designed based on the complete current loop. Generally, in the SPM motor, the current reference of the d axis is set to zero. The error between the reference speed and measured speed is sent to the speed controller to produce the current reference of the q axis. Then, the error between the reference and

measured currents are through other two PI controllers to determine the DQ reference frame stator voltage.

Figure 2.8 shows the block diagram of the decoupled *dq* current control strategy. Both i_d and i_q are controlled with a PI regulator to match their reference values i_{dref} and i_{qref}. Since the bandwidth of the inner current control loop is much higher than that of speed loop, the effect of the back-emf on the q axis current can be ignored at the control design stage.

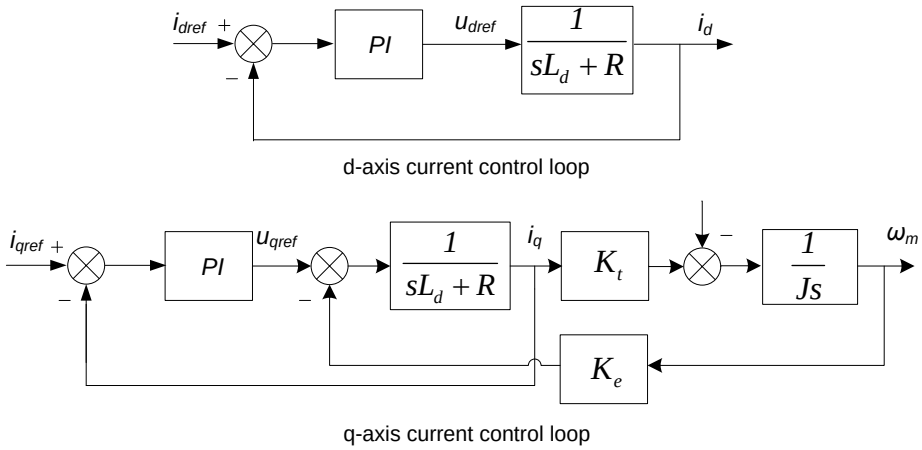

Figure 2.8 Decoupled dq current control loop.

Assume the PI current controller has the general form of $\frac{k_{ii} + k_{pi}s}{s}$, where k_{ii} and k_{pi} are the integral and proportional gains, respectively. Using the pole-zero cancelling technique, the relationship between k_{ii} and k_{pi} can be found, i.e. $k_{pi}/k_{ii} = L_d/R$. Hence, the closed loop transfer function for both d and q axis currents is:

$$\frac{i_{d,q}(s)}{i_{dref,qref}(s)} = \frac{\frac{k_{ii}}{Rs}}{1+\frac{k_{ii}}{Rs}} = \frac{1}{\frac{R}{k_{ii}}s+1} \tag{2.21}$$

The speed control loop needs to be designed based on the current control loop. Assuming the bandwidth of the current control is sufficiently higher, the closed-loop speed control system can be represented by the following block diagram:

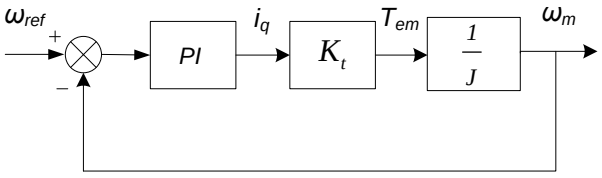

Figure 2.9 Speed control loop.

Suppose the PI current controller has the form of $\frac{k_{is}+k_{ps}s}{s}$, where k_{is} and k_{ps} are the integral and proportional gains of the speed controller. Through similar design procedure, the closed loop transfer function of the speed control can be derived.

$$\frac{w_m(s)}{w_{ref}(s)} = \frac{\frac{k_{is}+k_{ps}s}{s}\cdot\frac{K_t}{J}}{1+\frac{k_{is}+k_{ps}s}{s}\cdot\frac{K_t}{J}} \tag{2.22}$$

Based on the above design and the motor parameters, the current controller values of k_{ii} and k_{pi} are obtained as 4502.52 and 7.58, and the speed controller values of k_{is} and k_{ps} are obtained as 233.085 and 1.137, respectively.

2.5 Simulation Results

In this section, the developed PMSM model will be tested under two cases, speed change and load change.

2.5.1 Speed Change

For this test, the PMSM motor is used to supply a constant load of 0.6Nm, while a speed change will be employed to test the performance of the PMSM motor.

2.5.1.1 Under Healthy Condition

Figure 2.10 shows the speed response of the PMSM rotor under healthy condition, where the blue and red dash curves represent the measured electrical speed and the speed reference, respectively.

At the time point of 0.14s, the speed reference is increased from 800rpm to 1000rmp within 0.06s. Clearly, the actual speed can match the reference accurately, which verifies the proposed control design.

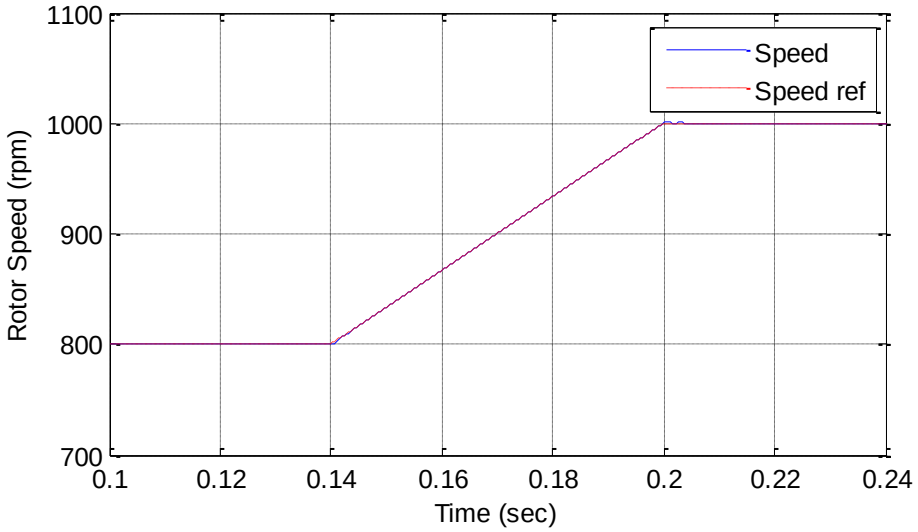

Figure 2.10 PMSM speed response under healthy conditions.

Figure 2.11 indicates the behaviour of the electrical torque under this speed change. As it can be seen, along with the speed change, the torque has increased from 0.6Nm to 0.78Nm with slight oscillations. When the speed control becomes constant, the torque ramps down back to 0.6Nm.

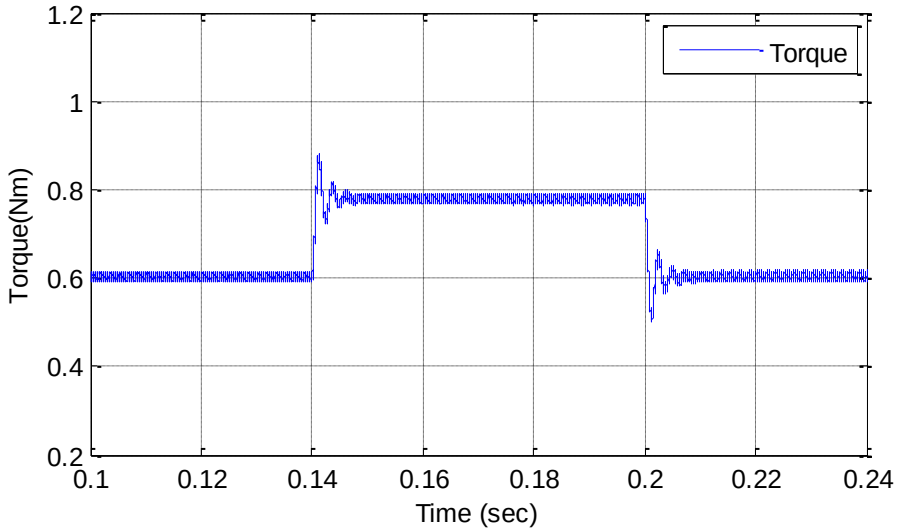

Figure 2.11 PMSM motor torque under healthy conditions.

Figure 2.12 shows the waveform of the three-phase currents during the speed change. When the speed ramps from 800rpm to 1000rpm (i.e. from 0.14s to 0.2s), the phase current amplitude increases from 3.4A to 4.3A.

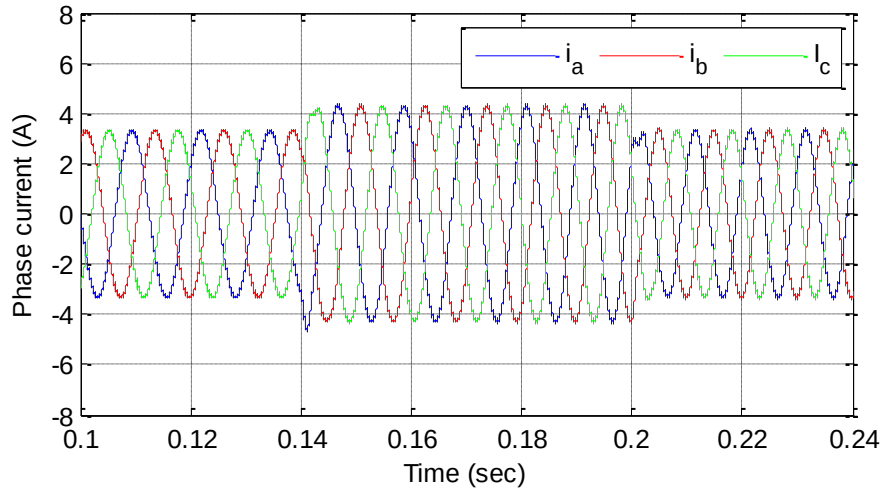

Figure 2.12 Waveform of three-phase current of PMSM under normal conditions.

Figure 2.13 shows the current waveforms in the two winding parts of the phase A, where the blue trace line represents the phase current, and the red trace is the short-circuit current. As expected, the fault current is equal to zero under healthy conditions.

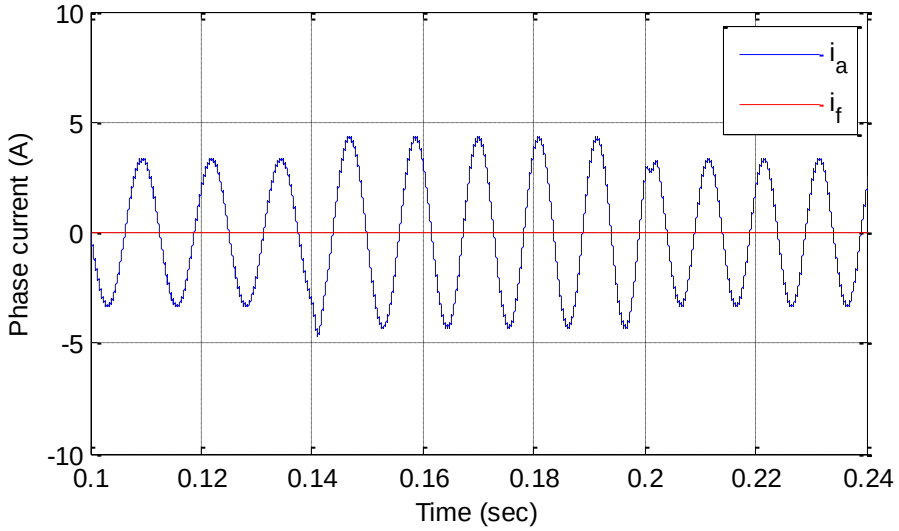

Figure 2.13 Current waveforms in phase A winding under normal conditions.

2.5.1.2 Under Fault Condition

A short-circuit fault of 2 turns is introduced into phase A at the time point of 0.24s. Figure 2.14 shows the comparison of the speed response with the normal and faulty windings, while Figure 2.15 highlights the comparison of the output torque under healthy and faulty cases. It can be seen that, when the short-circuit fault occurs, a 2nd order harmonic has been introduced to both speed response and electromagnetic torque waveforms.

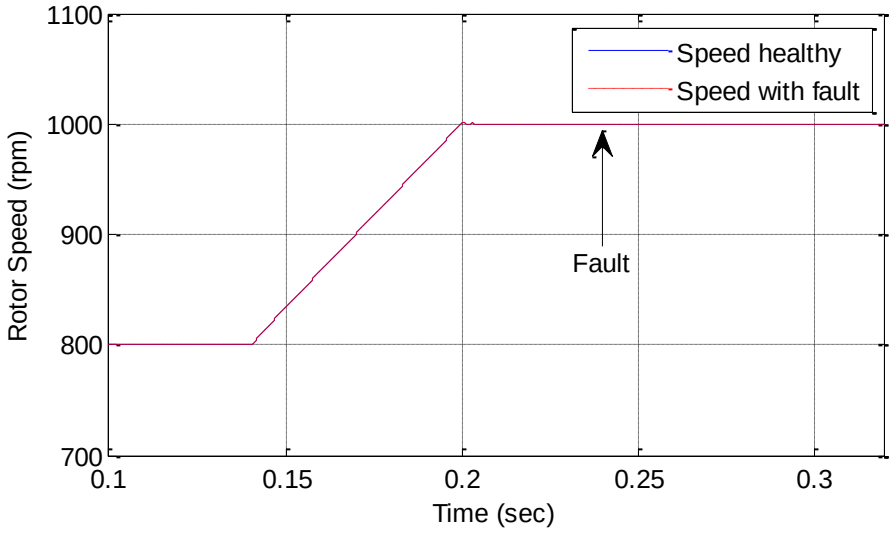

(a) Original view.

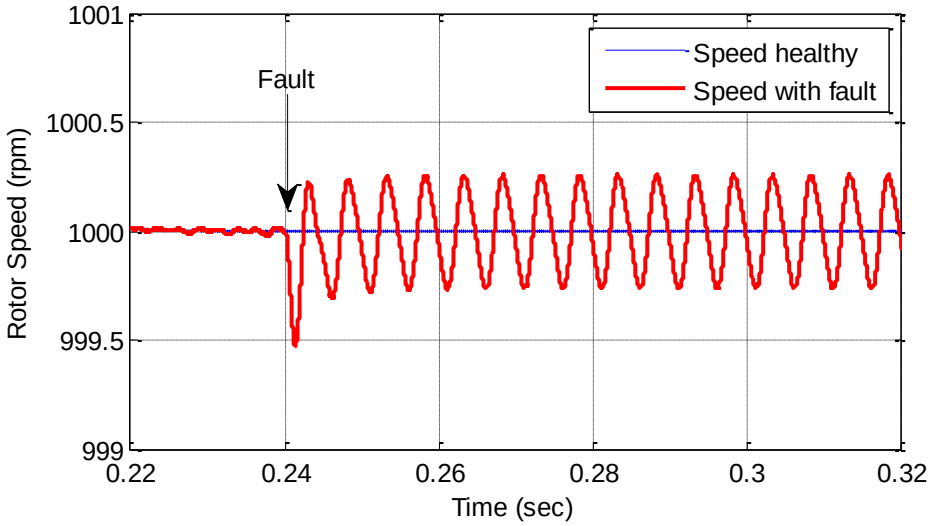

(b) Zoomed-in view.

Figure 2.14 Speed response under normal and faulty conditions.

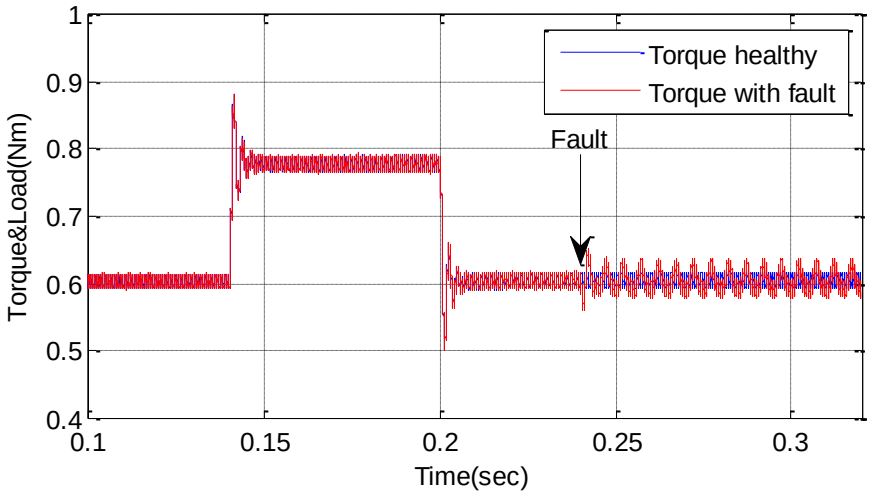

Figure 2.15 Torque response under normal and fault conditions.

Figure 2.16 presents the current waveform under the inter-turn short-circuit fault. It can be observed that, after 0.24s, the faulty phase current (i.e. phase A) has relatively larger amplitude than the other two.

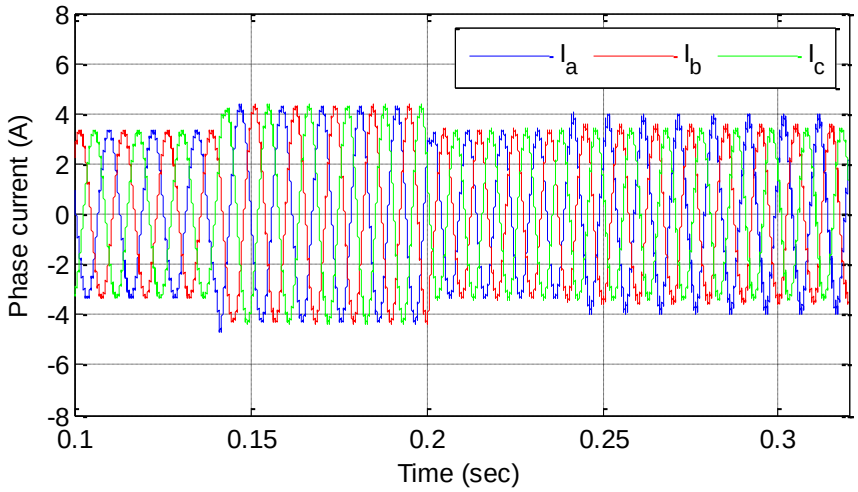

Figure 2.16 Waveform of three-phase currents under faulty conditions.

Due to the very small number of the short-circuit turns, both the motor torque and speed changes in an insignificant manner. However, due to the winding asymmetry, the three-phase currents become slightly unbalanced, which causes small harmonics in the motor speed and torque.

Figure 2.17 presents the waveforms of the short-circuit current i_f, the healthy current i_a and i_{a2}, where $i_{a2} = i_a - i_f$. Obviously, the amplitude of the short-circuit current i_f is significantly higher than that of the healthy current i_a, and

the direction of i_{a2} is opposite to other two currents. The peak value of i_a is 3.3A and the peak value of i_f is around 21A. The fault current simulation result is good match with the theoretical. Consequently, a torque is generated, which resists the output torque resulting in the 2nd harmonics when the system is under turn-to-turn short-circuit conditions.

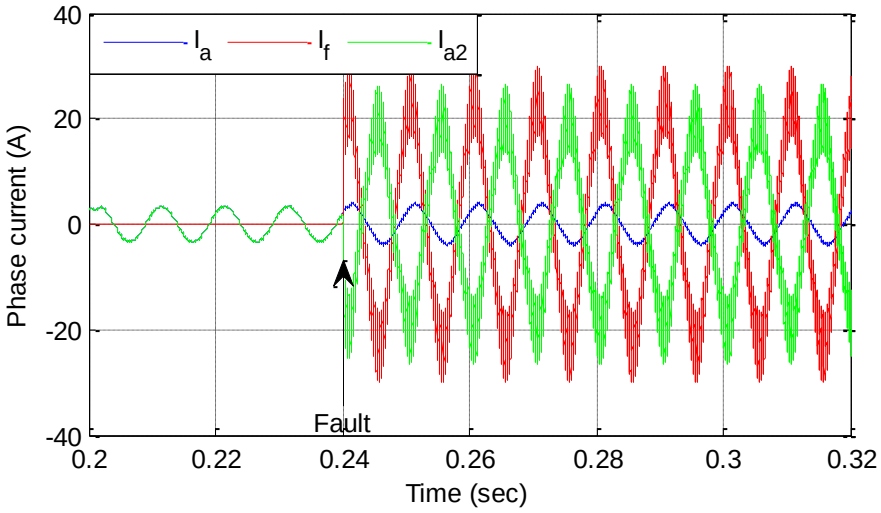

Figure 2.17 Current waveform in phase A winding under faulty conditions.

In order to examine the simulation result presented above, the analytical model discussed in Section 2.4 can be used for verification. Equation (2.23) lists system parameters under steady state.

$$\begin{aligned} &Speed=1000\ rpm;\\ &R=0.5\ \Omega;\\ &L=3.5\ mH;\\ &T_L=0.6\ Nm;\\ &K_t=1.77\times10^{-1}\ Nm/A. \end{aligned} \tag{2.23}$$

Based on the three-phase PMSM parameters, the back-emf and torque can be calculated by using (2.2) and (2.11).

$$\begin{aligned} &E(Peak)=6.78V;\\ &I(Peak)=3.3A; \end{aligned} \tag{2.24}$$

With the short-circuit fault of two turns, the fault current i_f can calculated as follows,

$$V_{a.rated} = \sqrt{(E + RI)^2 + (\omega LI)} = 10.48V\ (Peak)$$
$$\left|i_{f\_Peak}\right| = \left|\frac{V_{a.rated}}{R + j\omega\mu_f L}\right| = \left|\frac{10.48}{0.5 + j0.0608}\right| = 20.79A(Peak) \quad (2.25)$$

As it can be seen, a very good match between the theoretical analysis and simulation results has been demonstrated, which proves the accuracy of the PMSM modelling under inter-turn faults.

2.5.2 Load Change

For this test, the speed reference of the PMSM motor is fixed at 1000rpm, while a step change in load will be employed to test the motor performance.

2.5.2.1 Under Healthy Condition

Figure 2.18 shows the torque response of the PMSM under healthy condition, where the blue and red curves represent the electromagnetic torque and the load torque, respectively.

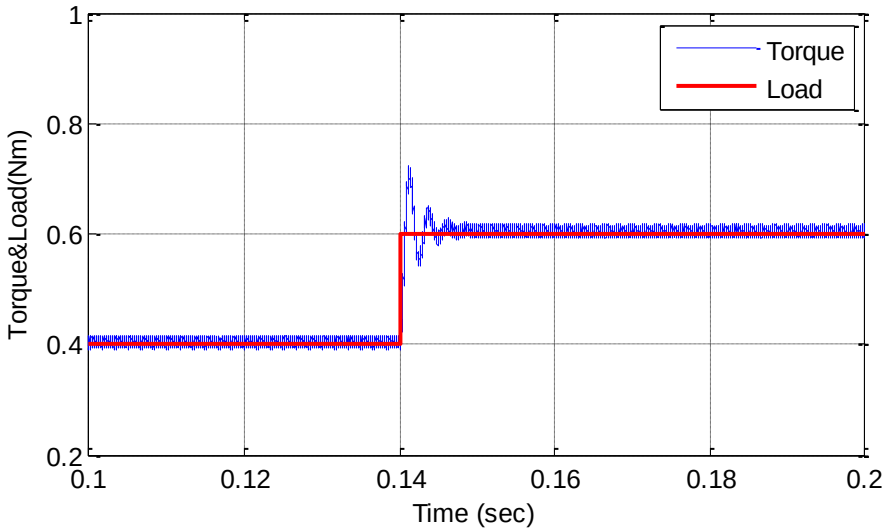

Figure 2.18 Torque response under healthy condition (with step change in load).

At the time point of 0.14s, the load torque has a step change from 0.4Nm to 0.6Nm. Clearly, the electromagnetic torque responds very quickly and reaches steady state within 0.01s.

Figure 2.19 presents the speed behaviour of the PMSM under the load step change, where the blue and red curves represent the measured electrical speed and the speed reference, respectively.

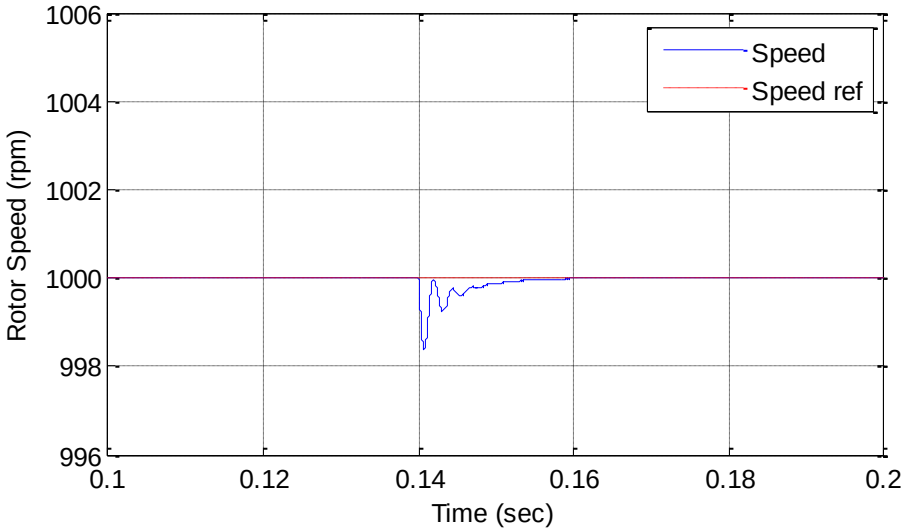

Figure 2.19 Speed response under healthy conditions.

Along with the load torque change at 0.14s, the speed drops down about 2rpm, and then increases back to 1000rpm when the torque response becomes constant.

Figure 2.20 shows the waveform of the three-phase current when the load change applies. When the load torque changes from 0.4Nm to 0.6 Nm at the time point of 0.14s, the amplitude of the three-phase increases from 2.2 A to 3.3A accordingly.

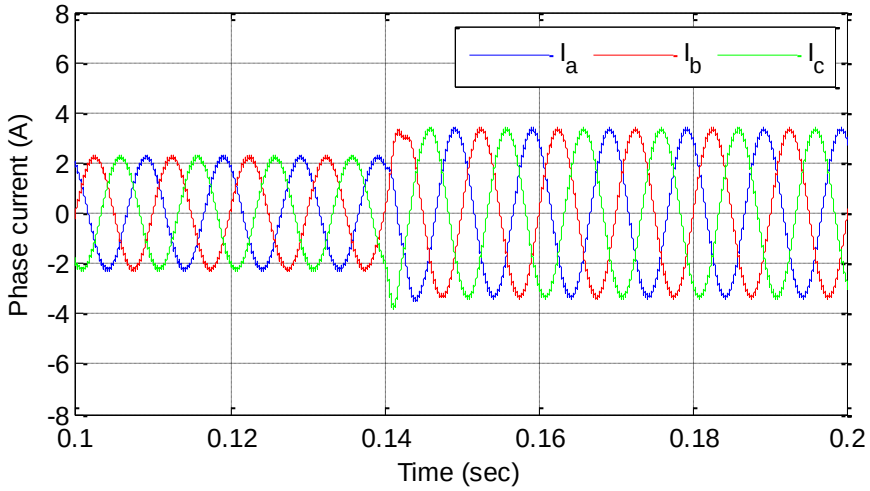

Figure 2.20 Current response under healthy conditions.

Figure 2.21 presents the current of the two parts of phase A winding, which is very similar to Figure 2.13. As expected, the fault current is equal to zero under healthy conditions.

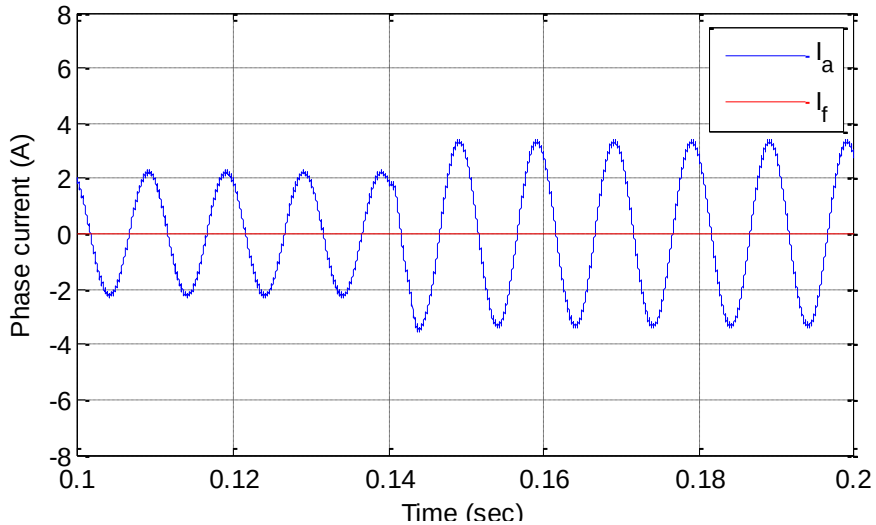

Figure 2.21 Current waveform in phase A winding under healthy conditions.

2.5.2.2 Under Fault Condition

A short-circuit fault of 2 turns is introduced into the phase A winding at the time point of 0.25s. Figure 2.22 shows the comparison of the output torque under healthy and faulty conditions, while Figure 2.23 shows the corresponding speed response comparison. Clearly, when the short-circuit fault occurs, a 2nd order harmonic has been introduced to both speed response and electromagnetic torque waveforms.

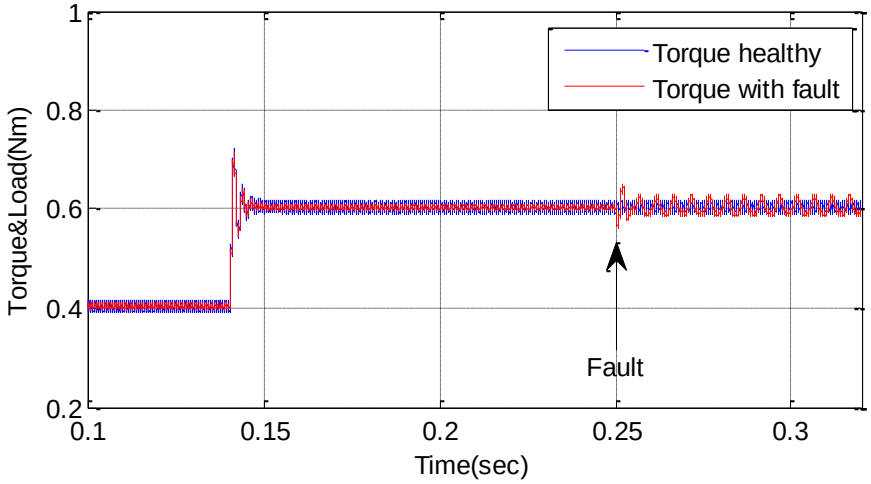

Figure 2.22 Torque response under normal and fault conditions.

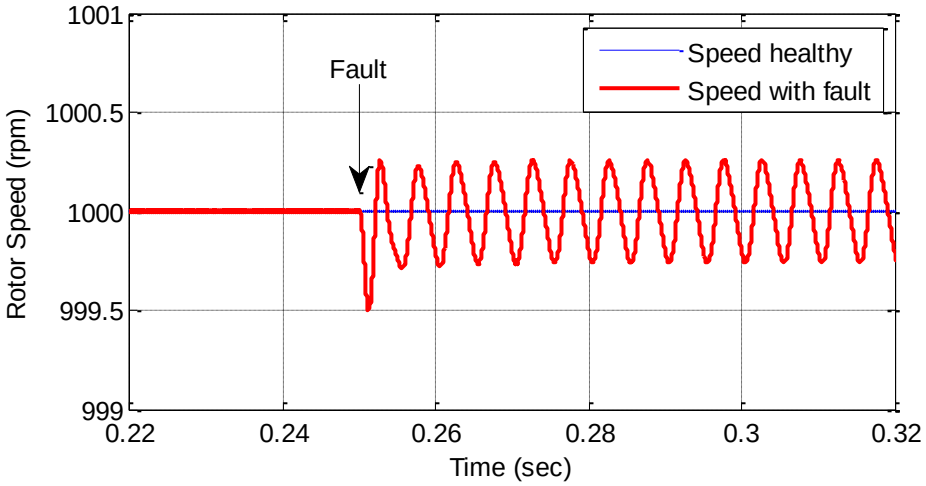

Figure 2.23 Speed response under normal and fault conditions.

Figure 2.24 shows the waveform of the three-phase current under the short-circuit fault. When the fault occurs at 0.25s, the amplitude of the faulty phase current increases a bit.

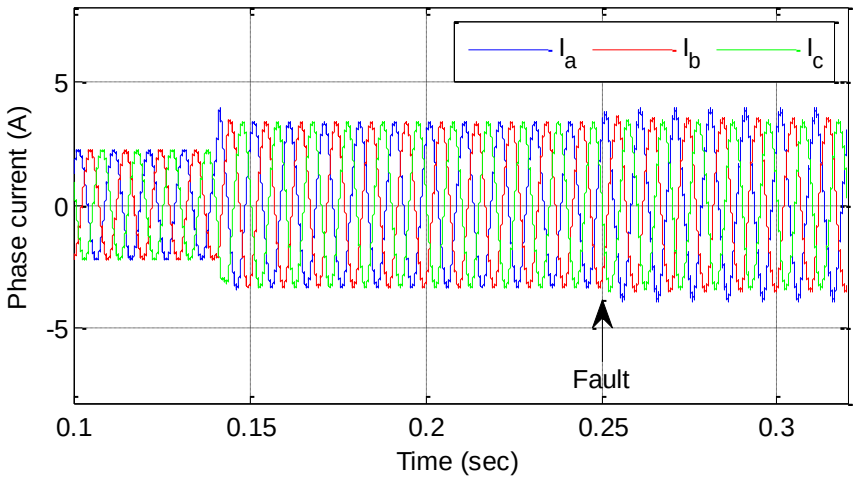

Figure 2.24 Waveform of three-phase currents under fault condition.

Figure 2.25 presents the waveform of the short-circuit current and the healthy part current in phase A. The amplitude of the short-circuit current i_f is significantly higher than that of the healthy current, and the direction of i_{a2} is opposite to other two currents. The fault current value calculated by (2.19) is 20.79A, which is very close the simulation result 21A.

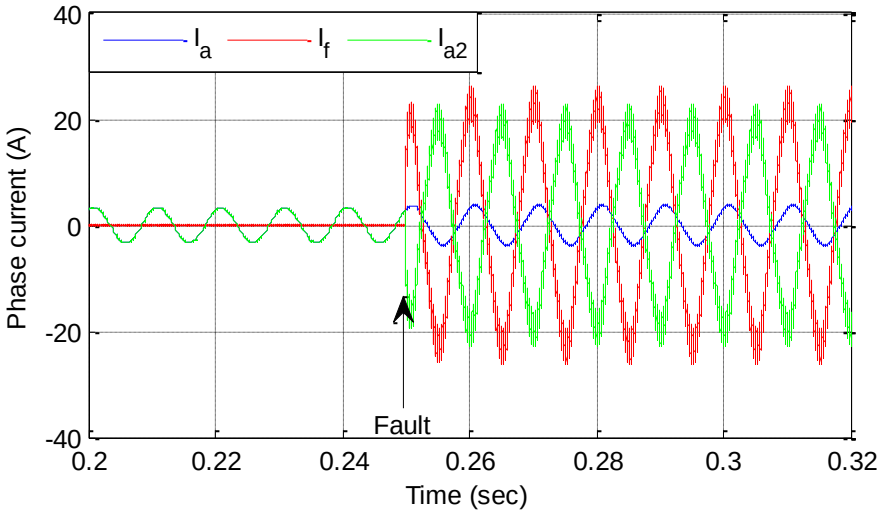

Figure 2.25 Current waveform in phase A winding under faulty conditions.

2.6 Summary

In this chapter, the modelling of the PMSM with inter-turn short-circuit faults has been presented. Firstly, the fundamental theory of PM machine equation under ABC frame and DQ frame has been introduced. Then, the PMSM model has been discussed in detail to provide a clear understanding of the basic concepts. Finally, a very good match between the simulation results and the theoretical analysis has been demonstrated.

CHAPTER 3

FAULT DETECTION TECHNIQUE 1: NEGATIVE SEQUENCE ANALYSIS

3.1 Introduction

In this chapter, the traditional fault detection techniques used for both induction motors and PMSMs are first reviewed and studied. Following that, the concept of symmetrical components is introduced, which forms the basis of the proposed negative sequence components detection approach. Then, two kinds of methods are discussed to perform the calculation of the negative sequence components of the PMSM: one is three-phase sequence analyser and another is second order generalised integrator based approach. The influence of motor load and speed changes on the negative sequence components are investigated, which will help to draw a robust and accurate algorithm for the inter-turn short-circuit fault detection.

3.2 Fault Detection Techniques

3.2.1 Fault Detection for Induction Motors

Motor current signature analysis (MCSA) is one of the most common approaches for the fault detection of induction motors [18, 43-45]. By applying signal processing algorithms, the MCSA analyses motor current waveforms and can provide early machine diagnosis and protection. However, it requires long computation time, due to the complexity in mathematics.

Due to the interaction between electrical and mechanical behaviour, inter-turn faults and some unbalanced electrical faults of induction motors can be reflected by vibration phenomenon [46, 47]. Based on the measurement of such signals, vibration signature analysis (VSA) analyses and identifies possible faults of inductor motors. The main drawbacks of this approach are that.it demands a number of measurement sensors, which is costly, and is sensitive to environment noises.

It has been shown that the use of axial flux (AX) is able to reveal magnetic circuit imbalances [48-50]. Based on this, different methods have been proposed for AX analysis, in order to diagnose motor faults. Theoretically, a perfectly balanced machine should have an axial flux of zero. However, small asymmetries always exist in practice, due to physical discrepancies of stator windings; for example, this fact implies that any motor will have a small but non-negligible axial leakage flux, and so this approach demands special care to obtain reliable data.

Apart from aforementioned methods, many other approaches have been reported in literature for the fault detection of the induction motor, e.g., thermal monitoring, gas in oil analysis [11, 15, 29]. However, since this research work focuses on the diagnosis of short-circuit faults of the PMSM, they are beyond the scope of this study and will not be discussed here.

3.2.2 Fault Detection Technique for PMSMs

Generally, faults in PMSMs can be divided into three categories, which are electrical, magnetic and mechanical faults, respectively [15, 51]. For electrical faults, it mainly includes abnormal connection of the stator windings, stator open turns and short-circuit turns etc [41]. Magnetic faults consist of partial or total demagnetization of the rotor magnets. Mechanical faults cover bearing and eccentricity faults, (while the latter one further involves static eccentricity, dynamic eccentricity and mixed eccentricity [51]). The eccentricity faults are mainly caused by the manufacturing imperfections and imprecision, and can lead to magnetic and dynamic problems of the PMSM [51]. Since this research work is dedicated to the inter-turn short-circuit failures, some principal fault detection techniques are introduced as follows.

Based on the sequence components of the stator current, Reference [52] has demonstrated an approach to the detection of open-circuit faults in multi-phase PMSM drives. By using the second-order generalized integrator (SOGI) for the generation of the quadrature signal, the fundamental negative sequence current can be evaluated. The Cumulative Sum (CUSUM) algorithm was adopted to define the decision criterion.

In [53], the author proposed a simplified on-line short-circuit fault detection scheme for interior permanent magnets synchronous machines (IPMSM), by looking at a change in positive sequence component supplied by a current-controlled voltage source inverter (CCVSI). According to the difference between the DQ axis voltage reference in the look-up table and the actual voltage references output from the current controller, the fault can be indicated without using any voltage sensor.

Wavelet transformation has been employed in [21] to diagnose the inter-turn short-circuit faults of PMSMs. The harmonic components of the stator current are analysed and transformed into the DQ axis, and the wavelet approach is applied to extend the analysis to transitory failures.

In this research work, a novel fault detection scheme is presented to assess the inter-turn short-circuit fault of the PMSMs. The proposed technique is based on

the negative sequence components of stator currents and impedances, which will be discussed in the following sections.

3.3 Symmetrical Components

The method of symmetrical components was first proposed by C. L. Fortescue [54] in 1918. It states that any unbalanced n-phase quantities, i.e. either voltage, current or impedance, can be represented by n symmetrical sets of balanced phasors. For example, considering an unbalanced three-phase system shown in Figure 3.1, each of the three phasors is displaced 120 degrees from the others in a clockwise rotation sequence.

According to Fortescue's methodology, for this given system, there are three sets of independent components: positive, negative and zero sequence quantities. The positive sequence quantities have the same phase sequence as the three-phase system. The negative sequence quantities are displaced 120 degrees from the others, but in a counter-clockwise rotation sequence (i.e. A-C-B). The zero sequence quantities are equal in magnitude in phase with each other but have no rotation sequence [54].

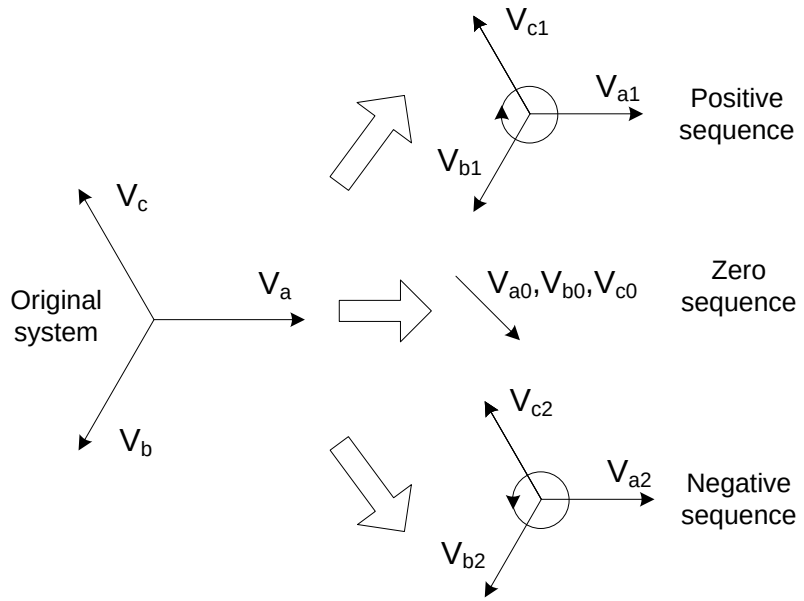

Figure 3.1 Symmetrical components of unbalanced three-phase system.

The symmetrical components can be used as an effective tool to determine any unbalanced variables (e.g. current or voltage) as in (3.1),

$$\begin{aligned} I_a &= I^+ + I^- + I^0 & V_a &= V^+ + V^- + V^0 \\ I_b &= \alpha^2 I^+ + \alpha I^- + I^0 & V_b &= \alpha^2 V^+ + \alpha V^- + V^0 \\ I_c &= \alpha I^+ + \alpha^2 I^- + I^0 & V_c &= \alpha V^+ + \alpha^2 V^- + V^0 \end{aligned} \tag{3.1}$$

$$\alpha = e^{j2\pi/3}$$

where V_a, V_b and V_c represent the three-phase unbalanced line to neutral voltages; I_a, I_b and I_c are the phase current of the three windings; V^+, V^- and V^0 are the positive, negative and zero sequence components of the voltage; I^+, I^- and I^0 are the positive, negative and zero sequence components of the current; the α operator shifts a vector by an angle of 120 degrees anti-clockwise, and the α^2 operator performs a 240 degrees counter-clockwise phase shift.

By using (3.1), the symmetrical components of the current and voltage for the unbalanced three-phase system can be calculated as below,

$$\begin{aligned} I^+ &= \frac{1}{3}(I_a + \alpha I_b + \alpha^2 I_c) & V^+ &= \frac{1}{3}(V_a + \alpha V_b + \alpha^2 V_c) \\ I^- &= \frac{1}{3}(I_a + \alpha^2 I_b + \alpha I_c) & V^- &= \frac{1}{3}(V_a + \alpha^2 V_b + \alpha V_c) \\ I^0 &= \frac{1}{3}(I_a + I_b + I_c) & V^0 &= \frac{1}{3}(V_a + V_b + V_c) \end{aligned} \tag{3.2}$$

$$1 + \alpha + \alpha^2 = 0$$

Then, the symmetrical component set can be written as in (3.3), where the variable x can be either current or voltage.

$$\begin{bmatrix} x^+ \\ x^- \\ x^0 \end{bmatrix} = \frac{1}{3}\begin{bmatrix} 1 & \alpha & \alpha^2 \\ 1 & \alpha^2 & \alpha \\ 1 & 1 & 1 \end{bmatrix}\begin{bmatrix} x_a \\ x_b \\ x_c \end{bmatrix} \tag{3.3}$$

Following this, the negative sequence impedance can be defined and calculated, as shown in [46, 55] (3.4),

$$Z^- = \frac{V^-}{I^-} \tag{3.4}$$

In the following sections, the concept of symmetrical components will be utilised to diagnose the inter-turn short-circuit faults of the PMSM.

3.4 Three-phase Sequence Analyser

3.4.1 General Structure

In this section, the three-phase sequence analyser provided by MatLab-Simulink is utilised to calculate the negative sequence components. For a specified frequency, this block first applies a Fourier analysis over a sliding window of one cycle of the three input signals. Then, it evaluates the phasors values and derives the positive sequence, negative sequence, and zero sequence.

Figure 3.2 shows the block diagram of a three-phase sequence analyser for negative sequence components calculation. It should be pointed out that, due to the use of the sliding window for the Fourier transformation, one cycle of simulation has to be completed before the outputs give the correct magnitude and angle. Consequently, the evaluation of the symmetrical components is always delayed by one cycle of the fundamental frequency. The calculation procedure of the sequence components can be found in (3.3).

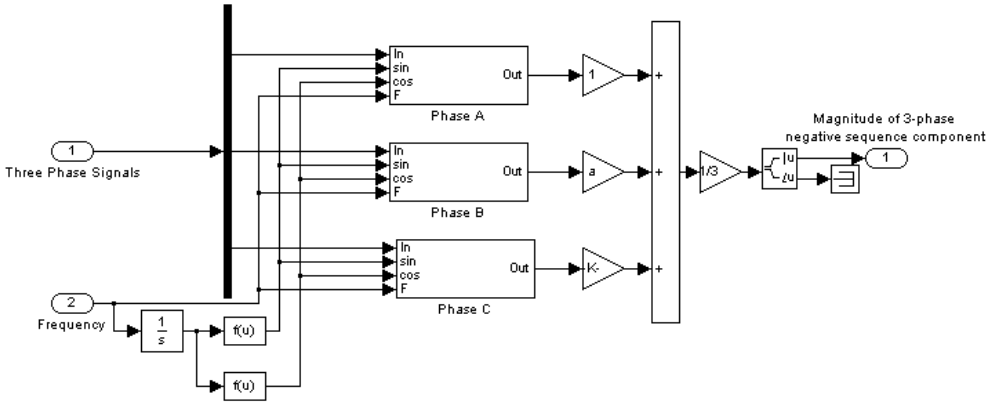

Figure 3.2 Block diagram of three-phase sequence analyser for negative sequence components calculation.

3.4.2 Simulation Results

Figure 3.3 shows the waveform of the three-phase current when the amplitude changes. The three-phase current amplitude decreases from 2A to 1A at time=1sec, while the fundamental frequency remains at 5Hz.

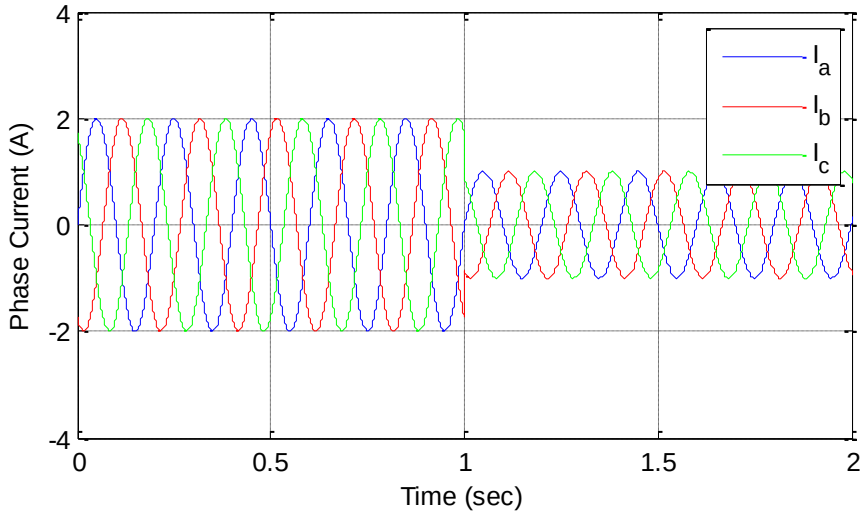

Figure 3.3 Three-phase current response under balanced system.

Figure 3.4 shows the corresponding symmetrical components response, where the blue and red curves represent the positive sequence current and negative sequence currents, respectively.

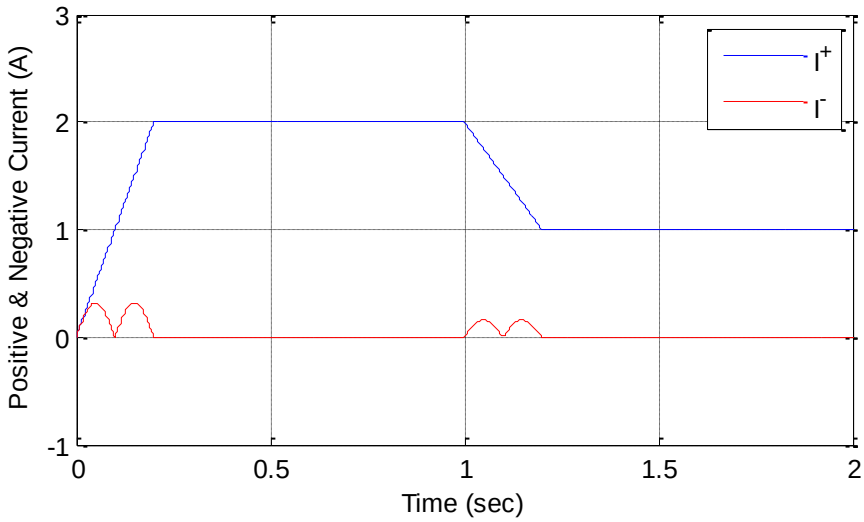

Figure 3.4 Symmetrical components response under balanced system.

Since the system is balanced, the positive sequence current represents the amplitude of the three-phase current, while the negative one is zero in steady

state. As it can be seen, due to the sliding window employed for the Fourier analysis, it always takes 0.2s (i.e. one cycle= $1/f$, f is the fundamental frequency 5Hz) for the positive sequence current to reach the steady state and give an accurate result. Another observation is, during the transient (i.e. from 0 to 0.2s, from 1s to 1.2s), the negative sequence current is not zero.

Figure 3.5 shows the current waveform of the unbalanced system. At the time point of 1s, the amplitude of the current is reduced to 1A and the system becomes unbalanced. The current of phase B has relatively lower amplitude than other two phases.

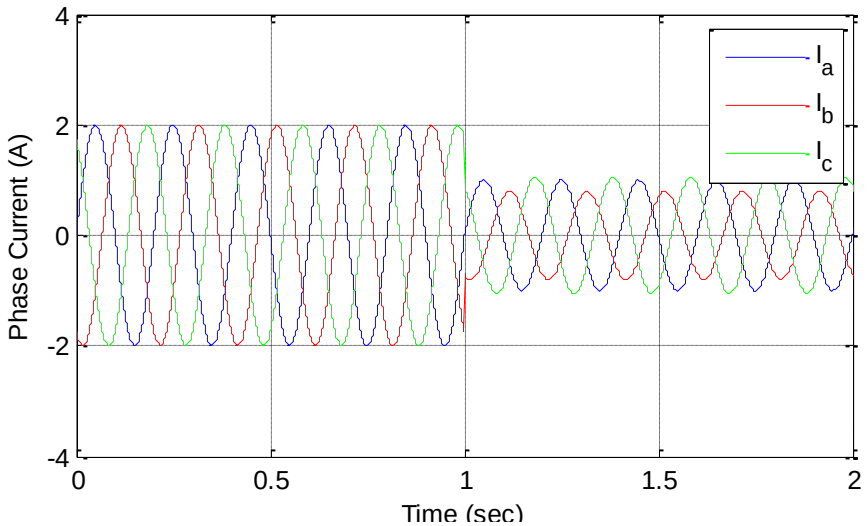

Figure 3.5 Three-phase current response under unbalanced system.

Figure 3.6 shows the corresponding symmetrical components response, where the blue and red curves represent the positive sequence current and negative sequence currents, respectively.

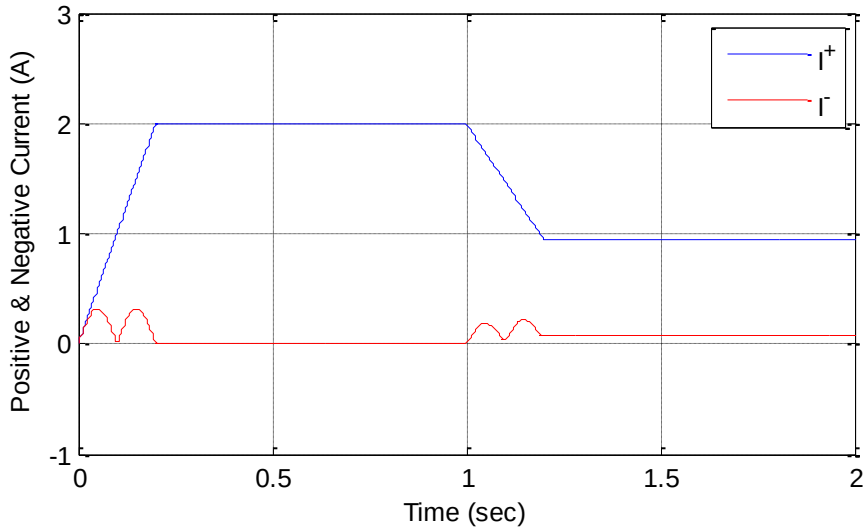

Figure 3.6 Symmetrical components response under unbalanced system.

It can be seen that, the early values (before 1s) are the same as in Figure 3.4, while the latter part is significantly different. Due to the unbalance, the positive sequence current is reduced to 0.95 (lower than 1 in previous case), and the negative sequence current in steady state is 0.05 (not 0 anymore). The significant difference in the negative sequence current can be utilised to detect the unbalanced three-phase current, and thus diagnose possible inter-turn short-circuit faults.

3.5 Negative Sequence Calculation based on SOGI

3.5.1 General Structure

The second order generalised integrator (SOGI) was originally proposed by M. Ciobotaru for a single-phase phase locked loop (PLL) structure [56]. Due to its simple implementation and effectiveness in orthogonal system generation, it is also considered in this work to perform the negative sequence component calculation.

Figure 3.7 shows the block diagram of the SOGI based negative sequence calculation system. It mainly consists of three stages: firstly, the αβ transformation is used to transform the three-phase quantities (i.e. voltages and currents) into αβ frame; then, the resultant αβ components are filtered and

quadrature signals are produced; the output of two SOGIs enables the calculation of the negative components.

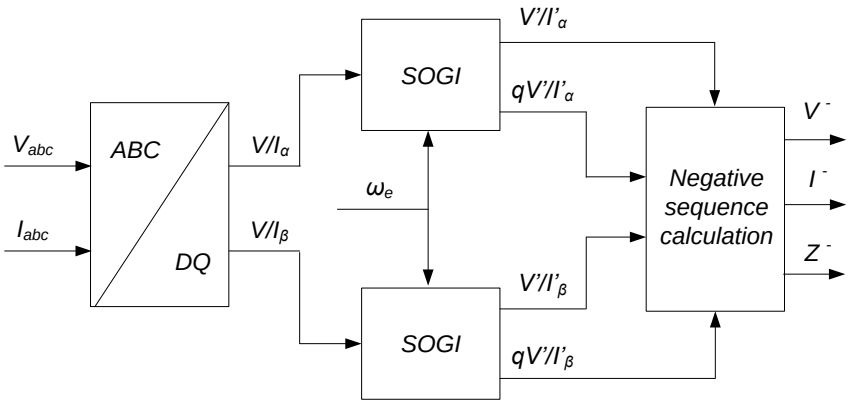

Figure 3.7 Block diagram of the proposed negative sequence calculation system.

3.5.2 Equation Derivation

According to Lyon's method, the symmetrical components can be applied in the time domain by using the Lyon transformation[54, 57]. Take voltage for example, equation (3.5) represents the instantaneous negative sequence components V_{abc}^{-} of an unbalanced sinusoidal voltage vector $V_{abc}=[v_a\ v_b\ v_c]^T$ [58].

$$V_{abc}^{-}=\begin{bmatrix} v_a^{-} & v_b^{-} & v_c^{-} \end{bmatrix}^T=[T_{-}]V_{abc}$$
$$[T_{-}]=\frac{1}{3}\begin{bmatrix} 1 & \alpha^2 & \alpha \\ \alpha & 1 & \alpha^2 \\ \alpha^2 & \alpha & 1 \end{bmatrix},\ \alpha=e^{j\frac{2\pi}{3}} \tag{3.5}$$

With the Clarke transformation [59], the voltage vector V_{abc} can be transferred from the *abc* to *αβ* reference frames as in (3.6).

$$V_{\alpha\beta}=\begin{bmatrix} v_\alpha & v_\beta \end{bmatrix}^T=[T_{\alpha\beta}]V_{abc} \tag{3.6}$$
$$[T_{\alpha\beta}]=\frac{2}{3}\begin{bmatrix} 1 & -\frac{1}{2} & -\frac{1}{2} \\ 0 & \frac{\sqrt{3}}{2} & -\frac{\sqrt{3}}{2} \end{bmatrix}$$

Then, the instantaneous negative sequence voltage on the $\alpha\beta$ reference frame can be found,

$$\begin{aligned} V_{\alpha\beta}^{-} &= \left[T_{\alpha\beta}\right]\mathrm{v}_{abc}^{-} = \left[T_{\alpha\beta}\right]\left[T^{-}\right]V_{abc} \\ &= \left[T_{\alpha\beta}\right]\left[T^{-}\right]\left[T_{\alpha\beta}\right]^{-1}V_{\alpha\beta} \\ &= \frac{1}{2}\begin{bmatrix} 1 & q \\ -q & 1 \end{bmatrix}V_{\alpha\beta} \end{aligned} \tag{3.7}$$

where $q=e^{-j\frac{\pi}{2}}$ is an operator corresponding to a 90 degree phase shift of the original signal.

Following (3.7), the expression for calculating the negative sequence components of a generic variable x can be written as in (3.8), where the variable x can be either current or voltage.

$$\left[X_{\alpha\beta}^{-}\right] = \frac{1}{2}\begin{bmatrix} 1 & q \\ -q & 1 \end{bmatrix}\left[X_{\alpha\beta}\right] \tag{3.8}$$

3.5.3 Principle of SOGI

The generation of the orthogonal signals of the $\alpha\beta$ components is achieved by two SOGIs. Figure 3.8 presents the general structure of a SOGI, which is defined as [60, 61]. Variable ω_f is the resonant frequency of the SOGI, which is usually set to be the synchronous frequency ω_e of a three-phase sinusoidal system.

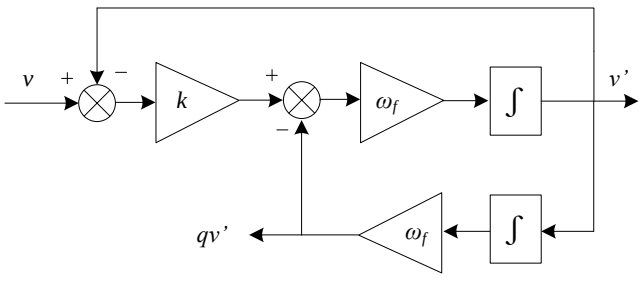

Figure 3.8 General structure of SOGI.

The closed loop transfer functions are defined as in (3.9) and (3.10), where *v'(s)* is the filter output; *s* is the Laplace operator; *k* and ω_f set the damping factor and the resonant frequency of the system.

$$D(s)=\frac{v'}{v}(s)=\frac{k\omega_f s}{s^2+k\omega_f s+\omega_f{}^2} \tag{3.9}$$

$$Q(s)=\frac{qv'}{v}(s)=\frac{k\omega_f{}^2}{s^2+k\omega_f s+\omega_f{}^2} \tag{3.10}$$

The corresponding Bode plot of the SOGI system is shown in Figure 3.9

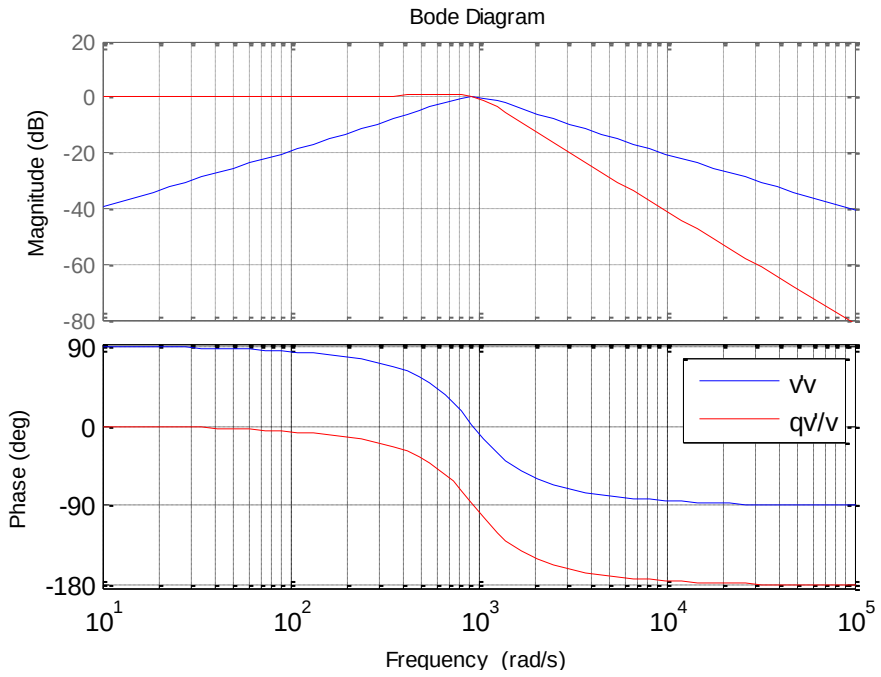

Figure 3.9 Bode plots of the SOGI system.

If the input signal *v(s)* is sinusoidal and the frequency is $\omega_f{}'$, it can be expressed as a phasor **v** [62]. The SOGI system can produce two output signals: the direct filter output signal, *v'(s)*, will be in phase with the input signals for fundamental frequency components, the in-quadrature output signal, *qv'(s)*, is always 90 degree shifted with respect to *v'(s)* (refer to Figure 3.9). The expressions of the two signals can be calculated from (3.11) and (3.12).

$$v' = Dv \begin{cases} |D| = \dfrac{k\omega_f \omega_f'}{\sqrt{\left(k\omega_f \omega_f'\right)^2 + \left(\omega_f^2 - \omega_f'^2\right)^2}} \\ \underline{|D} = tan^{-1}\left(\dfrac{\omega_f'^2 - \omega_f^2}{k\omega_f \omega_f'}\right) \end{cases} \tag{3.11}$$

$$qv' = Qv \begin{cases} |Q| = \dfrac{\omega_f'}{\omega_f}|D| \\ \underline{|Q} = \underline{|D} - \dfrac{\pi}{2} \end{cases} \tag{3.12}$$

The output of α and β components SOGI, v'_α and v'_β are used in (3.8) to calculate the negative sequence components. Based on that, the negative sequence components can be derived by using (3.13) and (3.14).

$$\left|X^-\right|' = \sqrt{\left(X_\alpha^-\right)^2 + \left(X_\beta^-\right)^2} \tag{3.13}$$

$$\left|Z^-\right| = \frac{\sqrt{\left(V_\alpha^-\right)^2 + \left(V_\beta^-\right)^2}}{\sqrt{\left(I_\alpha^-\right)^2 + \left(I_\beta^-\right)^2}} \tag{3.14}$$

3.5.4 Simulation Results

Figure 3.10 shows the waveform of the three-phase current when the amplitude changes. The three-phase current amplitude increases from 3.2A to 3.85A at time=0.15sec, while the fundamental frequency remains at 100Hz.

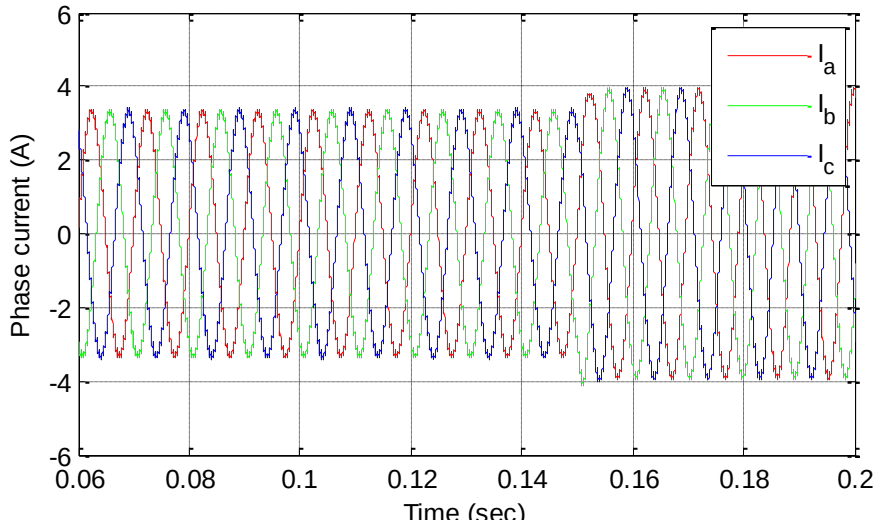

Figure 3.10 Three-phase current response under balanced system.

Figure 3.11 compares the corresponding positive sequence components obtained by the two calculation systems, where the blue curve represents the output from the SOGI system, and the green one is from the three-phase sequence analyser.

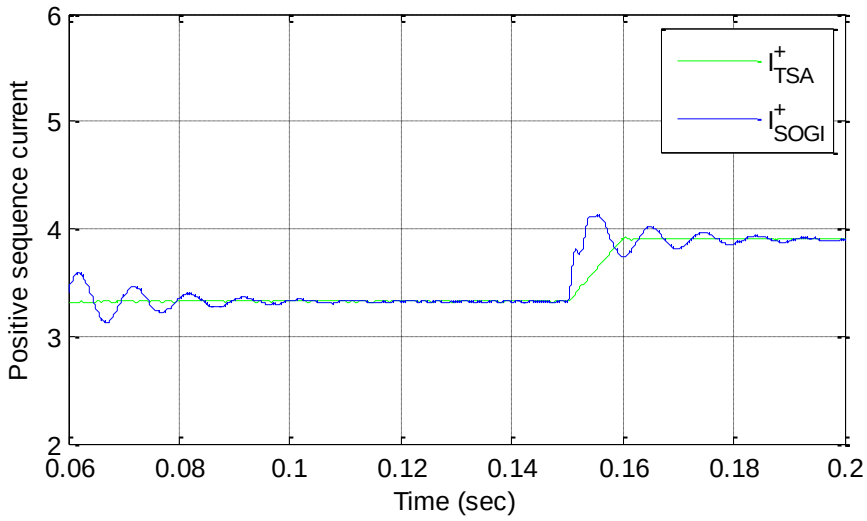

Figure 3.11 Comparison of positive sequence components.

Clearly, when the three-phase sequence analyser is employed, it always takes one fundamental period (i.e. 0.01s) to reach the steady state, due to the use of the Fourier analysis. Compared with this, the SOGI system can respond to the amplitude change instantaneously and does not exhibit any delay. However, the output positive sequence component oscillates seriously, and thus takes much more time to reach the steady state. In the following study, the three-phase sequence analyser will be employed to obtain negative sequence components for fault detection purpose.

3.6 PMSM under Asymmetrical Components

For a three-phase PMSM, several effects can cause asymmetries in the three-phase quantities, such as inherent motor defects, inter-turn short-circuit, unbalanced phase windings, and load or speed fluctuations, etc. The negative sequence component can be used to detect these asymmetries. As discussed in [63], a considerable increase in the negative sequence current takes place under the inter-turns short-circuit fault of the PMSM. However, unbalanced phase

windings (i.e. back-emf unbalanced) can produce a similar asymmetry. In order to produce an accurate and robust fault detection system, some modifications to this approach are needed.

In this section, the negative sequence analysis based approach is applied to diagnose inter-turn short-circuit faults of the PMSM. Based on the measurement of the voltage and current variables, the negative sequence components of the system are calculated by using the three-phase sequence analyser. Meanwhile, the PMSM drive is tested with either speed or load fluctuations, in order to obtain the behaviour of the negative components, under such conditions.

3.6.1 Speed Fluctuation

In this sub-section, the PMSM motor is set to supply a constant load of 0.6Nm, with 2% asymmetrical components of back-emf in the phase A. The speed reference ramps up and down between 800 rpm and 1000rpm, as Figure 3.12 shows, in order to give a complete performance test under speed fluctuation. A short-circuit fault of 2 turns is injected into phase A time = 0.5s.

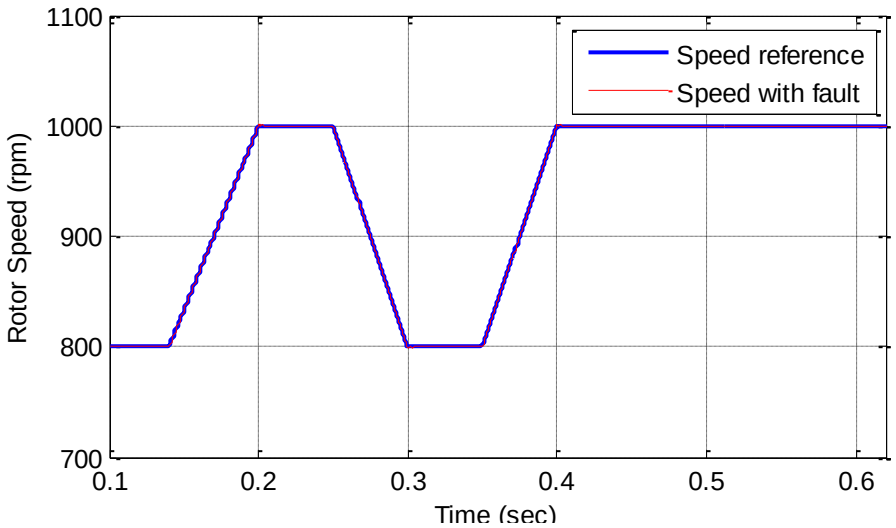

Figure 3.12 PMSM speed response under speed fluctuation test.

Figure 3.13 presents the corresponding negative sequence current under this testing condition. As can be noticed, although the inter-turn short-circuit fault can be revealed immediately after its occurrence, six false alarms are also

generated at 0.14s, 0.2s, 0.25, 0.3, 0.35 and 0.4, whose values are almost higher than that of the real fault conditions.

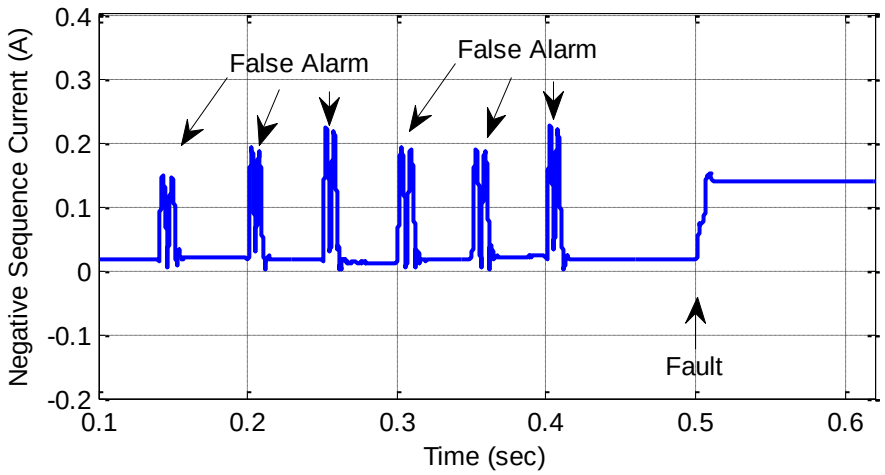

Figure 3.13 Negative sequence current under speed fluctuation and fault conditions.

Obviously, these six false alarms are caused by the speed fluctuation. When a speed change occurs, it brings a non-stationary symmetry condition which generates a considerable increment on the magnitude of the negative sequence current. As a result, a false alarm may arise in the detection system.

Figure 3.14 shows the corresponding negative sequence impedance under this testing condition. Similarly, the negative sequence impedance fluctuates signicantly during the speed change of the PMSM.

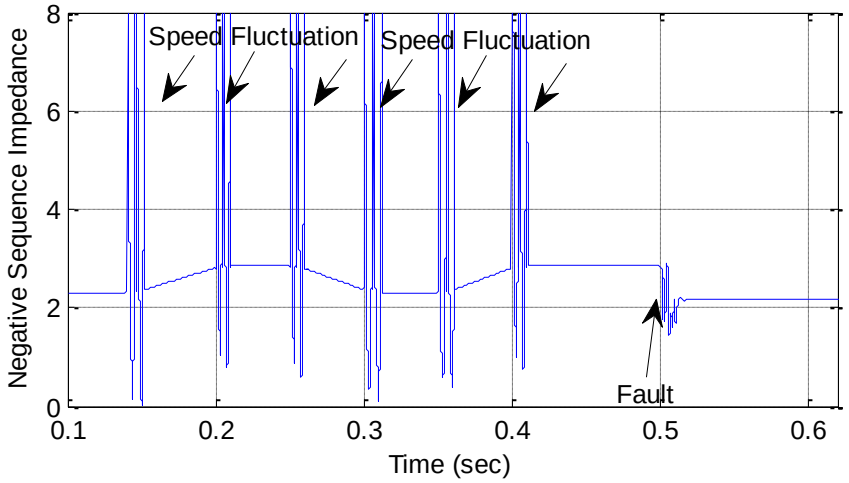

Figure 3.14 Negative sequence impedance under speed fluctuation and fault conditions.

Obviously, using this information only will lead to a false alarm, so some filtering algorithm is required to remove the false alarms.

Figure 3.15 shows the waveform of the negative sequence current, when a moving average filter is utilised for signal processing.

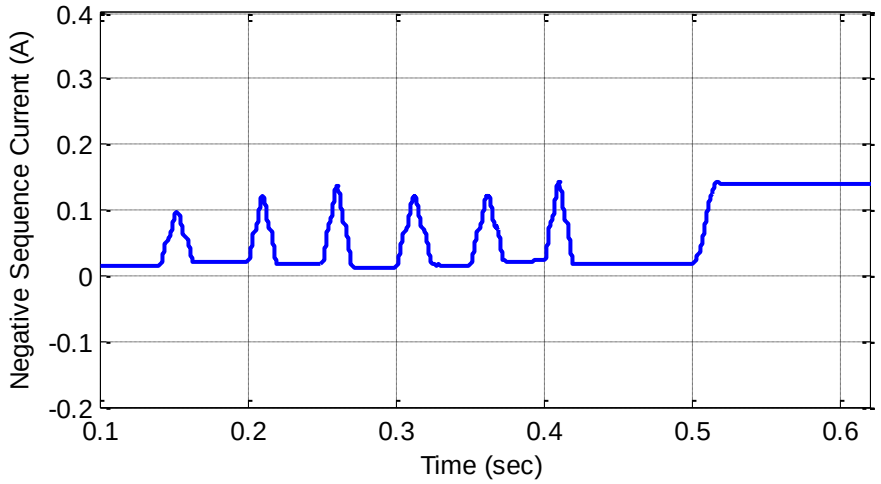

Figure 3.15 Negative sequence current with moving average filter under speed fluctuation and fault condition.

In this case, the moving average filter has averaged the high frequency component produced by the speed change over half cycle, as shown in Figure 3.16. The negative sequence current still experiences a high value either under speed fluctuation or the inter-turn short-circuit fault, though the waveform becomes much smoother, and the time constant of false alarm= $2\times\pi/\omega$, ω is the electrical angular speed (refer to section 3.4.2).

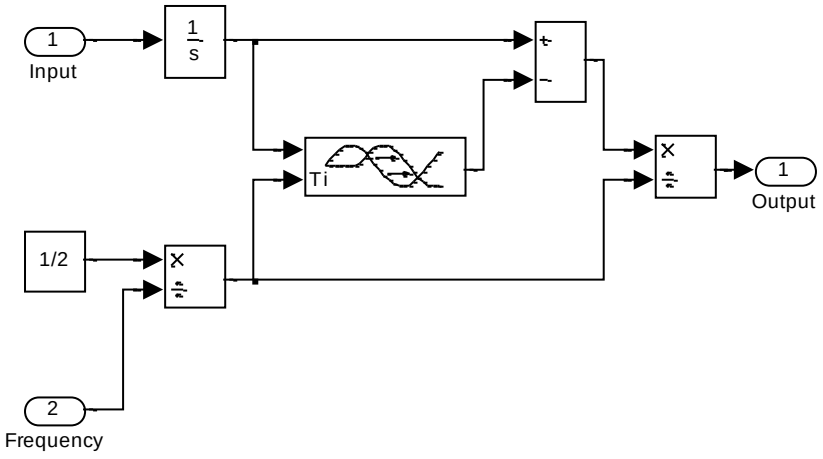

Figure 3.16 Block diagram of moving average filter.

Figure 3.17 gives the corresponding waveform of the negative sequence impedance, when the moving average filter is employed. As it can be noticed, the negative sequence impedance experiences a considerable increase when the speed changes. In contrast, it drops significantly (i.e. from 2.2 to 1.7) as the inter-turn short-circuit takes place.

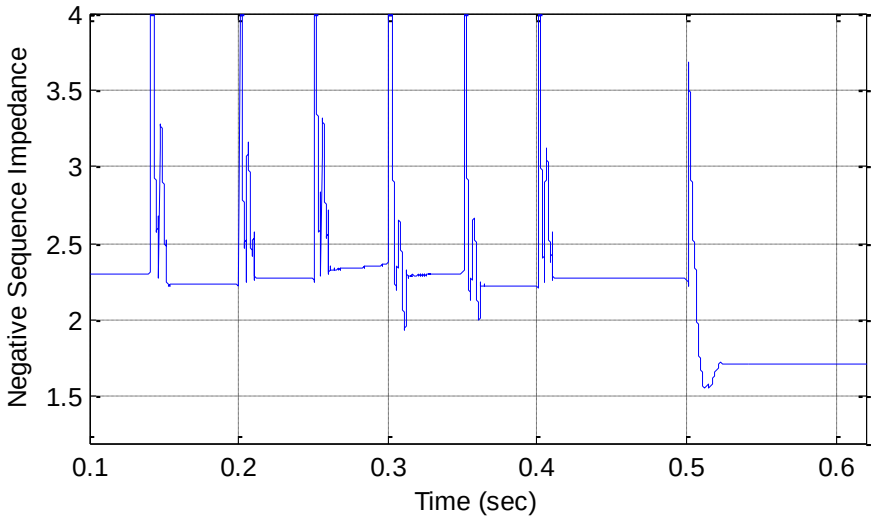

Figure 3.17 Negative sequence impedance with moving average filter under speed fluctuation and fault condition.

3.6.2 Load fluctuation

In this sub-section, the speed reference of the PMSM motor is fixed at 1000rpm with 2% asymmetrical components set in the back-emf of Phase A. A step change in load is considered to examine its possible influence on the negative sequence components.

As shown in Figure 3.18, the load torque steps up and down between 0.4Nm and 0.6Nm, in order to give a complete performance test under load fluctuation. A short-circuit fault of 2 turns is introduced into phase A at 0.5s. The blue and red curves represent the electromagnetic torque and load torque, respectively.

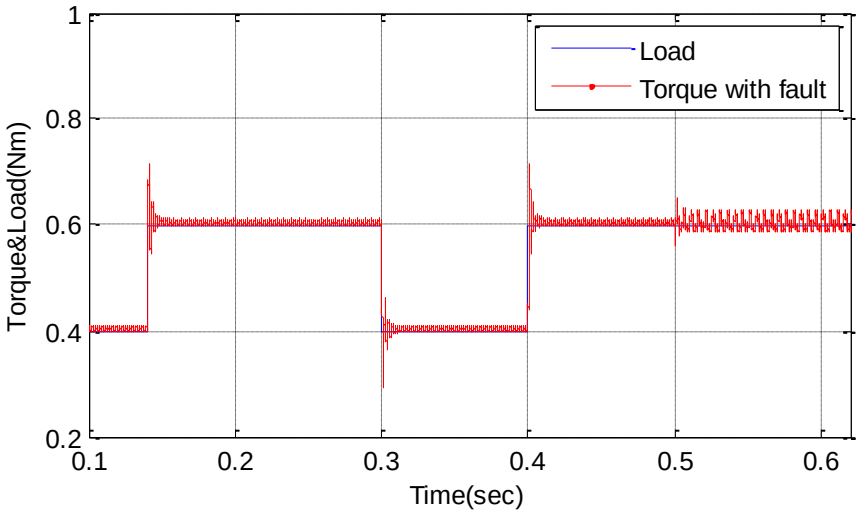

Figure 3.18 PMSM torque response under torque fluctuation test.

Figure 3.19 gives the waveform of the negative sequence current under this testing condition. It can be noted that, the value of the negative sequence current is not equal to zero when the load is constant due to imbalance in the phase back-emf. When the step change is applied at 0.14s, 0.3s and 0.4s the values of the negative sequence current increase significantly, but the duration of the false alarm time is around 0.01s (i.e. one cycle). Once the torque settles down, it decreases back to the original value. When the inter-turn short-circuit fault occurs, the negative sequence current can reflect it immediately by an increase in the amplitude from 0.01A to 0.13A.

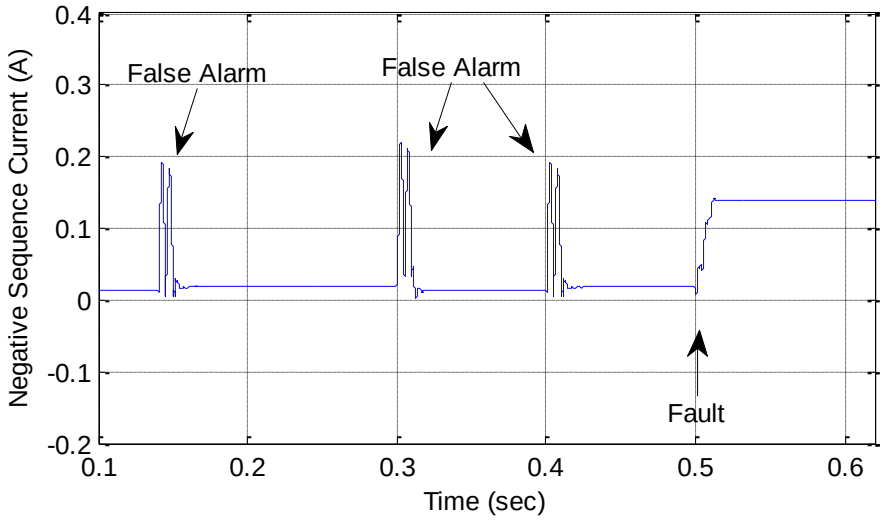

Figure 3.19 Negative-sequence current under load fluctuation and fault conditions.

Figure 3.20 shows the waveform of the negative sequence impedance under this test. Similarly, the negative sequence impedance is affected by both the load fluctuation and the short-circuit fault.

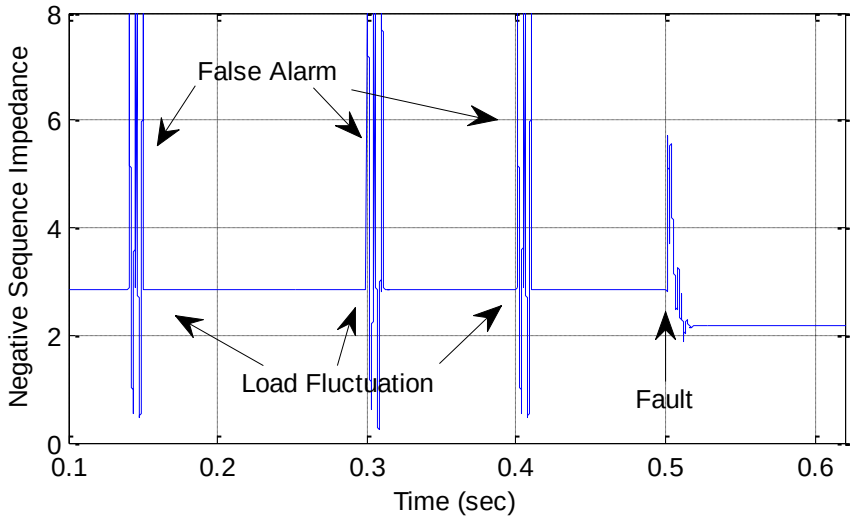

Figure 3.20 Negative sequence impedance under load fluctuation and fault conditions.

With the aim of smoothing the diagnosis signals, the moving average filter is also employed for this testing. Figure 3.21 and Figure 3.22 show the waveforms of the negative sequence current and impedance, when the moving average filter is implemented.

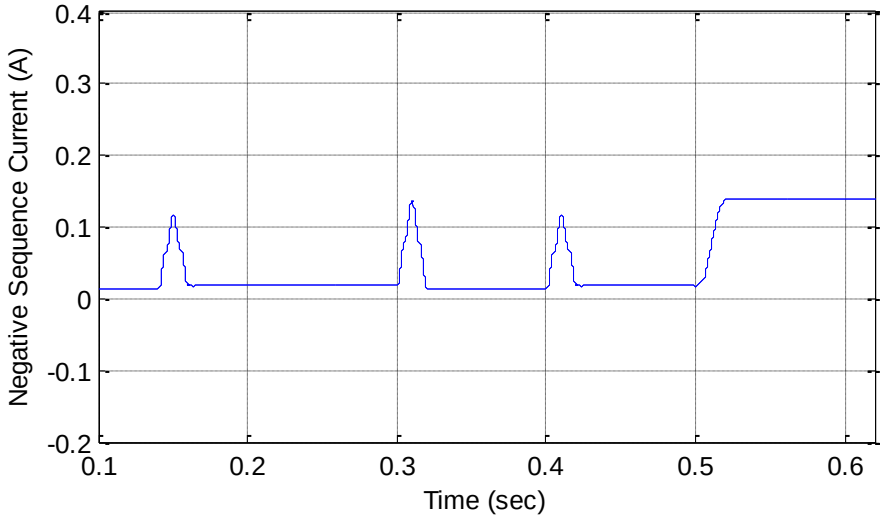

Figure 3.21 Negative sequence current with moving average filter under load fluctuation and fault condition.

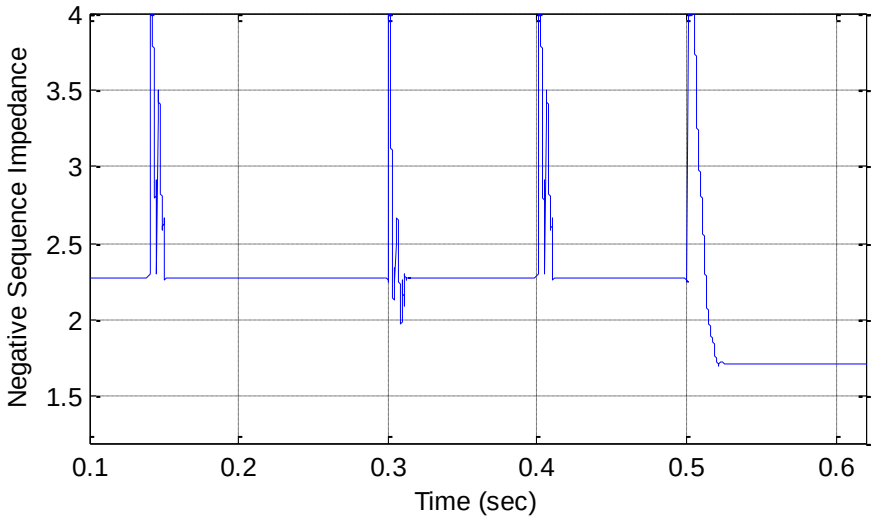

Figure 3.22 Negative sequence impedance with moving average filter under load fluctuations and fault condition.

3.6.3 Discussion

Obviously, the use of the moving average filter does help to smooth the two diagnosis signals, but the false alarm caused by the load fluctuation cannot be eliminated, which makes it very difficult to diagnose the short-circuit faults by using the information from one signal (i.e. either current or impedance).

The behaviour observed from the negative sequence current and impedance is summarised in Table 3.1. It can be seen that, during the fluctuations, both the negative sequence current and impedance increase to a higher level. Under fault condition, the negative sequence current starts to increase, while the negative sequence impedance is decreasing. It should be pointed out that the decrease of the negative sequence impedance depends on the severity of the fault, and it may not reduce significantly for imbalance PMSM systems. With the aim of improving the accuracy of fault detection, a combination of the negative sequence current and impedance is adopted in this work, which will be discussed in Chapter 4.

Table 3.1 Relationship between the sequence components under load change, speed change and fault condition.

Sequence Component	Load change	Speed change	Fault condition
Negative sequence current	↑	↑	↑
Negative sequence impedance	↑	↑	~↓

3.7 Summary

In this chapter, the traditional fault detection techniques used for both induction motors and PMSMs are reviewed and studied. Following that, the concept of symmetrical components is introduced, and two kinds of methods are discussed to perform the calculation of the negative sequence components of the three-phase PMSM. Finally, the simulation results have been provided to reveal the influence of load and speed fluctuations on the negative sequence components. By using both the information of the negative sequence current and impedance, the inter-turn short-circuit faults can be distinguished effectively.

CHAPTER 4

FAULT DETECTION TECHNIQUE 2: FUZZY LOGIC APPROACH

4.1 Introduction

Previous research work has demonstrated clearly that, the inter-turn short-circuit faults can be reflected by using the negative sequence current or impedance in the system steady state. However, as shown in the simulation results, the false alarm caused by load or speed fluctuation cannot be eliminated, which makes it very difficult to diagnose the short-circuit faults by using the information from one signal only (i.e. either current or impedance). For this reason, a novel fuzzy logic based approach is considered in this work for the fault detection of the PMSMs, in order to utilise the information of both the negative sequence current and impedance to draw a clear and accurate detection result.

In this chapter, the concept of conventional classical sets is first reviewed as the basis of fuzzy logic. Following that, the principle, membership function and rule based inference of fuzzy logic are presented and discussed. Based on the information of the negative sequence components analysed in the previous chapter, a fuzzy logic based fault detection scheme is developed, in order to reduce the influence of speed and load changes on the detector output. The end of the chapter provides simulation results using the MATLAB/Simulink environment.

4.2 Fuzzy Logic Foundation

4.2.1 Classical Sets

For classical set theory, a universe set is defined as a collection of elements that have the same characteristics, and each qualified element is called the member of the set [64]. Some classical sets may be contained inside the universe set. Generally, the sets are denoted by capital letters, and the elements are represented by lower case letters.

Figure 4.1 shows an example to support the understanding of the above definitions. Considering a universe set of U, the solid circle is its boundary and the points inside it are its elements. A classical set of V with square-shape boundary is contained by the universe set U. Several points, a, b, c, x, y and z, are distributed inside the set U, but some are out of the classical set V.

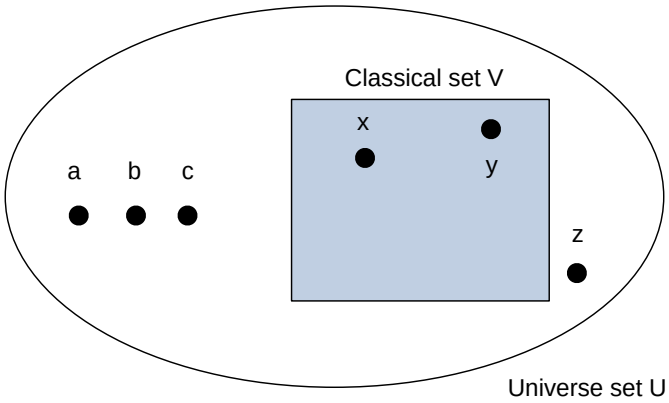

Figure 4.1 Example of classical set theory.

If the element *a* belongs to the set U, the relationship can be represented as $a \in U$. Similarly, the symbol $\notin$ indicates one element does not belong to a set, for example $b \in V$. Table 4.1 summarises the notation and definition for the example given in Figure 4.1.

Table 4.1 Notations and definitions of the set example shown in Figure 4.1.

Notation	Definition
$a,b,c,x,y,z \in U$	a,b,c,x,y,z belong to the universe set U
$x,y \in V$	x,y belong to the classical set V
$a,b,c,z \notin V$	a,b,c,z do not belong to the classical set V

Using a characteristic function to distinguish between elements contained and not contained in a set is known as mapping the universe set into the determined set.

$$\mu_U(a) = \begin{cases} 1 & if \quad a \in U \\ 0 & if \quad a \notin U \end{cases} \tag{4.1}$$

4.2.1.1 Classical Sets Operations

In order to explain the operations of classical sets, Figure 4.2 shows two sets as an example: V and W, which exist in the Universal set U.

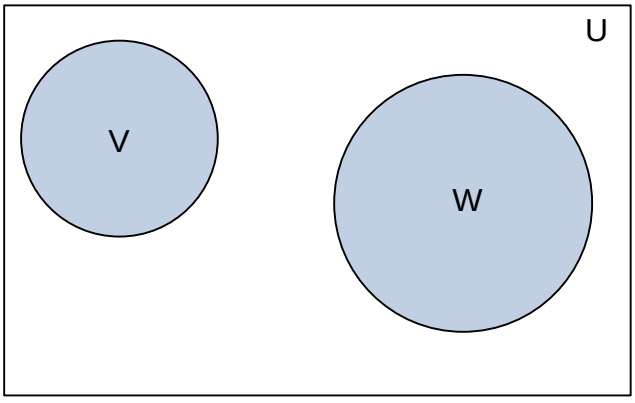

Figure 4.2 Set V and W in the universe set U.

Figure 4.3 shows the union between the set V and set W, often denoted in classical set theory as V∪W. The union of two sets includes all elements existing in either set V, W or both.

$$V \cup W = \{x | x \in V \text{ or } x \in W\} \tag{4.2}$$

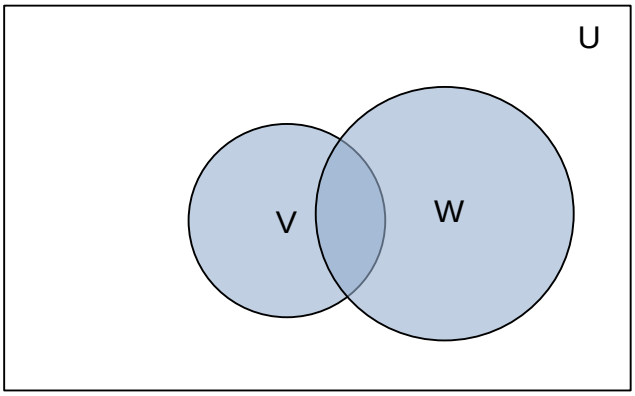

Figure 4.3 Union of set V and set W in the universe set U.

Figure 4.4 shown below portrays the intersection of the two set V and W, which represents that all the elements in the universe set U that belong to both set V and set W.

$$V \cap W = \{x | x \in V \text{ and } x \in W\} \tag{4.3}$$

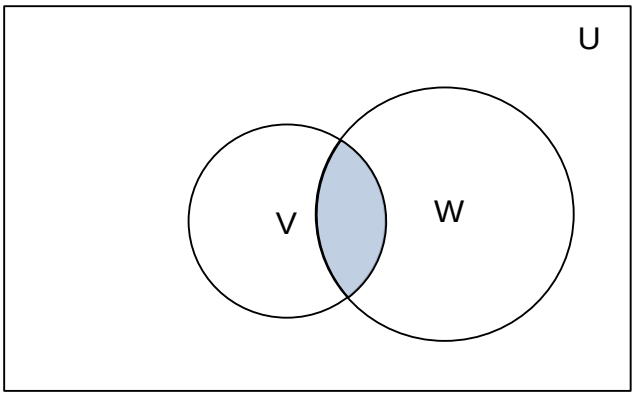

Figure 4.4 Intersection of set V and set W in the universe set U.

Figure 4.5 depicts the difference of the two sets V and W, which represents the element in set V that only belongs to set V. It can be denoted as V|W.

$$V|W = \{x | x \in V \text{ and } x \notin W\} \tag{4.4}$$

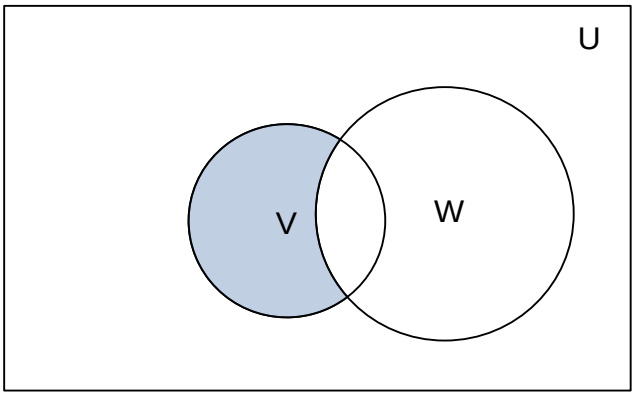

Figure 4.5 Difference of set V and set W in the universe set U.

The complement of a set is defined as the element in the universe set that does not belong to the set. Figure 4.6 shows the complement of set V in the universe set U.

$$\overline{V} = \{x | x \notin V \quad x \in U\} \tag{4.5}$$

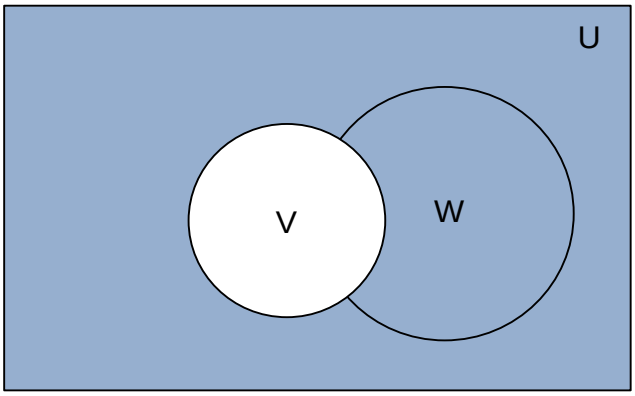

Figure 4.6 Complement of set V in the universe set U.

4.2.2 Fuzzy Sets

Fuzzy logic, also known as fuzzy set theory, was first introduced by L. Zadeh in 1965 [65], a concept which is founded on classical or crisp set theory. In the classical set theory, each elements of the universe set is issued a value of 0 or 1 to represent FALSE or TRUE by the characteristic function [66]. In comparison to a classical set, the boundary of a fuzzy set is not defined. The fuzzy set is formed in a way that contains elements which have varying degree of membership. In other words, the characteristic function can take a value in the interval ranging between 0 and 1.

The membership μ_V of an element x for a fuzzy set V is denoted by,

$$\mu_V : X \rightarrow [0, 1] \tag{4.6}$$

$$V = \{(x, \mu_V(x)) | x \in V, \ \mu_V(x) \in [0,1]\} \tag{4.7}$$

where $\mu_V(x)$ is the degree of membership of element x in the fuzzy set V. Fuzzy sets can be categorised as either continuous or discrete. In the discrete fuzzy set V, a member x, which has a relative membership μ can be represented as μ/x [64]. The set V can be written as follows, where $x_1, x_2 \cdots x_n$, are members of the discrete set V and μ_1; $\mu_2 \cdots \mu_n$; are the degrees of membership.

$$\begin{aligned} &V = \mu_1/x_1 + \mu_2/x_2 + \ldots \ \ldots \ \ldots + \mu_n/x_n \\ &or \\ &V = \sum_{i=1,n} \mu_i/x_i \end{aligned} \tag{4.8}$$

A continuous fuzzy set can be denoted as,

$$V = \int_X \frac{\mu(x)}{x} \tag{4.9}$$

Figure 4.7 shows a fuzzy set of negative sequence impedances, which defines all the values of the negative sequence impendence magnitudes at low, middle or high. Obviously, the concepts of the low, middle and high values of the negative sequence impedances are determined by the data from simulation analysis, and the details of definitions are described in the Section 4.3.1.

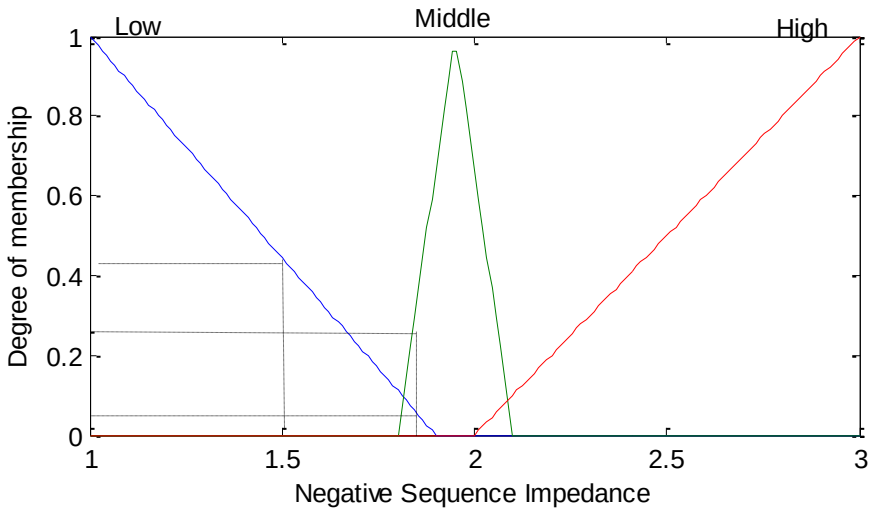

Figure 4.7 Fuzzy set of negative sequence impedance.

Thus, we can have the following fuzzy values of the membership level in the three sets:

$$\mu_{Low}(Z^-)=\begin{cases}1 & 1.0<Z^- \\ \dfrac{1.9-Z^-}{1.9-1} & 1.0\le Z^-<1.9 \\ 0 & Z^-\ge 1.9\end{cases} \tag{4.10}$$

$$\mu_{Middle}(Z^-)=\begin{cases}0 & 1.8<Z^- \\ \dfrac{Z^--1.8}{1.95-1.8} & 1.8\le Z^-<1.95 \\ \dfrac{2.1-Z^-}{2.1-1.95} & 1.95\le Z^-<2.1 \\ 0 & Z^-\ge 2.1\end{cases} \tag{4.11}$$

$$\mu_{High}(Z^-)=\begin{cases}0 & 2.0<Z^- \\ \dfrac{Z^--2.0}{3.0-2.0} & 2.0\le Z^-<3.0 \\ 1 & Z^-\ge 3.0\end{cases} \tag{4.12}$$

For example, when the calculated negative sequence impedance value is 1.5, the corresponding membership degree is 0.44 in the set Low, and 0.0 in the set Middle and High. If the value of the negative sequence impedance is 1.85, it may be judged to be Low or Middle, i.e. $\mu_{Low}(1.85)=0.04$, $\mu_{Middle}(1.85)=0.37$.

4.2.2.1 Fuzzy Sets Operations

Fuzzy set operations are derived from the classical set theory and thus have similar forms. Considering a given element *x* of the universe U, the operations of union, intersection and complement are listed below [64].

Union (i.e. Or):

$$\mu_{V\cup W}(x)=\mu_V(x)\cup\mu_W(x)=max(\mu_V(x),\mu_W(x)) \tag{4.13}$$

Intersection (i.e. And):

$$\mu_{V\cap W}(x)=\mu_V(x)\cap\mu_W(x)=min(\mu_V(x),\mu_W(x)) \tag{4.14}$$

Complement (i.e. Not):

$$\overline{\mu_V(x)} = 1 - \mu_V(x) \tag{4.15}$$

Take the Low and Middle sets of Figure 4.7 for example,

$$\begin{aligned} Low &= 0.27/1.65 + 0.16/1.75 + 0.04/1.85 + 0/1.95 + 0/2.05 \\ Middle &= 0/1.65 + 0/1.75 + 0.33/1.85 + 1/1.95 + 0.33/2.05 \end{aligned} \tag{4.16}$$

The union of the fuzzy sets Low and Middle

$$= 0.27/1.65 + 0.16/1.75 + 0.33/1.85 + 1/1.95 + 0.33/2.05 \tag{4.17}$$

The intersection of the fuzzy sets Low and Middle

$$= 0/1.65 + 0/1.75 + 0.04/1.85 + 0/1.95 + 0/2.05 \tag{4.18}$$

The complement of the fuzzy set Low

$$= 0.73/1.65 + 0.84/1.75 + 0.67/1.85 + 0/1.95 + 0.67/2.05 \tag{4.19}$$

4.2.3 Fuzzy (Rule-Based) System

Generally, a fuzzy rule has the form as in (4.20), where V and W are two classical sets that are defined on two universe sets X and Y, respectively.

$$\textit{If x is V, then y is W} \tag{4.20}$$

The if-part of the sentence is called the premise of the rule; the then-part of the sentence is called the conclusion of the rule. It typically expresses an inference such that if there is a fact, then another fact can inferred or derived [64, 67]. It should be pointed out that, both the premise and conclusion of a rule may contain multiple parts [68].

Figure 4.8 shows a simple Mamdani model of two-rule system. It has two crisp values inputs *x* and *y* and a single output *z**. Equation (4.21) gives the If-Then rules used in the fuzzy system,

$$\begin{aligned} &\textit{If x is } A_1 \textit{ and y is } B_1\textit{, then z is } C_1 \\ &\textit{If x is } A_2 \textit{ and y is } B_2\textit{, then z is } C_2 \end{aligned} \tag{4.21}$$

where A_1 , A_2, B_1, B_2, C_1 and C_2 are the fuzzy sets.

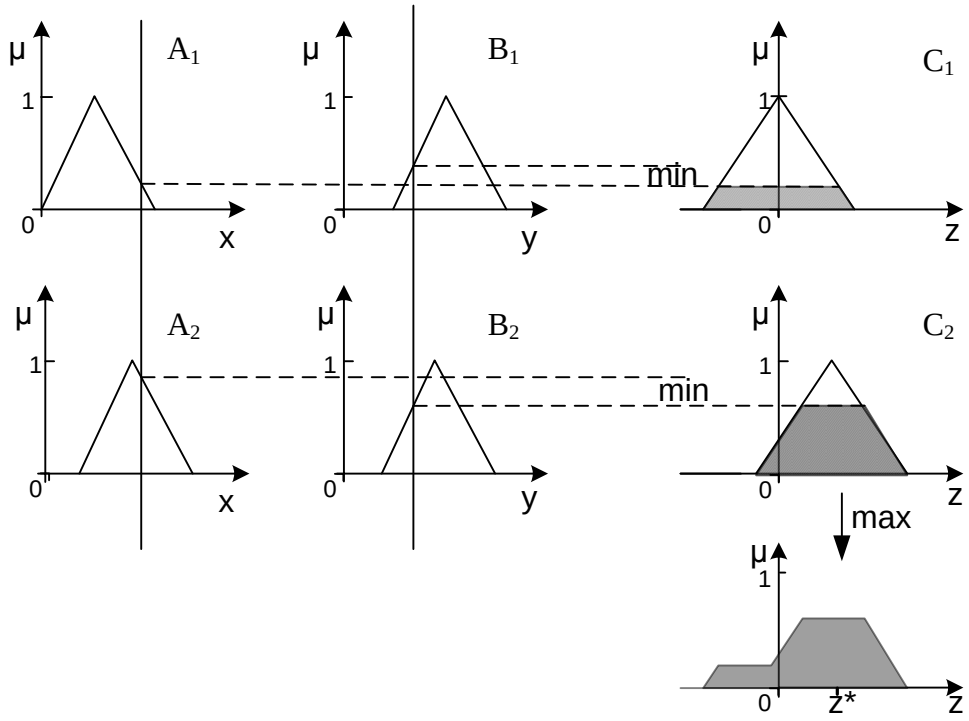

Figure 4.8 The Mamdani fuzzy inference system.

The operation of the Mamdani fuzzy interface system is explained as follows: for the given value *x*, membership values $\mu_{A1}(x)$ and $\mu_{A2}(x)$ are derived; for the given value *y*, the membership values $\mu_{B1}(y)$ and $\mu_{B2}(y)$ are calculated; then for each rule, find the minimum of the membership value $min(\mu_{A1}(x), \mu_{B1}(y))$ and $min(\mu_{A2}(x), \mu_{B2}(y))$; Based on it, the fuzzy sets C_1 and C_2, are truncated to get the sets C'_1 and C'_2; for each value in the truncated sets, take the *max* operation to get the final output fuzzy set C.

4.2.4 Defuzzification

The output from the Mamdani model is a fuzzy set. To be able to use it, it is often necessary to convert it to a single scalar quantity, which is known as defuzzification. Several methods can be found in the literature, such as Max-membership method, Centroid of Gravity (COG) method, Weight average method and Mean-of-Maxima method [64]. In this work, the COG method is applied for the fuzzy set defuzzification.

The COG method, also known as the centre of area or centre of gravity, is an essentially technique for finding mid-point of the final output fuzzy set. It utilises a weighted average of the membership grades. Figure 4.9 shows graphical representation of the COG method, while (4.22) gives the mathematical expression,

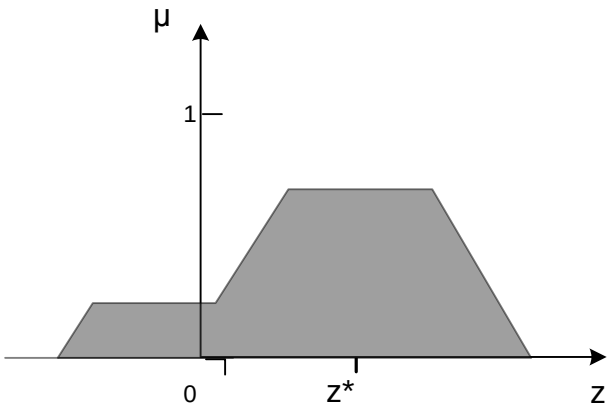

Figure 4.9 Centroid of Gravity (COG) method [69].

$$z^* = \frac{\int \mu_C(z) \cdot z dz}{\int \mu_C(z) dz} \tag{4.22}$$

where $\mu_C(z)$ is the membership value of the fuzzy set C, and z* is represents the centre of the shaded area.

4.3 Fault Detection based on Fuzzy Logic

The inter-turn short-circuit fault of the PMSMs can be detected by observing the information of the negative sequence components (i.e. both the current and impedance). However, it is very difficult to interpret the obtained component values as a linear relationship and to further derive a clear and precise detection algorithm.

The fuzzy logic approach can be considered as a promising solution, since the numerical data (i.e. values of the negative sequence components) can be treated in a linguistic manner. Two major subsections should be taken into account,

which are the membership function of the system input and the fuzzy rule based inference.

4.3.1 Membership Function

Based on the definitions presented in Section 4.2, the fuzzy logic approach is employed for fault detection of the inter-turn short-circuit faults of the PMSMs. The first input is Negative Sequence Current, and it can be divided into three membership functions, which are Negative Sequence Current Low (NCL), Negative Sequence Current Medium (NCM), and Negative Sequence Current Big (NCB), respectively.

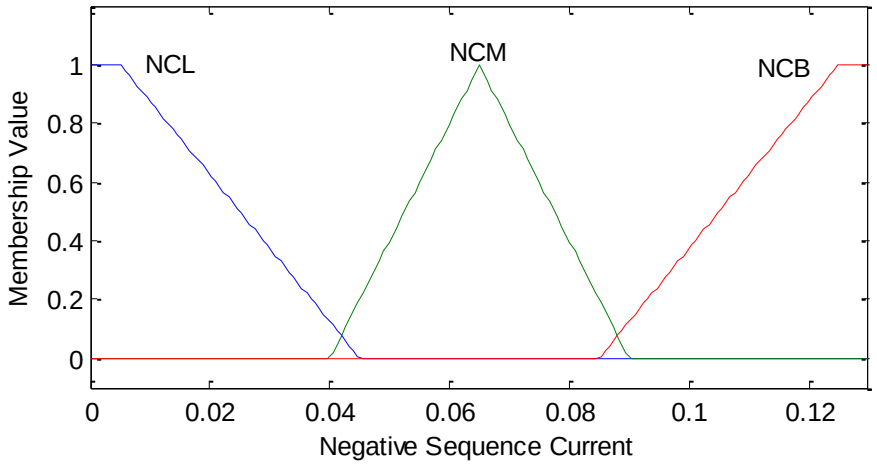

Figure 4.10 Membership functions for the first input (Negative Sequence Current).

Figure 4.10 shows the membership functions of the Negative Sequence Current. It should be pointed out that, the set of the membership function should be designed according to the individual system under consideration. For example, the value of the negative sequence current for a PMSM is determined by many factors such as inherent unbalance caused by winding discrepancy etc. [5]. The simulation result given in Chapter 3 has shown that, when the system is in steady state under normal condition, the value of the negative sequence current is very small but does not have a constant value.

According to the simulation results, the negative sequence current with 2 short-circuit turns is 0.13A (refer to Figure 3.19). Hence, the range of the negative sequences current under fault conditions can be chosen to be between 0.085

and 0.13. Since the value of the negative sequence current is proportional to the number of the short-circuit turns, any other faults with higher short-circuit turns can be detected effectively. By taking the system imbalance into account, the range of the NCL is chosen to be between 0 and 0.045. Accordingly, the range of the NCM can be determined, which is between 0.04 and 0.09.

Similarly, three membership functions can be developed for the negative sequence impedance, which are Negative Sequence Impedance Low (NIL), Negative Sequence Impedance Medium (NIM), and Negative Sequence Impedance Big (NIB), as shown in Figure 4.11.

When short-circuit faults occur, the value of the negative sequence impedance will decrease, and the change is proportional to the number of short-circuit turns. Considering that the target PMSM has a negative sequence impedance of 2.3 under normal condition and 1.7 with 2 turns short-circuit fault (refer to Figure 3.20), the range of NIL is chosen to be between 0 and 1.9, and the boundary of NIB is selected at 2.

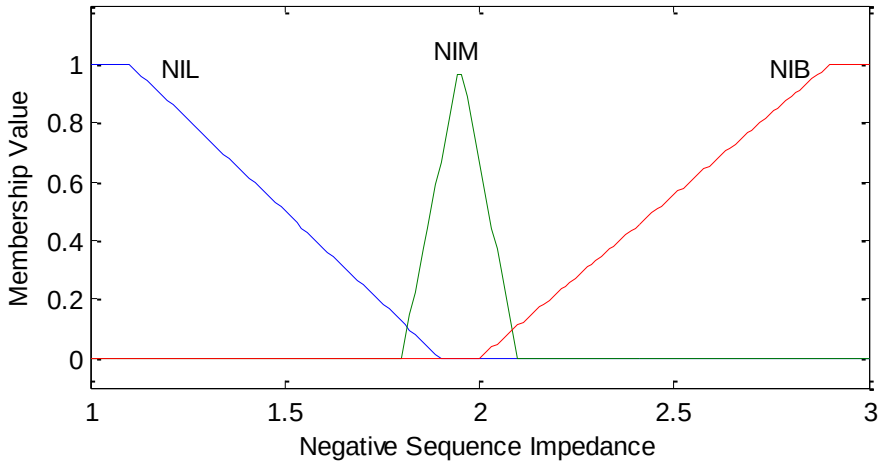

Figure 4.11 Membership functions for the second input "Negative Sequence Impedance".

Based on the two membership functions and the conclusion drawn in Table 3.1, Figure 4.12 shows the corresponding health and fault indicator, where H and F represent the health and fault operation, respectively.

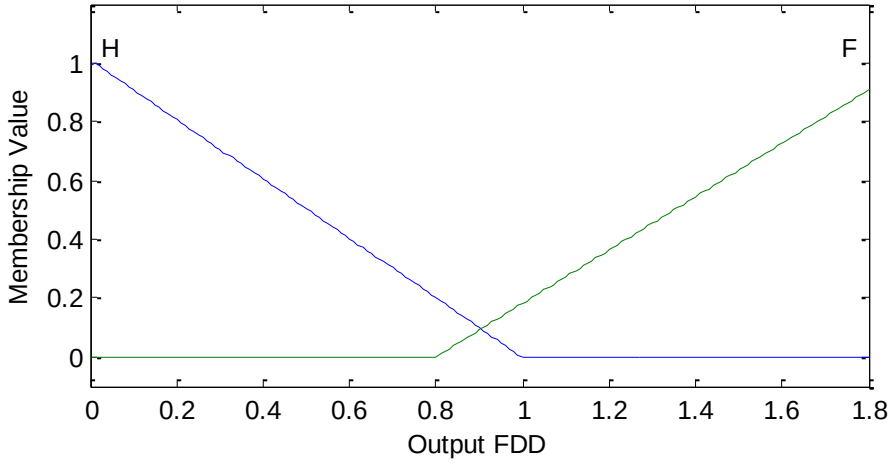

Figure 4.12 Membership function for the output "Health and Fault Indicator".

As expected, the use of the two negative sequence components can eliminate the influence of the false alarms and produces a very good fault detection result.

4.3.2 Rule based Inference

With the aim of relating the input and the output, a rule based inference system has been developed. The Input signals of the system are the calculated negative sequence current and negative sequence impedance of the PMSM. And a total of six rules are employed to clearly state the motor operating condition in a quantitative manner [70].

- Rule (1) If I^- is NCL and Z^- is NIM, then OP is H;
- Rule (2) If I^- is NCL and Z^- is NIB, then OP is H;
- Rule (3) If I^- is NCM and Z^- is NIB, then OP is H;
- Rule (4) If I^- is NCM and Z^- is NIL, then OP is F;
- Rule (5) If I^- is NCB and Z^- is NIL, then OP is F;
- Rule (6) If I^- is NCB and Z^- is NIM, then OP is F.

For instance, if the negative sequence current is Low (NCL) and the negative sequence impedance is Big (NIB), the system considers the PMSM is in normal condition and outputs an indicator of Healthy (H); if the negative sequence current is Big (NCB) and the negative sequence impedance is Low (NIL), then the output detector response is Fault (F).

Based on the above rules, the inter-turn short-circuit fault condition of the PMSM can be distinguished by using a quantitative representation of the two negative sequence components.

Figure 4.13 presents the fuzzy inference diagram for a healthy PMSM where rule (2) is solicited. As it can be seen, the value of I^- is 0.016 which indicates a low negative sequence current (i.e. NCL). The graph in the first column have the membership functions of $\mu_{Low}(I^-)$=0.7, $\mu_{Low}(I^-)$=0.7, $\mu_{Middle}(I^-)$=0.0, $\mu_{Big}(I^-)$=0.0, $\mu_{Big}(I^-)$=0.0. Likewise, the second column (Z^-) is at value of 2.3 which implies a high negative sequence impedance, and thus have the membership function of $\mu_{Middle}(Z^-)$=0.0, $\mu_{Big}(Z^-)$=0.3, $\mu_{Low}(Z^-)$=0.0, $\mu_{Low}(Z^-)$=0.0, $\mu_{Big}(Z^-)$=0.0. The fuzzy output for the five rules is the AND result between the first input I^- and the second input Z^-. According to (4.14), this operation result should be min(0.7,0.0), min(0.7, 0.3), min(0.0, 0.0), min(0.0, 0.0), min(0.0, 0.0), which only produces $\mu_{Healthy}$=0.3.

Now the Centroid of Gravity (COG) method can be applied to produce a crisp output value, for the value of $I^-$is 0.016 and the value of Z^- is 2.3, the fuzzy output element output value can be calculated using (4.22), Under this condition, the PMSM is judged to be as healthy.

$$OP = \frac{\int \mu_H(z)\cdot z dz}{\int \mu_H(z) dz} = \frac{0.3\times 0.672 + 0.3\times(1-0.672)}{0.3\times 2} = 0.418 \tag{4.23}$$

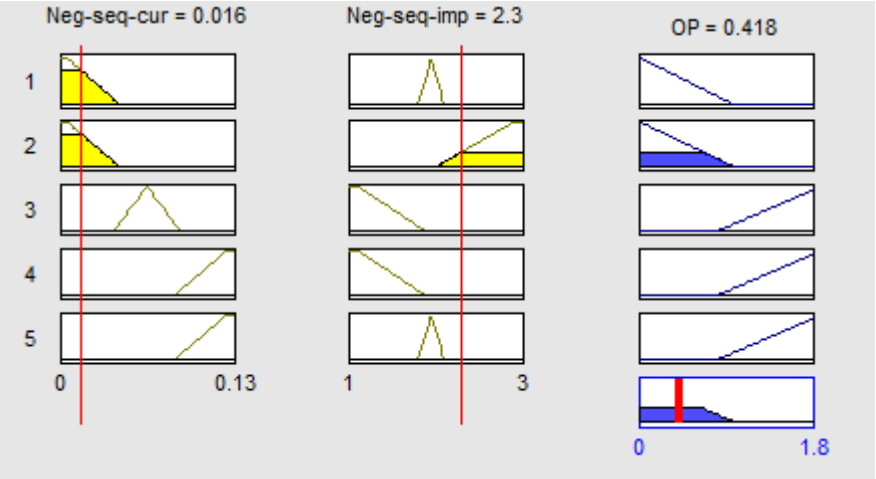

Figure 4.13 Fuzzy inference diagram for a healthy PMSM.

Figure 4.14 shows the fuzzy inference diagram for a faulty PMSM where rule (5) is solicited. The value of I^- is 0.13 which brings a high negative sequence current (i.e. NCB), and the value of Z^- is 2.3 which indicates a large impedance (i.e. NIL). Under this condition, the PMSM is considered to be faulty (OP=1.45).

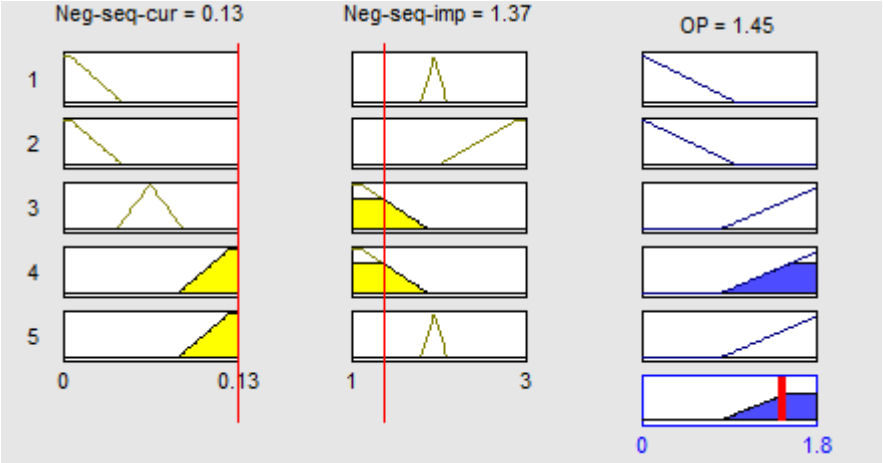

Figure 4.14 Fuzzy inference diagram for a faulted PMSM.

Figure 4.15 shows the fuzzy inference diagram for a PMSM under speed and load fluctuations, where rule (3) is solicited. The value of I^- is 0.0696, which gives a medium negative sequence current (i.e. NCM), and the value of Z^- is 2.3 which implies a large impedance (i.e. NIB).

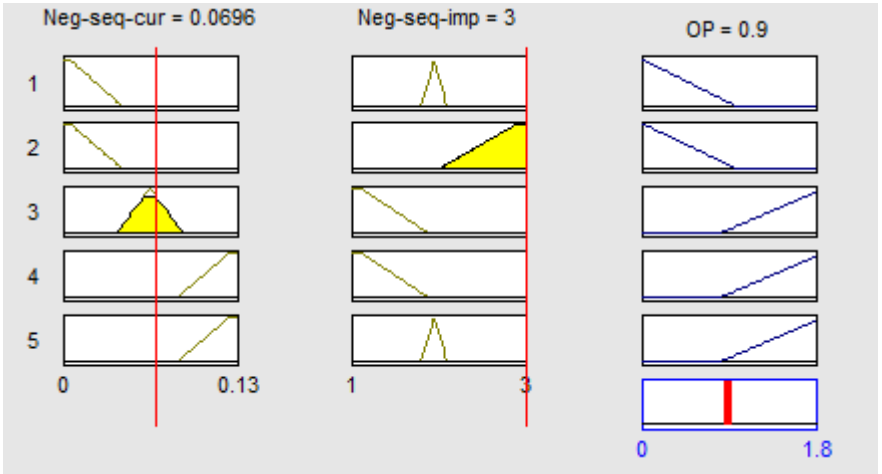

Figure 4.15 Fuzzy inference diagram for a PMSM under speed and load fluctuations.

Under this case, the status of the PMSM is judged to be healthy. Clearly, the use of the fuzzy logic system can reduce the influence of speed or load changes on the fault detection effectively.

Figure 4.16 shows the surface plot of the detector response of the FDD system, where the x-axis and y-axis represent the negative sequence current and impedance, and the z-axis is the output of the detector response.

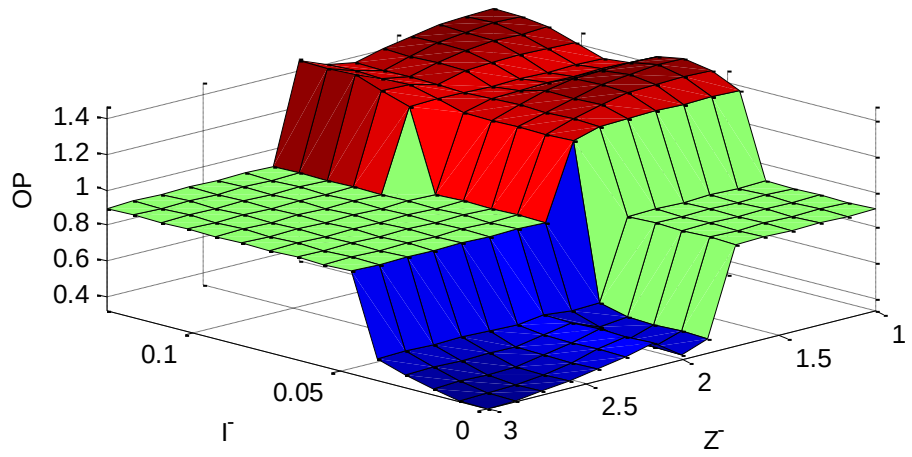

Figure 4.16 Surface plot of the detector response.

The red surface part implies that the PMSM has an inter-turn short-circuit fault, since the negative sequence current is medium or large and impedance is small or medium. Similarly, the blue surface part represents that the PMSM is under normal operating condition, as the negative sequence current is low or medium and the impedance is medium or large.

It should be pointed out that, the two green surface parts repeat the conditions which are not covered by the rules defined above, i.e. the condition where both the negative sequence current and impedance are either high or small. According to the analysis carried out in Chapter 3, these two conditions will never occur together, since the negative sequence current and impedance are always inversely proportional to each other.

4.4 Simulation Results

In this section, the proposed fuzzy logic based fault detection scheme is utilised for the PMSM short-circuit fault detection using the MATLAB/Simulink environment. The disturbance caused by both the load torque fluctuation and the speed fluctuation is taken into account, in order to test the developed FDD system in a practical situation.

4.4.1 Speed Disturbance (2 Turns)

In this sub-section, the speed ramps from 800rpm to 1000rpm between 0.14s and 0.2s, an inter-turn short-circuit fault of 2 turns is injected into phase A at t time=0.24s.

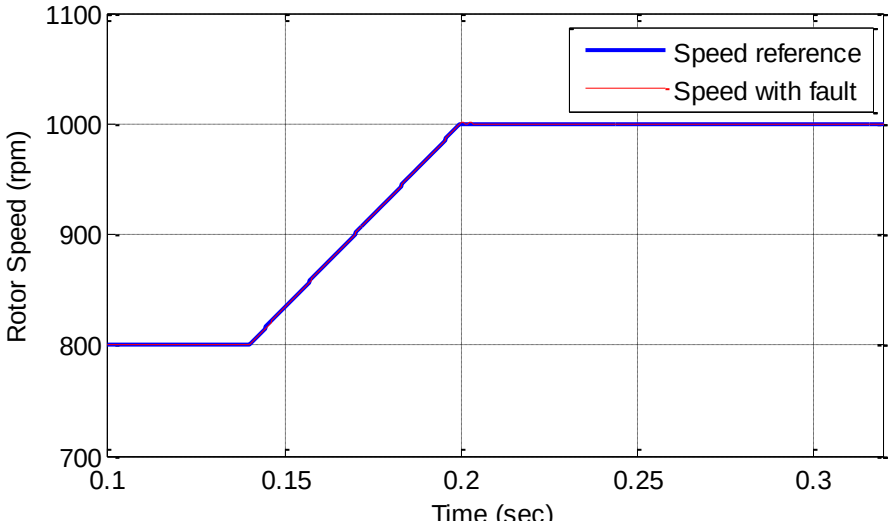

Figure 4.17 PMSM speed response with fault condition.

Figure 4.18 shows the waveform of the filtered negative sequence current. Due to the speed ramp, the value of the negative sequence current has been influenced, and two spikes have been introduced at 0.14s and 0.2s, respectively. The peak value of these two spikes is quite high, which are 0.1 and 0.12 (i.e. NCB). Obviously, using only the negative sequence current to diagnose the fault will lead to a fault alarm.

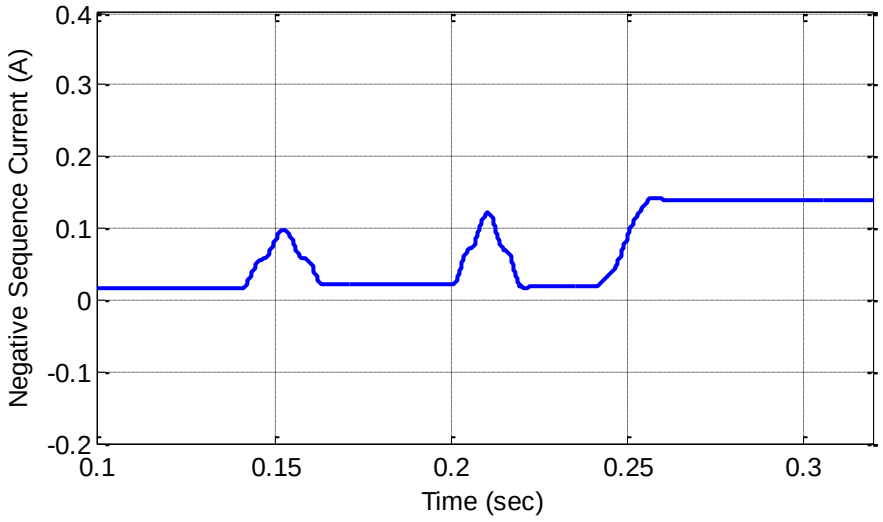

Figure 4.18 Filtered negative sequence current under speed disturbance.

Figure 4.19 shows the corresponding waveform of the negative sequence impedance. Clearly, when the speed changes, the value of the negative sequence impedance increases significantly, and the peak value is about 5.6 (i.e. NIB). At time=0.24s, the short-circuit fault is introduced, and the value of the negative sequence impedance drops to 1.71 (i.e. NIL).

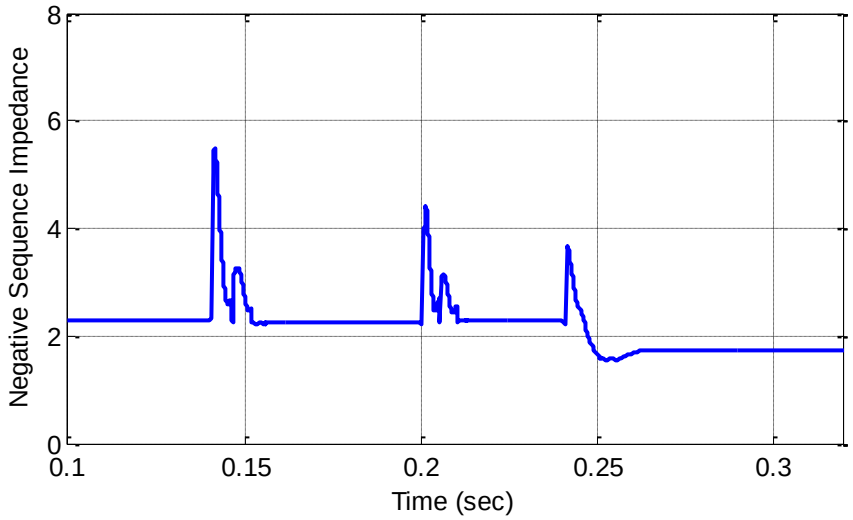

Figure 4.19 Filtered negative sequence impedance under speed disturbance.

By using both the information of the negative sequence current and impedance, Figure 4.20 shows the fault indicator under the speed disturbance and fault condition. Clearly, the proposed fault detection scheme is capable of diagnosing the fault accurately and quickly (less than one cycle delay) under speed disturbance.

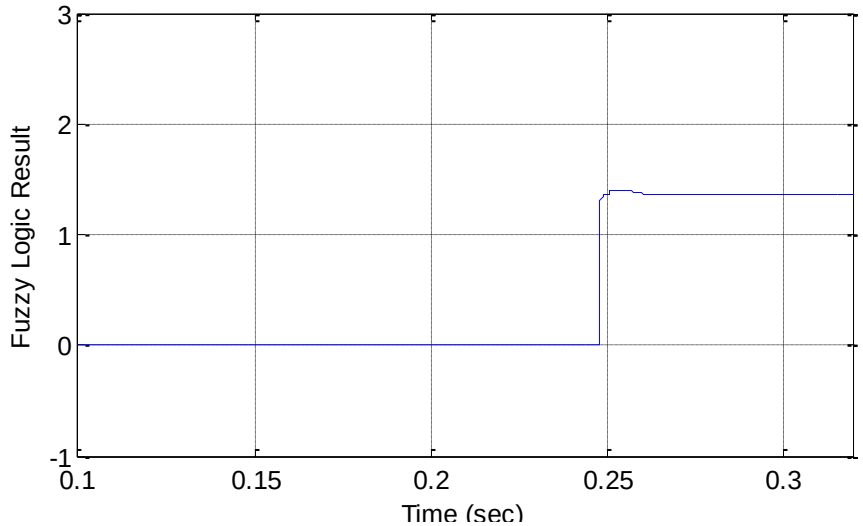

Figure 4.20 Fault indicator under speed disturbance and fault condition.

4.4.2 Load Disturbance (2 Turns)

In this sub-section, the speed reference of the PMSM motor is fixed at 1000rpm, and a step change in load is considered to examine the possible influence on the negative sequence components.

As shown in Figure 4.21, the load torque has a step change from 0.4Nm to 0.6Nm at time=0.14s. After that, a short-circuit fault of 2 turns is introduced into phase A at time=0.24s.

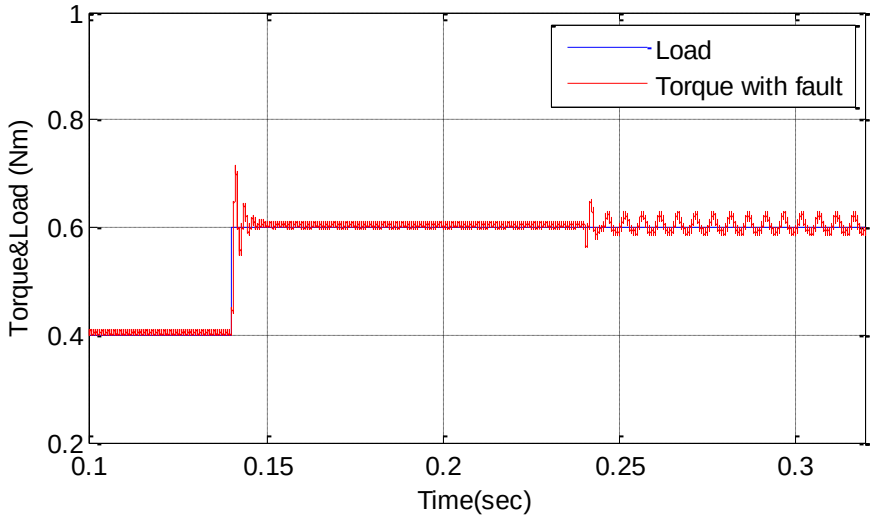

Figure 4.21 PMSM torque response under fault condition.

Figure 4.22 and Figure 4.23 show the two negative sequence components under the load disturbance and fault condition. The negative sequence current

is affected noticeably, manifesting spikes when the load changes at 0.14s, and reaches 0.11A (i.e. NCB). Using only the negative sequence current will definitely result in a false alarm. Similarly, the negative sequence impedance increases largely (i.e. NIB) under this load disturbance.

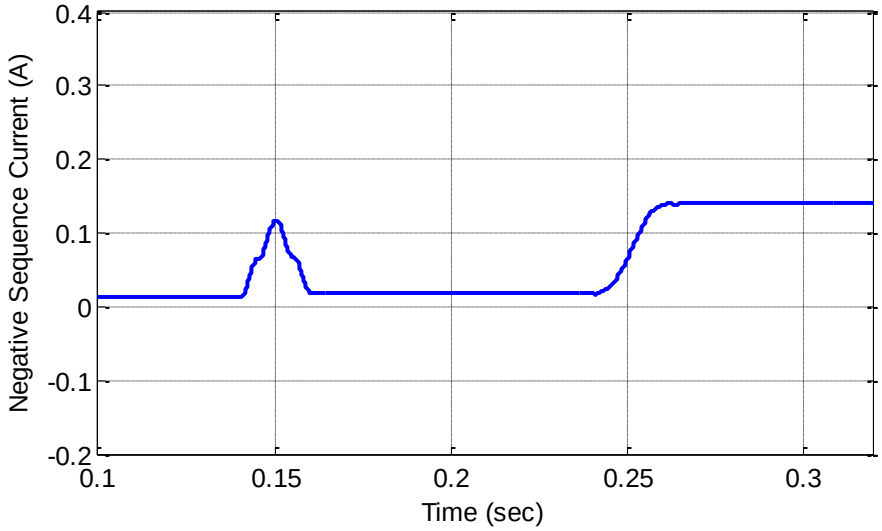

Figure 4.22 Filtered negative sequence current under load disturbance and 2 turns fault.

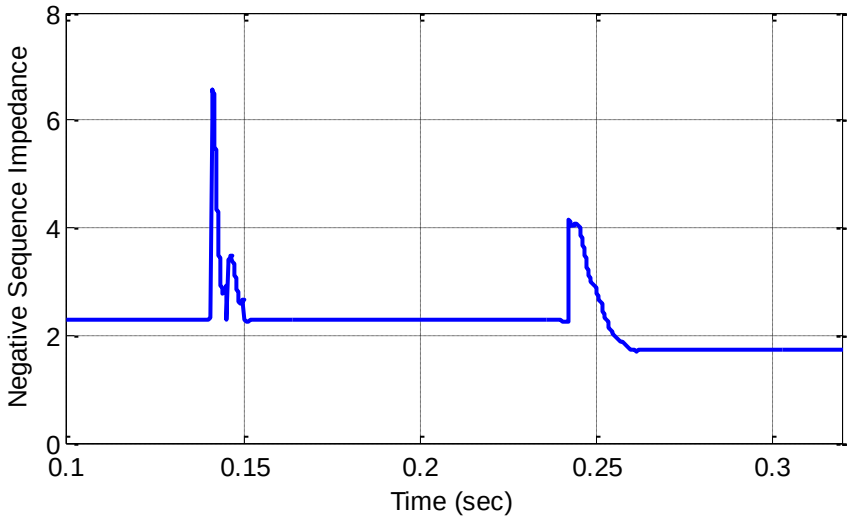

Figure 4.23 Filtered negative sequence impedance under load disturbance and 2 turns fault.

When the system is under the fault condition, the value of the negative sequence current increased from 0.01 (i.e. NCL) to 0.14 (i.e. NCB). Meanwhile, the value of the negative sequence impedance decreased from 2.3 (i.e. NIB) to 1.7 (i.e. NIL).

By using both the information of the negative sequence current and impedance, Figure 4.24 shows the fault indicator under the load disturbance and 2 turns fault condition. Clearly, the influence of the load disturbance can be filtered successfully, and the fault can be detected effectively and quickly (within two cycle delays).

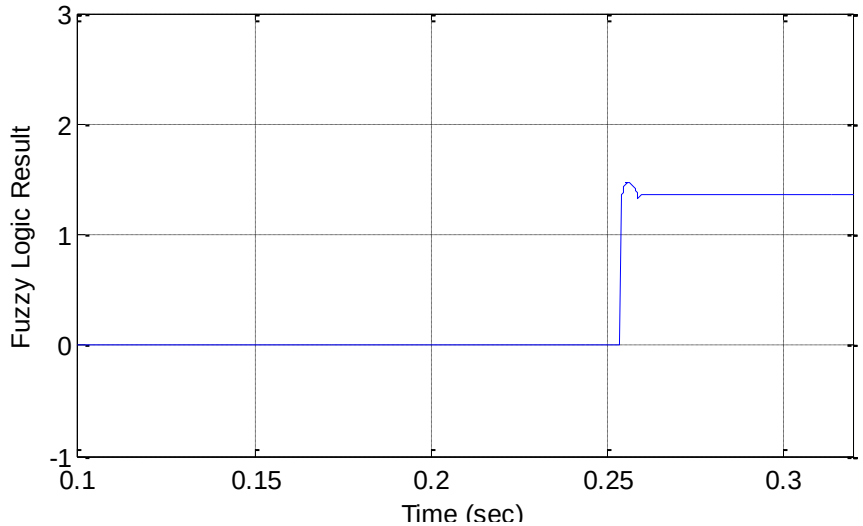

Figure 4.24 Fault indicator under load disturbance and 2 turns fault.

4.4.3 Load Disturbance (10 Turns)

In this sub-section, the speed reference of the PMSM motor is fixed at 500rpm, and the load torque has a step change from 0.2Nm to 0.4Nm at time=0.14s. A short-circuit fault of 10 turns is introduced into phase A at time=0.24s, as illustrated in Figure 4.25.

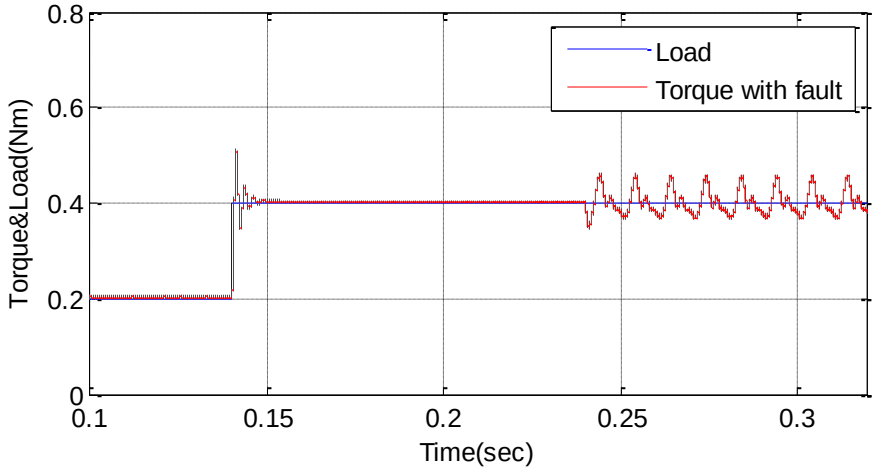

Figure 4.25 Torque response under fault condition.

Figure 4.26 shows the waveform of the negative sequence current under the load disturbance. Compared with Figure 4.22, the negative sequence current value is much higher (i.e. 0.55 (NCB) versus 0.11 (NCB)), due to the 10 short-circuit turns.

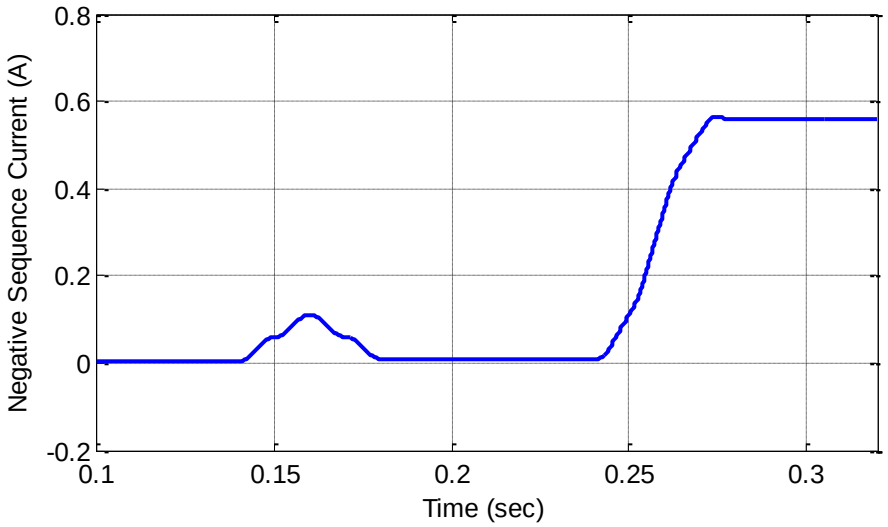

Figure 4.26 Filtered negative sequence current under load disturbance 10 turns fault.

Figure 4.27 shows the waveform of the negative sequence impedance under the load disturbance. In comparison to the previous test condition (refer to Figure 4.19), the value of the negative sequence impedance becomes lower, i.e. changing from 1.7 to 1.284.

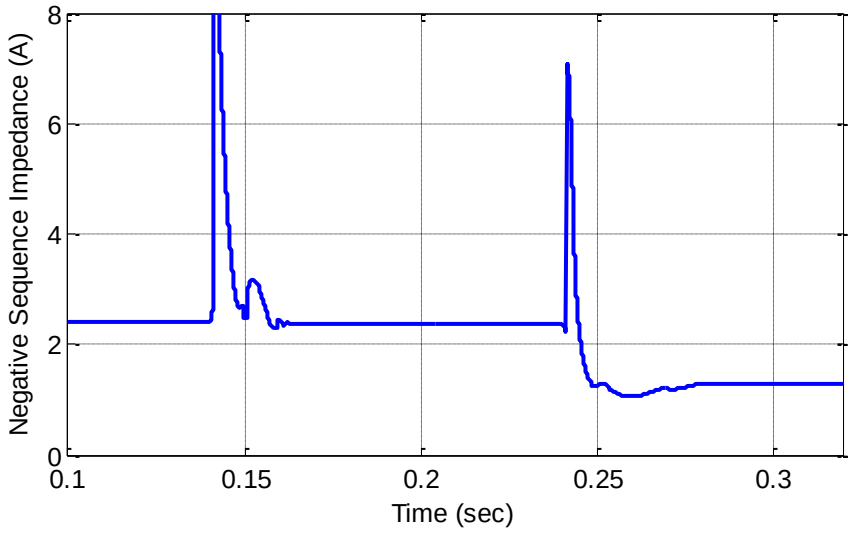

Figure 4.27 Filtered negative sequence impedance under load disturbance and 10 turns fault.

By using both the information of the negative sequence current and impedance, Figure 4.28 shows the fault indicator under the load disturbance and 10 turns fault condition. The proposed fuzzy logic approach is capable of detecting the short-circuit fault less than one cycle delay under motor speed fluctuation condition.

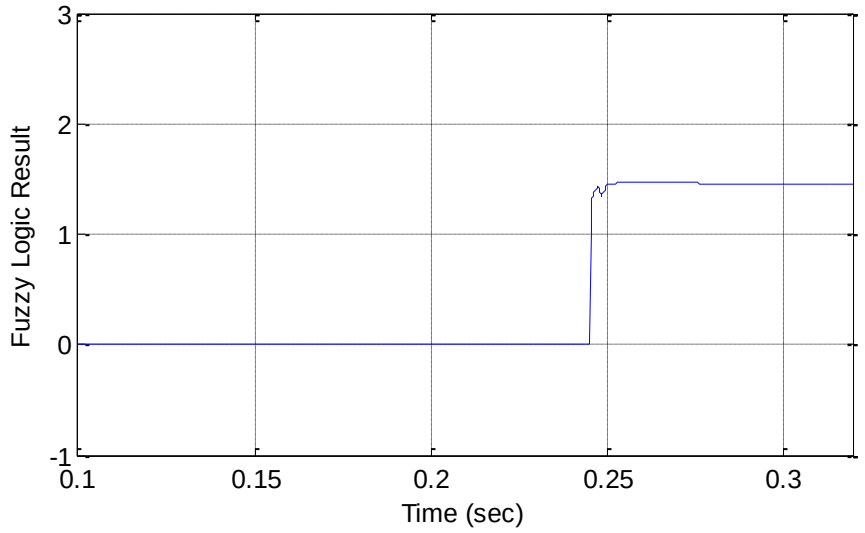

Figure 4.28 Fault indicator under load disturbance and 10 turns fault.

4.5 Summary

In this chapter, a fuzzy logic based fault detection approach is proposed for the diagnosis of the inter-turn short-circuit fault of the PMSMs. Firstly, the fundamental theory of classical set and fuzzy set was introduced. Then, the membership function and the rule based inference of the fuzzy logic were discussed in detail to provide a clear understanding of basic concepts. Finally, the simulation shows that the proposed approach is capable of diagnosing the faulted phase accurately and quickly under load or speed fluctuations.

CHAPTER 5

CONCLUSIONS AND FUTURE WORK

5.1 Conclusions

In the last two decades, the permanent magnet synchronous machine has attracted more and more interests and been applied widely in modern industries and special applications, such as hybrid automobile, aerospace drives and military power drives. Owing to the high energy product of rare-earth permanent magnet, the PMSMs hold excellent torque density, wide constant power speed range and high conversion efficiency in comparison of traditional machines. However, the use of the permanent magnet for the creation of the magnetic field brings a significant drawback for the machine, which is the weak fault tolerance capability. Taking an inter-turn short-circuit fault as an example, a few short-circuit turns lead to huge increase in the faulting winding current, and thus to excessive heat generation. This may further propagate and eventually cause a catastrophic failure.

Based on the above reason, fault detection of the PMSMs has become crucially important and necessary, especially for applications demanding high security and reliability (e.g. aerospace and automotive sectors). This forms the basic motivation of this research work.

In this thesis, the modelling of PMSM with an inter-turn short-circuit faults have been presented first. Based on the classical three-phase circuit coordinates, the dynamic description of the PMSM under the ABC frame has been reviewed and transformed into the DQ frame. The developed PMSM model can represent the motor operation under the normal and short-circuit fault conditions. The simulation results have shown a good correlation to the theoretical analysis.

Following this, a winding inter-turn short-circuit fault detection technique for the PMSM has been addressed by applying sequence component theory. Two different ways for the derivation of the sequence component have been demonstrated, and a three-phase sequence analyser is used to obtain the negative sequence components for fault detection purpose. Although either the negative sequence current or impedance can reflect the occurrence of a fault, the influence of the motor speed or load fluctuation introduces disturbances and, thus, false alarms, which makes the fault detection system unreliable.

In order to overcome this problem, a fuzzy logic approach has been considered to process both the negative sequence current and impedance information, in order to eliminate the disturbance of the load or speed fluctuation while the true short-circuit fault can be diagnosed effectively and quickly. Based on a number of different measured data from the simulation result, the fuzzy logic system has been adjusted and tested. The simulation results have shown that the proposed fault detection approach is capable of diagnosing the faulting phase accurately and quickly under both load and speed fluctuations.

5.2 Future Work

Although the feasibility of the developed fault detection and diagnosis system has been validated successfully, there are still some aspects that need to improve and study further for practical applications.

Although the most common fault of the PMSMs, i.e. inter-turn short-circuit type fault, has been studied and modelled in this thesis, the work on the PMSM fault modelling could be further improved. For the considered fault model, several assumptions were made for simplicity, such as sinusoidal distribution of magneto motive force and the flux, and non-saturated magnetic field etc. These assumptions may introduce model errors, and compromise the fidelity of the model. Advanced modelling techniques could be employed to improve accuracy.

Second, only the stator winding turn-to-turn short-circuit fault has been considered. In practice, the PMSM may suffer from different faults, such as inverter faults, air gap eccentricity, partial demagnetisation, etc. For a comprehensive FDD system, different type of faults should be detected and identified. The influence of other faults on the developed technique should also be assessed.

Likewise, the effects of harmonics in the determination of the fault indicator should also be studied. And finally, the proposed system should be tested in a prototype drive system with controllable fault injections.

Appendix A

SIMULINK MODELS

A.1 Simulink Models

In this Appendix, the detailed structure of the MatLab Simulink models developed for the FDD of the PMSM is presented as follows.

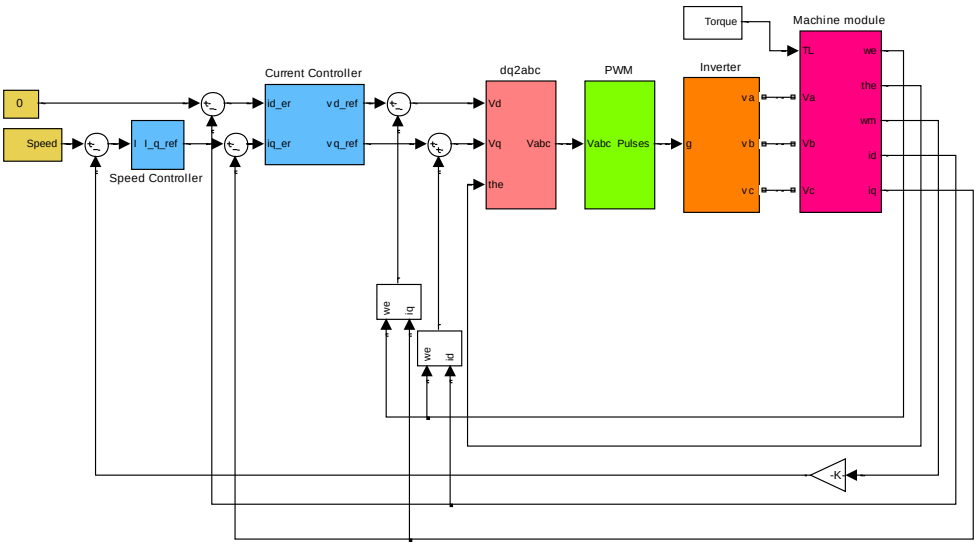

Figure A.1 Simulink model of vector controlled PMSM.

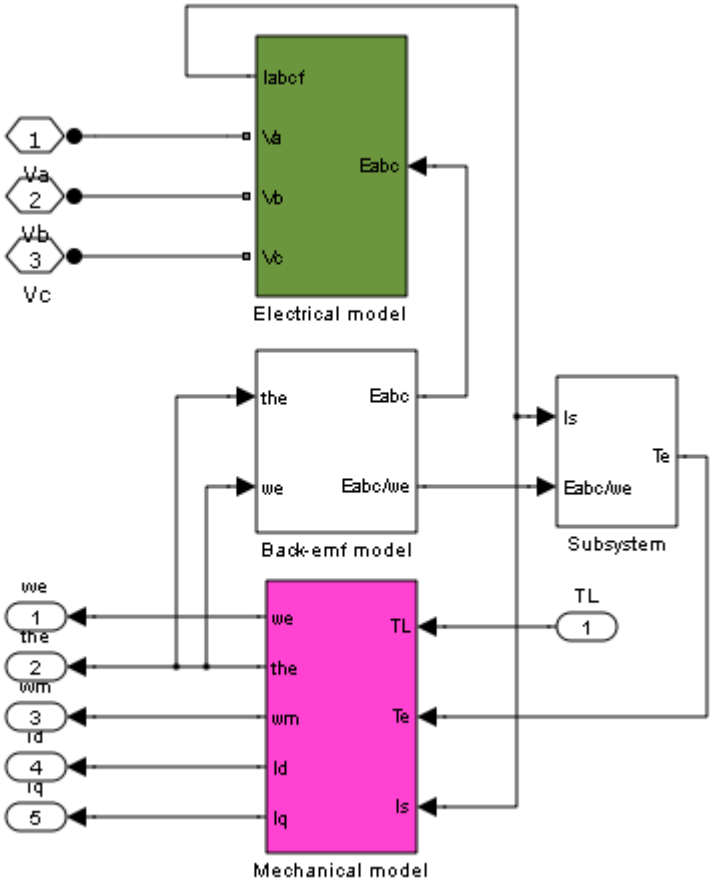

Figure A.2 Subsystem of the PMSM.

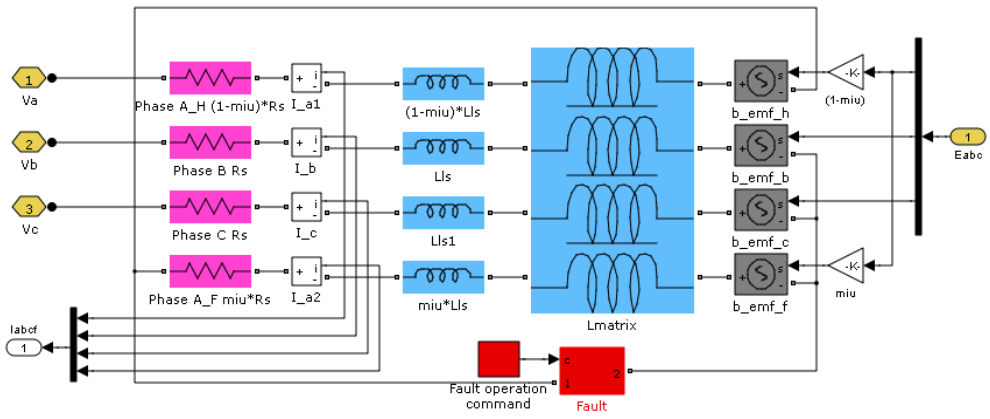

Figure A.3 Subsystem of the electrical model.

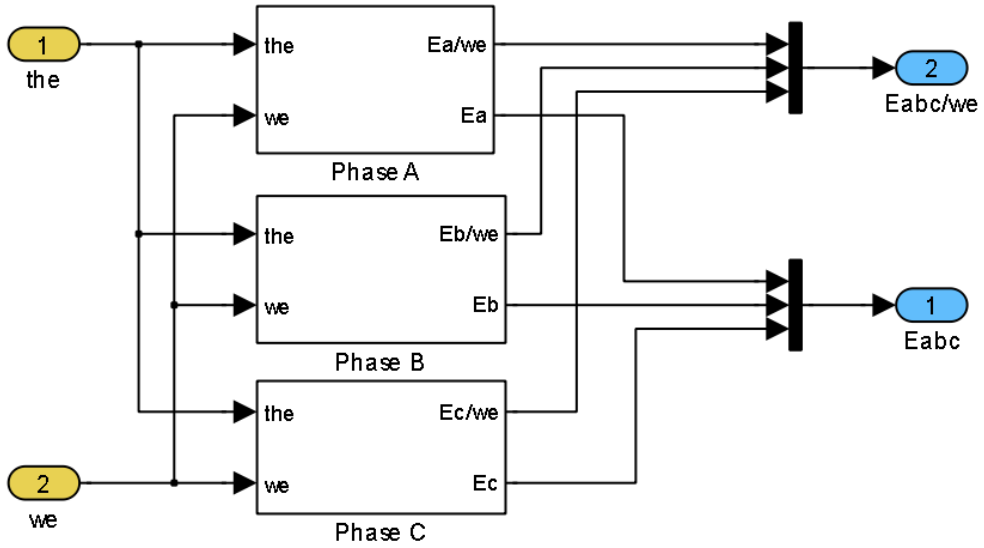

Figure A.4 Subsystem of back-emf model.

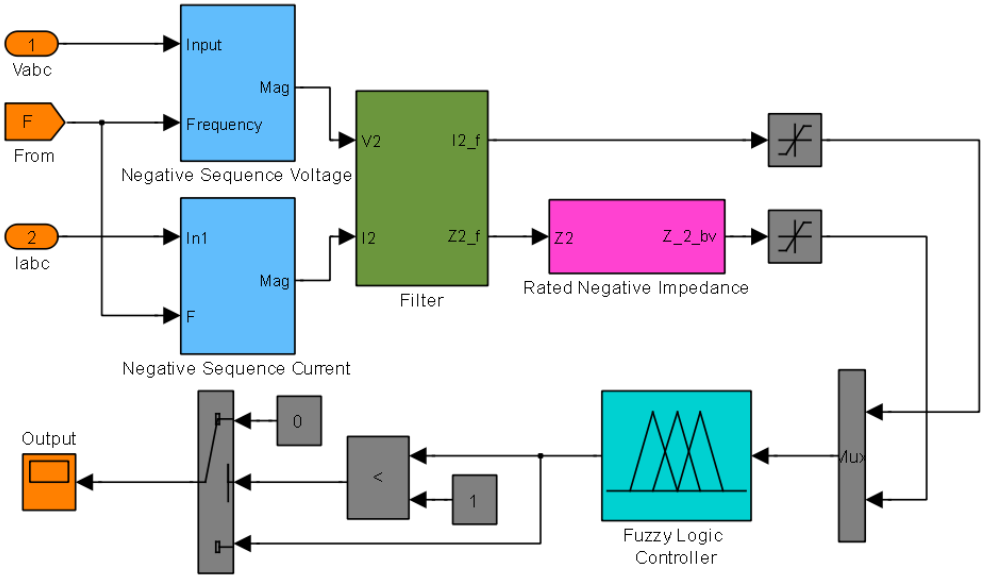

Figure A.5 Simulink model of FDD.

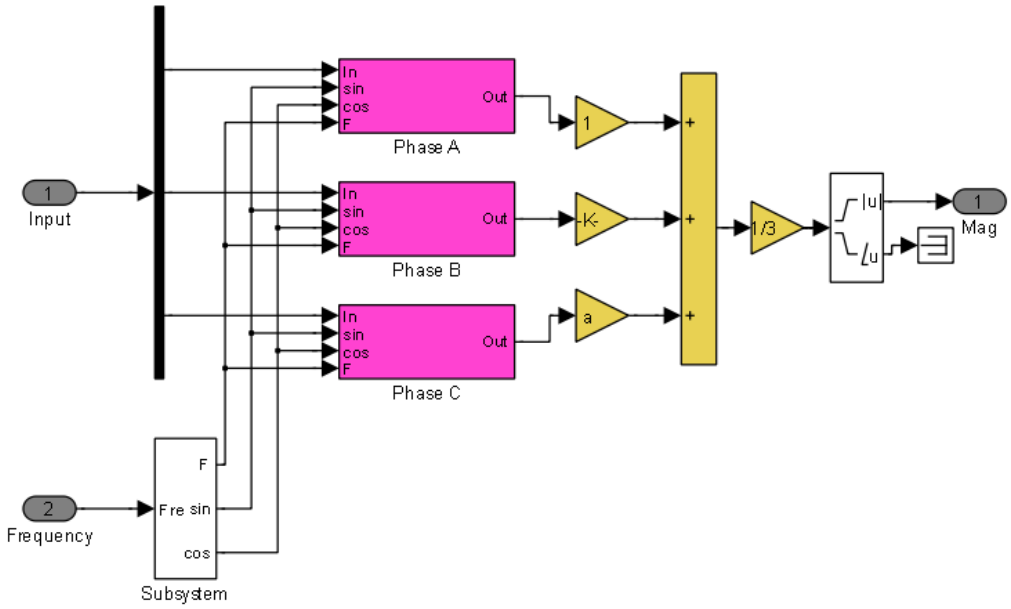

Figure A.6 Subsystem of negative sequence components model.

References

[1] T. J. E. Miller, *Brushless Permanent-magnet and Reluctance Motor Drives*: Clarendon Press, Oxford, 1989.

[2] T. Miyamoto, H. Sakurai, H. Takabayashi, and M. Aoki, "A development of a permanent magnet assembly for MRI devices using Nd-Fe-B material," *IEEE Trans. Magn.*, vol. 25, no. 5, pp. 3907-3909, 1989.

[3] G. Pellegrino, A. Vagati, P. Guglielmi, and B. Boazzo, "Performance comparison between surface-mounted and interior PM motor drives for electric vehicle application," *IEEE Trans. Ind. Electron.*, vol. 59, no. 2, pp. 803-811, Feb 2012.

[4] L. Liu, "Robust fault detection and diagnosis for permanent magnet synchronous motors," Ph.D. dissertation, Dep. of Mech. Eng., Florida State Univ., 2006.

[5] Quiroga Mendez and J. Eduardo, "stator winding fault detection for a PMSM using fuzzy logic classifier and neural network model identification," M.S. thesis, Dept. Mech. Eng., Florida State Univ., 2008.

[6] C. Angeli, "Diagnostic expert systems: from expert's knowledge to real—time systems," in *Advanced Knowledge Based Systems :Model, Applications & Search* vol. 1, ed, 2010, pp. 50-73.

[7] H. Mohamed Basri, K. Lias, W. A. Wan Zainal Abidin, K. M. Tay, and H. Zen, "Fault detection using dynamic parity space approach," in *Proc. IEEE Power Eng. and Optimiza. Conf. (PEDCO'2012)* Melaka, Malaysia, 2012, pp. 52-56.

[8] K. Warwick, A. Ekwue, R. Aggarwal, and I. o. E. Engineers, *Artificial Intelligence Techniques in Power Systems*: Institution of Electrical Engineers, 1997.

[9] G. K. Singh and S. a. Ahmed Saleh Al Kazzaz, "Induction machine drive condition monitoring and diagnostic research—a survey," *Electric Power Systems Research*, vol. 64, pp. 145-158, 2003.

[10] J. Robinson, C. Whelan, and N. K. Haggerty, "Trends in advanced motor protection and monitoring," *IEEE Trans. Ind. Appl.*, vol. 40, pp. 853-860, 2004.

[11] S. Nandi and H. A. Toliyat, "Condition monitoring and fault diagnosis of electrical machines-a review," in *Proc. 34th. Annu. Conf. IEEE Ind. Applicat. Conf. (IAS'99)*, Phoenix, AZ, 1999, pp. 197-204.

[12] "IEEE Recommended Practice for the Design of Reliable Industrial and Commercial Power Systems - Redline," *IEEE Std 493-2007 (Revision of IEEE Std 493-1997) - Redline*, pp. 1-426, 2007.

[13] O. Ojo, O. Osaloni, and P. Kshirsagar, "Models for the control and simulation of synchronous type machine drives under various fault conditions," in *Proc. 37th. Annu. Conf. IEEE Ind. Appl. Conf. (IAS'02)*, Pittsburgh, PA, 2002, pp. 1533-1540.

[14] A. A. Abdallah, V. Devanneaux, J. Faucher, B. Dagues, and A. Randria, "Modelling of surface-mounted permanent magnet synchronous machines with stator faults," in *Proc. 30th. Annu. Conf. IEEE Ind. Electon. Soc. (IECON'04)*, Busan, Korea, 2004, pp. 3031-3036.

[15] S. Nandi, H. A. Toliyat, and L. Xiaodong, "Condition monitoring and fault diagnosis of electrical motors-a review," *IEEE Trans. Energy Convers.*, vol. 20, pp. 719-729, 2005.

[16] A. L. Nelson and C. Mo-Yuen, "Characterization of coil faults in an axial flux variable reluctance PM motor," *IEEE Trans. Energy Convers.*, vol. 17, pp. 340-348, 2002.

[17] A. Gandhi, T. Corrigan, and L. Parsa, "Recent advances in modeling and online detection of stator interturn faults in electrical motors," *IEEE Trans. Ind. Electron.*, vol. 58, pp. 1564-1575, 2011.

[18] W. T. Thomson and M. Fenger, "Current signature analysis to detect induction motor faults," in *IEEE Ind. Appl. Mag.* vol. 7, ed, 2001, pp. 26-34.

[19] W. Qing and S. Nandi, "Fast single-turn sensitive stator inter-turn fault detection of induction mchines based on positive and negative sequence third harmonic components of line currents," in *Proc. 43th. Annu. Conf. IEEE Ind. Appl. Conf. (IAS'08)*, Edmonton, Canada, 2008, pp. 1-8.

[20] J. Cusido, L. Romeral, J. A. Ortega, J. A. Rosero, and A. Garcia Espinosa, "Fault detection in induction machines using power spectral density in wavelet decomposition," *IEEE Trans. Ind. Electron.*, vol. 55, pp. 633-643, 2008.

[21] J. A. Rosero, L. Romeral, J. Cusido, A. Garcia, and J. A. Ortega, "On the short-circuiting fault detection in a PMSM by means of stator current transformations," in *Proc. IEEE Power Electron. Specialists Conf. (PESC'07)*, Orlando, Florida, 2007, pp. 1936-1941.

[22] P. S. Barendse, B. Herndler, M. A. Khan, and P. Pillay, "The application of wavelets for the detection of inter-turn faults in induction machines," in *Proc. IEEE Int. Electric Machines and Drives Conf. (IEMDC'09)*, Miami, United States, 2009, pp. 1401-1407.

[23] J. Rosero, L. Romeral, E. Rosero, and J. Urresty, "Fault detection in dynamic conditions by means of discrete wavelet decomposition for PMSM running under bearing damage," in *Proc. 24th IEEE Appl. Power Electron. Conf. and Exposition (APEC'09)*, Washington,USA, 2009, pp. 951-956.

[24] A. Bouzida, O. Touhami, R. Ibtiouen, A. Belouchrani, M. Fadel, and A. Rezzoug, "Fault diagnosis in industrial induction machines through discrete wavelet transform," *IEEE Trans. Ind. Electron.*, vol. 58, pp. 4385-4395, 2011.

[25] H. Jun, Z. Jianzhong, C. Ming, and W. Zheng, "Fault diagnosis of mechanical unbalance for permanent magnet synchronous motor drive system under nonstationary condition," in *Proc. IEEE Int. Energy Convers. Congr. Expo. Conf. (ECCE' 2013)*, Denver, Colorado, 2013, pp. 3556-3562.

[26] C. Siwei, Z. Pinjia, and T. G. Habetler, "An Impedance Identification Approach to Sensitive Detection and Location of Stator Turn-to-Turn Faults in a Closed-Loop Multiple-Motor Drive," *IEEE Trans. Ind. Electron.*, vol. 58, pp. 1545-1554, 2011.

[27] J. C. Urresty, J. R. Riba, H. Saavedra, and L. Romeral, "Detection of inter-turns short circuits in permanent magnet synchronous motors operating under transient conditions by means of the zero sequence voltage," in *Proc. 14th Euro. Conf. Power Electron. Appl. (EPE '11)*, Birmingham, United Kingdom, 2011, pp. 1-9.

[28] L. A. Pereira, D. da Silva Gazzana, and L. F. A. Pereira, "Motor current signature analysis and fuzzy logic applied to the diagnosis of short-circuit faults in induction motors," in *Proc. 31st IEEE Ann. Conf. Ind. Electron. Soc. (IECON '05)*, Raleigh, NC, 2005, pp. 275-280.

[29] A. Siddique, G. S. Yadava, and B. Singh, "Applications of artificial intelligence techniques for induction machine stator fault diagnostics: review," in *Proc. 4th IEEE Int. Symp. on Diagnostics for Electric Mach., Power Electron. and Drives, (SDEMPED'03)*, Atlanta, Georgia, USA, 2003, pp. 29-34.

[30] M. Bouzid, G. Champenois, N. M. Bellaaj, L. Signac, and K. Jelassi, "An Effective Neural Approach for the Automatic Location of Stator

Interturn Faults in Induction Motor," *IEEE Trans. Ind. Electron.,* vol. 55, pp. 4277-4289, 2008.

[31] B. C. Mecrow, A. G. Jack, J. A. Haylock, and J. Coles, "Fault tolerant permanent magnet machine drives," in *Proc. 17th IEEE Int. Conf. on Elect. Mach. and Drives*, 1995, pp. 433-437.

[32] J. A. Haylock, B. C. Mecrow, A. G. Jack, and D. J. Atkinson, "Operation of fault tolerant machines with winding failures," *IEEE Trans. Energy Convers.*, vol. 14, pp. 1490-1495, 1999.

[33] Y. Lee, "A stator turn fault detection method and a fault-tolerant operating strategy for interior PM synchronous motor drives in safety-critical applications," Ph.D dissertation, Dep. of Elect. Comput. Eng., Georgia Institute of Technology, 2007.

[34] D. Min, A. Keyhani, and T. Sebastian, "Fault analysis of a PM brushless DC Motor using finite element method," *IEEE Trans. Energy Convers.,* vol. 20, pp. 1-6, 2005.

[35] O. A. Mohammed, Z. Liu, S. Liu, and N. Y. Abed, "Internal Short Circuit Fault Diagnosis for PM Machines Using FE-Based Phase Variable Model and Wavelets Analysis," *IEEE Trans. Magn.,* vol. 43, pp. 1729-1732, 2007.

[36] T. R. Jawad Ahmed Farooq, Abdesslem Djerdir, Abdellatif Miraoui, "Modelling and simulation of stator winding inter-turn faults in permanent magnet synchronous motors," *Int. J. Comput. Math. in Elect. Electron. Eng. (COMPEL'08),* vol. 27, pp. 887-896, 2008.

[37] D. Bao and W. Huo, "High precision BLDCM servo control with nonlinear identification," in *Informatics in Control, Automation and Robotics*. vol. 2, Y. Dehuai, Ed., ed: Springer, 2012, pp. 761-768.

[38] P. Pillay and R. Krishnan, "Modeling of permanent magnet motor drives," *IEEE Trans. Ind. Electron.,* vol. 35, pp. 537-541, 1988.

[39] R. H. Park, "Two-reaction theory of synchronous machines generalized method of analysis-Part I," *AIEE Tran.,* vol. 48, pp. 716-727, 1929.

[40] T. Boileau, B. Nahid-Mobarakeh, and F. Meibody-Tabar, "Back-EMF based detection of stator winding inter-turn fault for PM synchronous motor drives," in *Proc. IEEE Conf. on Vehicle Power and Propulsion (VPPC'07)*, Arlington, USA, 2007, pp. 95-100.

[41] L. Romeral, J. C. Urresty, J. R. Riba Ruiz, and A. Garcia Espinosa, "Modeling of Surface-Mounted Permanent Magnet Synchronous Motors With Stator Winding Interturn Faults," *IEEE Trans. Ind. Electron.,* vol. 58, pp. 1576-1585, 2011.

[42] B. Vaseghi, B. Nahid-Mobarakeh, N. Takorabet, and F. Meibody-Tabar, "Experimentally validated fynamic fault model for PMSM with stator

winding inter-turn fault," in *Proc. IEEE Ind. Appl. Soc. Ann. Meeting (IAS '08)*, Edmonton, Canada 2008, pp. 1-5.

[43] M. E. H. Benbouzid, "A Review of Induction Motors Signature Analysis as a Medium for Faults Detection," *IEEE Trans. Ind. Electron.*, vol. 47, 2000.

[44] R. R. Schoen, T. G. Habetler, F. Kamran, and R. G. Bartheld, "Motor bearing damage detection using stator current monitoring," in *Proc. 29h Ann. Conf. Ind. Appl. Soc. (IAS '94)*, Denver, USA, 1994, pp. 110-116.

[45] L. Eren and M. J. Devaney, "Bearing damage detection via wavelet packet decomposition of the stator current," *IEEE Trans. Instrum. Meas.*, vol. 53, pp. 431-436, 2004.

[46] I. Albizu, I. Zamora, and A. J. Mazon, "Techniques for on-line diagnosis of stator shorted turns in induction motors," *Electric Power Components and Systems*, vol. 34, pp. 97-114, 2006.

[47] F. C. Trutt, J. Sottile, and J. L. Kohler, "Condition monitoring of induction motor stator windings using electrically excited vibrations," in *Proc. 37th Ann. Conf. Ind. Appl. Soc. (IAS '02)*, Pittsburgh, PA, USA, 2002, pp. 2301-2305.

[48] W. T. Thomson, R. A. Leonard, and A. J. Milne, "Failure identification of offshore induction motor systems using on-condition monitoring," in *Proc. 4th Int. Conf on National*, Birmingham, UK, 1984.

[49] J. Penman, M. N. Dey, A. J. Tait, and W. E. Bryan, "Condition monitoring of electrical drives," *IEE Proc. B Electric Power Appl.*, vol. 133, pp. 142-148, 1986.

[50] J. Penman, H. G. Sedding, B. A. Lloyd, and W. T. Fink, "Detection and location of interturn short circuits in the stator windings of operating motors," *IEEE Trans. Energy Convers.*, vol. 9, pp. 652-658, 1994.

[51] B. M. Ebrahimi, J. Faiz, and M. J. Roshtkhari, "Static-, Dynamic-, and Mixed-Eccentricity Fault Diagnoses in Permanent-Magnet Synchronous Motors," *IEEE Trans. Ind. Electron.*, vol. 56, pp. 4727-4739, 2009.

[52] F. Meinguet, E. Semail, and J. Gyselinck, "An on-line method for stator fault detection in multi-phase PMSM drives," in *Proc. IEEE Vehicle Power and Propulsion Conf. (VPPC'10)*, Lille, France, 2010, pp. 1-6.

[53] Y. Lee and T. G. Habetler, "An On-Line Stator Turn Fault Detection Method for Interior PM Synchronous Motor Drives," in *Proc. 22th IEEE Applied Power Electronics Conf. (APEC'07)*, Anaheim, USA, 2007, pp. 825-831.

[54] C. L. Fortescue, "Method of Symmetrical Co-Ordinates Applied to the Solution of Polyphase Networks," *AIEE Tran.*, vol. 37, pp. 1027-1140, 1918.

[55] F. Fang, Y. Shiyuan, H. Xinguo, and W. Zhengguo, "Application of the Prony's method for induction machine stator fault diagnosis," in *Proc. Int. Conf. on Elect. Mach. Syst. (ICEMS'08)*, Wuhan, China, 2008, pp. 827-831.

[56] M. Ciobotaru, R. Teodorescu, and F. Blaabjerg, "A new single-phase PLL structure based on second order generalized integrator," in *Proc. 37th IEEE Power Electron. Specialists Conf. (PESC'06)*, Jeju, South Korea, 2006, pp. 1-6.

[57] W.V.Lyon, *Applications of the Method of Symmetrical Components*. New York: McGraw-Hill Book Company, 1937.

[58] P. Rodriguez, A. Luna, M. Ciobotaru, R. Teodorescu, and F. Blaabjerg, "Advanced grid synchronization system for power converters under unbalanced and distorted operating conditions," in *Proc. 32th Ann. Conf. on IEEE Ind. Electron. (IECON'06)* Paris, France, 2006, pp. 5173-5178.

[59] W. C. Duesterhoeft, M. W. Schulz, and E. Clarke, "Determination of instantaneous currents and voltages by means of alpha, beta, and zero components," *AIEE Tran.*, vol. 70, pp. 1248-1255, 1951.

[60] Y. Xiaoming, W. Merk, H. Stemmler, and J. Allmeling, "Stationary-frame generalized integrators for current control of active power filters with zero steady-state error for current harmonics of concern under unbalanced and distorted operating conditions," *IEEE Trans. Ind. Appl.*, vol. 38, pp. 523-532, 2002.

[61] R. Teodorescu, F. Blaabjerg, U. Borup, and M. Liserre, "A new control structure for grid-connected LCL PV inverters with zero steady-state error and selective harmonic compensation," in *Proc. 19th Ann. IEEE Applied Power Electronics Conf. Exposition (APEC '04)*, California, USA, 2004, pp. 580-586.

[62] P. Rodriguez, R. Teodorescu, I. Candela, A. V. Timbus, M. Liserre, and F. Blaabjerg, "New positive-sequence voltage detector for grid synchronization of power converters under faulty grid conditions," in *Proc. 37th IEEE Power Electronics Specialists Conf. (PESC'06)*, Jeju, South Korea, 2006, pp. 1-7.

[63] J. Quiroga, L. Li, and D. A. Cartes, "Fuzzy logic based fault detection of PMSM stator winding short under load fluctuation using negative sequence analysis," in *Proc. American Control Conf. (ACC'08)*, Seattle, USA, 2008, pp. 4262-4267.

[64] T. J. Ross, *"Classical Sets and Fuzzy Sets", Fuzzy logic with engineering applications*: John Wiley & Sons, 2009.

[65] L. Zadeh, "Fuzzy Sets," *Information and Control*, vol. 8(3), pp. 338-359, 1965.

[66] S. Sivanandam, S. Sumathi, and S. Deepa, *Introduction to Fuzzy Logic Using MATLAB*. New York: Springer Berlin Heidelberg, 2007.

[67] J. Jantzen. (1998). *Tutorial on fuzzy logic*. Available: 26th Aug. 2014 http://ssdi.di.fct.unl.pt/scl/docs/fuzzy%20logic.pdf

[68] *If-Then Rules*. Available: Aug. 27,2014 http://www-rohan.sdsu.edu/doc/matlab/toolbox/fuzzy/fuzzytu5.html

[69] T. J. Ross, *Fuzzy Logic with Engineering Applications*. Chichester: John Wiley & Sons, Ltd, 2010.

[70] P. V. Goode and C. Mo-yuen, "Using a neural/fuzzy system to extract heuristic knowledge of incipient faults in induction motors. Part I-Methodology," *IEEE Trans. Ind. Electron.*, vol. 42, pp. 131-138, 1995.